Mével, C., Gillis, K.M., Allan, J.F., and Meyer, P.S. (Eds.), 1996
Proceedings of the Ocean Drilling Program, Scientific Results, Vol. 147

2. MELT MIGRATION THROUGH HIGH-LEVEL GABBROIC CUMULATES OF THE EAST PACIFIC RISE AT HESS DEEP: THE ORIGIN OF MAGMA LENSES AND THE DEEP CRUSTAL STRUCTURE OF FAST-SPREADING RIDGES[1]

James H. Natland[2] and Henry J.B. Dick[3]

ABSTRACT

Gabbroic rocks recovered by drilling and submersible at Hess Deep, eastern equatorial Pacific, record processes of melt migration and channelized magma flow that bear on the origin and persistence of magma lenses and the development of lower-crustal structure at the East Pacific Rise. Rocks from ODP Hole 894G near the summit of the intrarift ridge at Hess Deep, and sampled by submersible from an uplifted marginal horst on the nearby northern slope of the rift, are mainly gabbronorites and olivine gabbronorites that crystallized very near the base of sheeted dikes. North Slope gabbros were sampled without interruption right to the base of sheeted dikes, and differ from Site 894 principally in that the sequence contains oxide-rich ferrodiorites and is cut locally by narrow tonalite dikelets. The highly fractionated rocks plausibly represent the frozen residues of a narrow and thin magma lens which geophysical evidence suggests once lay beneath the axial neovolcanic zone of the East Pacific Rise and its feeder dikes. Site 894 rocks represent the now-frozen immediate substrate, upon which a magma lens once rested, and through which it was supplied with melt.

Bulk compositions and modal mineralogy (principally low abundances of oxide minerals) demonstrate that almost all the gabbroic rocks of Site 894, and North Slope gabbronorites deeper than about 200 m below the base of the dikes, are adcumulates with <7% (average 4.4%) of material crystallized from trapped intercumulus melt. Yet, in contrast to adcumulates in layered intrusions, none of these rocks crystallized in close proximity to a major magma body. Lithostratigraphic relationships at Site 894, and the presence of grain-size variations across sharp contacts in several of the North Slope dive samples, show that most crystallization and adcumulus crystal growth occurred in fracture networks or in narrow dike-like bodies averaging about 3 m, but ranging down to as little as 1 cm, in thickness. Expulsion of intercumulus melt was extremely efficient at all of these scales, and—based on evidence from drilling nearby at Site 895 at the crust-mantle transition—evidently was pervasive throughout the entire mass of gabbros down to the mantle. Melt expulsion was not only thorough, but occurred almost immediately, providing a nearly impermeable base into which dense, iron-rich magmas in the thin melt lens could not sink.

No gabbroic rock from either Site 894 or the North Slope is layered, although some of the rocks show preferred orientation of plagioclases. There are no monomineralic adcumulates; all are olivine-plagioclase-clinopyroxene or plagioclase-clinopyroxene adcumulates and mesocumulates which crystallized on cotectics. Strongly zoned plagioclases, some enclosed as broken crystals in clinopyroxene or orthopyroxene oikocrysts, and unusually high Cr-contents of clinopyroxenes, attest to initial stages of crystallization from primitive to moderately fractionated basaltic magmas, followed by post-cumulus migration of highly fractionated (ferrobasaltic to ferroandesitic) melts through an open crystal network, without complete reequilibration of the originally precipitated minerals. Some of the primitive magmas carried xenocrysts of highly calcic plagioclase (An_{80-95}) which probably crystallized in the upper mantle or lower crust. Grain boundaries of all phases show substantial mutual interpenetration suggesting that pressure solution assisted in expulsion of intercumulus melts, thus aided in adcumulus growth. Reduction in melt porosity proceeded nearly to completion in most rocks before oxide minerals (mainly ilmenite with lesser magnetite) began to crystallize. The distribution of oxides therefore indicates the very late-stage porosity structure of the partially molten rocks, just before they froze completely.

Formation of adcumulates at fast-spreading ridges evidently can take place simultaneously in fracture networks throughout the entire 4-km section of crystallizing gabbros with only a small melt lens at the top. The melt lens does not precipitate a sequence of layered cumulates which then subsides into lower parts of the crust. Adcumulus growth occurs under conditions of stress which produce incessant rifting and fracturing alternating with intervals of compaction beneath a substantial overburden of dikes and extrusives. It is aided by a permanently positive, albeit fluctuating, temperature gradient downward into the upper mantle. This gradient guarantees the potential for some melt to exist anywhere in the crust beneath the physical location of the basalt solidus at the top of the magma lens. A magma lens thus may be sustained as a steady-state feature between inflation-eruption events by porous flow of melt expelled from the entire column of developing adcumulates. Persistent flow is required since the lens never completely freezes. The lens itself is a pool of highly fractionated, iron-rich and even siliceous melt that collects at the low-temperature top of the gabbro column, perhaps at the porous base of a cracking front which extends through the sheeted dikes. It is available to mix with more primitive magmas during major inflation-eruption cycles.

The extreme efficiency of adcumulate formation throughout the entire thickness of the gabbroic layer supports the operation of nearly ideal in situ fractional crystallization during the development of the basaltic liquid line of descent. Extrusive basalts and dikes at the East Pacific Rise, on average, will show two- to three-fold enrichments in incompatible elements to the extent that the gabbroic layer is depleted in those elements as a consequence of the formation of gabbroic adcumulates. These variable enrichments are acquired by unavoidable mixing with different proportions of highly fractionated melts in the magma lens, which directly underlies the narrow locus of eruption along the axial rift.

[1]Mével, C., Gillis, K.M., Allan, J.F., and Meyer, P.S. (Eds.), 1996. *Proc. ODP, Sci. Results*, 147: College Station, TX (Ocean Drilling Program).
[2]Rosenstiel School of Marine and Atmospheric Science, University of Miami, 4600 Rickenbacker Causeway, Miami, FL 33149, U.S.A. jnatland@rsmas.miami.edu
[3]Woods Hole Oceanographic Institution, Woods Hole, MA 02543, U.S.A. hdick@whoi.edu

INTRODUCTION

We have conducted a study of rock textures and the compositions of constituent minerals in gabbroic rocks from Ocean Drilling Program (ODP) Hole 894G, which was drilled near the summit of the intrarift ridge at Hess Deep, eastern equatorial Pacific, during ODP Leg 147 in December 1992. The gabbroic rocks from this site represent the first sampling by drilling of lower crustal rocks produced at the fast-spreading East Pacific Rise.

Gabbros were cored for 127.5 m, with an average recovery of 35.4% (Gillis, Mével, Allan, et al., 1993), beginning at 18.6 m below seafloor (mbsf). This distance represents the length of the casing assembly emplaced without coring at the top of the hole, in order to stabilize a hard-rock guide base which was used to reenter the hole several times until coring conditions prevented further advance. Drilling at Hole 894F, a bare-rock spud-in without a guide base, recovered rock from the upper 25.7 m of the section at this level of exposure on the outcrop.

The low recovery, the difficulty of drilling, and the ultimate abandonment of the hole, were all a consequence of drilling on a sloping fault surface (Francheteau et al., 1990). However, faulting is the only reason these rocks were exposed in the first place. Leg 147 was the first test of our drilling technology under the more-or-less typical outcrop conditions of gabbros and peridotites on the seafloor. We may soon be able to drill farther and with higher recovery in such rocks, but for the present our science must be fashioned from limited materials obtained with some persistence.

Drilling difficulties notwithstanding, Site 894 is an important accomplishment. From the drilling, we know that it is located near the top of the gabbroic sequence exposed in the Hess Deep rift, slightly downslope and to the west of medium-grained, chloritized, aphyric basaltic breccias cored in Hole 894A, which are as metamorphosed as the high-level gabbros themselves. These presumably represent the hydrothermally altered base of the sheeted dike sequence. The site is also very near the gabbro-dike transition which was inferred from *Nautile* dive samples prior to the drilling (Francheteau et al., 1990). A long sequence of gabbros, locally interrupted by extrusive basalts, extends downslope nearly 2000 m from this location to the deepest part of the rift valley. There, both primitive gabbros and serpentinized peridotites were sampled during the *Nautile* dives (Francheteau et al., 1990; Hekinian et al., 1993). Site 894 also demonstrated that the strike of steeply dipping preferred mineral orientation (magmatic foliation) in some cored samples, restored with respect to a presumed north-south magnetic inclination, is also north-south. This unequivocally ties the rocks to the East Pacific Rise, which trends in the same direction about 65 km to the west. Even so, two east-west trending dikes of porphyritic diabase, evidently intruded from the tip of the Cocos-Nazca rift which is propagating into Hess Deep, were cored near the top of the hole. These are probably related to some of the fresh porphyritic extrusives which partially carapace the south flank of the intrarift ridge (Gillis, Mével, Allan, et al., 1993; Allan et al., this volume). The gabbros of Site 894 are locally intensely sheared and cataclastized, especially near the top of the hole at the fault surface. They were also pervasively metamorphosed to greenschist facies mineral assemblages during their exposure and uplift, and following their intrusion by dikes. But their primary structures, lithologies, and earliest metamorphic histories date from their emplacement beneath the East Pacific Rise.

The high-level gabbros of Site 894 invite comparison to the suite of gabbros sampled during *Alvin* dives from the steep southern slope of an uplifted marginal horst on the north side of the Hess Deep basin first discovered during a deep-tow survey in the 1970s (Klitgord and Mudie, 1974). The location is northeast of Site 894 (Fig. 1). The North Slope gabbros sequentially underlie pillow basalts and sheeted dikes which were produced at the East Pacific Rise at about 1.8 Ma (Lonsdale, 1988; Karson et al., 1992). Their exposure was accomplished by slope failure (Francheteau et al., 1992) rather than deep faulting, thus the rocks are generally fresher than the gabbros of Site 894, and are not at all sheared and brecciated. The samples of greatest interest here comprise a fairly detailed sequence obtained during three dives, each of them a vertical traverse upslope beginning in gabbros, with two of them proceeding into dikes. The most relevant comparisons to Site 894 are gabbro cumulates, which were sampled on steep, buttress-like ridges between the talus-strewn ramps of debris flows for about 300 m below the base of the dikes (Natland et al., 1990). The cumulates include oxide-bearing and oxide-rich ferrogabbros with narrow tonalite dikelets within a stratigraphy dominated by varitextured gabbronorites. The rocks are inferred to represent the residues of an axial magma lens frozen in place at the very top of the gabbroic layer (Natland, 1991c).

The magma lenses at fast-spreading ridges, which can be mapped for long distances using multichannel seismic techniques (e.g., Kent et al., 1990, 1993; Harding et al., 1989) are all that is left of what geophysicists used to construe as major magma chambers, extending from the base of the dikes to the mantle itself, and being more than 10 km wide at the base (e.g., Rosendahl, 1976; Orcutt et al., 1976). Now geophysics tells us that most of this is simply hot rock. The new techniques specify that seismically detectable melt at fast-spreading ridges only occurs in a narrow sill-like body some 900–1500 m wide (rarely wider), and probably only about 50 m thick, precisely beneath the axial neovolcanic zone (Kent et al., 1990, 1993). How much melt occurs below this, and where it is distributed, are not yet firmly established, but no more than about 5% of melt distributed throughout the rock mass down to the mantle would produce the seismic attenuation observed below the melt lens of the East Pacific Rise at 9°N (Burnett et al., 1989). Moreover, seismic gaps in the Moho reflection at the 9°N and 12.9°N nontransform offsets, just beneath or slightly offset from the magma-lens reflector, are only 2–6 km wide (Barth, 1994). Most melt flow from the mantle must be restricted to these narrow bands.

Thus, in considering the petrology and structure of the crust at a fast-spreading ridge, and how it forms, consistency with current geophysics implies that rocks beneath the melt lens, which are presumably the locus of most magma transport to the seafloor, are nonetheless almost entirely crystallized, and they are completely so (at the resolution of seismic imaging) within 450–750 m to either side of the precise center of spreading at the base of the dikes, and within 1500–3000 m to either side of the plate boundary at the base of the crust. The crystallization histories of gabbro samples from the North Slope of Hess Deep, and from Site 894, were nearly completed within 6400–11,000 yr (assuming a 7 cm/yr half spreading rate; Lonsdale, 1988). The entire course of magmatic differentiation, to the point of production at the North Slope of oxide ferrogabbros and tonalites (plagiogranites), was accomplished in the same span of time. High-level gabbros from the exposures in Hess Deep are consequently plausible representatives of magmas which crystallized within or just below former melt lenses, or of magmas which passed through melt lenses *en route* to dike injection and eruption. Careful study of these two rock suites should reveal the functioning of those magma lenses, perhaps explaining why they are persistent (steady-state) features, and how the process of magma transport was accomplished (Sinton and Detrick, 1992).

As a starting point, we shall be concerned with how much melt was still within the gabbro cumulates at the time they froze. Geophysics predicts less than 5%. In the world of layered intrusions, 5% is extremely little, so little that such rocks have been given the special name of *ad*cumulate (Wager et al., 1960; Wager and Brown, 1968), to indicate that compaction or infilling of an original loose collection of cumulus minerals was extremely efficient, and that residual melt porosities (Morse, 1986) were reduced to very low levels.

Adcumulates are actually an uncommon phenomenon in layered intrusions. That is, they only rarely constitute the bulk of an intrusion,

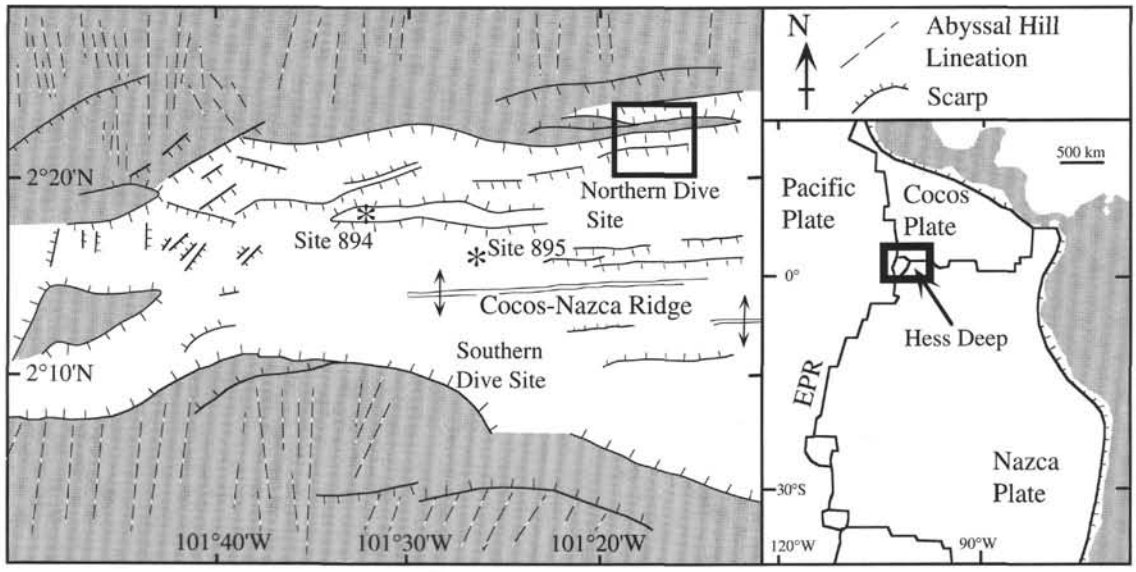

Figure 1. Schematic tectonic map of the western tip of the Cocos-Nazca rift showing the locations of Site 894 and the North Slope dive site, modified slightly from Gillis (unpubl. data). The inset on the right shows the location of the major plate boundaries, based on Lonsdale (1988) and Francheteau et al. (1992).

and in many layered intrusions they are rare (e.g., Skaergaard; Wager, 1963) or lacking altogether (e.g., Partridge River, Duluth Complex; Chalokwu and Grant, 1990). If adcumulates are an important part of the ocean crust, we then must consider why this is the case, and in particular, how such rocks can form in the absence of all but an extremely small lens of melt located right at the top of the stack of cumulates. In certain respects, we may also have to consider whether the cumulate terminology developed by Wager et al. (1960), which was later recast by Irvine (1982), actually is appropriate to describe gabbroic rocks of the ocean crust. Our textural terminology consequently will be as nongenetic as possible (cf., McBirney, 1993), at least at first.

A word on the methodology of this paper. The sequence of exposition might be compared to the making of a portrait, wherein preparation of the base and the background precede a general outline, and then detail is added to each part until the final image is produced. The eventual "image" to be rendered is the manner in which melts both produced these rocks and moved through them. Aspects of rock textures, crystallization histories, bulk compositions, and mineralogy are required to produce this final portrait, and are considered in that order. Then we shall stand back and view the entire portrait, and consider its overall impression. At this point, the base has been prepared, and we now describe the analytical palette.

METHODS

Thin sections were examined in both transmitted and reflected light. Modal measurements of the percentages of oxide minerals and the proportions of plagioclase to mafic minerals were made using a Leica Quantimet 500 image-analysis system, with the video camera attached to a Wild M3 zoom stereoscope (magnification range = 6.5×–40×) equipped with a polarizing stage. Measurements are made by isolating selected portions of a gray-scale range (0–256, black to white), so that they become precisely superimposed on the appropriate portions of the video image of a sample. The two measurements provide precise information pertinent respectively to residual melt porosities and processes of crystal sorting.

In particular, the very low percentages of oxide minerals in some of the rocks are difficult to measure by point counting. Image analysis, wherein each of the 385,000 pixels of the video image is equivalent to a point, allows rapid determination of oxide proportions as low as 0.01%, to two significant figures, summed from the approximately three images (at 6.5×) required for entire thin sections. The principal complication is distinguishing oxide minerals from sulfides, which may be equally abundant in some samples. This can be done rapidly using crystal outlines at 6.5×–16× in transmitted light with the stereoscope, then editing, or by making the measurements more laboriously at high magnification (40× or greater) on a standard petrographic microscope, and distinguishing oxides from sulfides in reflected light.

Image analysis also allows modifications of original images which enhance the gray-scale contrast between feldspars and mafic minerals. The remaining gray-scale overlaps, which in these rocks involve alteration phases, traces of cleavage and exsolution, inclusions within the primary silicates, and slide defects, can be efficiently removed by editing functions. Successively selected images of oxides, plagioclases, and mafic minerals can then be stacked (or not) as necessary, saved on disc, and printed out with contrasting tones via a visual graphics program such as Paintbrush®. Modal estimates obtained by image analysis for samples from both Site 894 and the North Slope, with some other relevant compositional parameters, are listed in Table 1.

Mineral analyses were determined bicoastally at four different institutions by six different analysts. Site 894 samples were analyzed using a JEOL superprobe at Massachusetts Institute of Technology and a Camebax electron probe at Scripps Institution of Oceanography. North Slope samples were analyzed at Scripps, and on a Cameca SX-50 electron probe at the University of California at Davis. Additional data were obtained using yet a third Cameca instrument at Lamont-Doherty Earth (then Geological) Observatory. Consistency of data was established by normalizing to the same standards which were available at all institutions.

Analysis strategies for the North Slope and Site 894 samples were somewhat different. Several different mineral grains, usually immediately adjacent to oxide minerals, in the North Slope gabbros were analyzed at one or two points each. The analyses were part of collaborations focusing on oxygen fugacities (Nilsson and Natland, 1991; Nilsson, 1993) and on the relationship of oxide minerals to rock magnetic properties (Gee et al., 1992). For samples of Site 894 (studied by Natland and Dick), fewer examples of each mineral were ana-

Table 1. Modal abundances of oxide minerals and silicates determined by quantitative image analysis.

Hole 894G			
Core, section, interval (cm)	% oxides	% plagioclase	% mafic silicates*
147-894G-			
1R-1, 8–10	0.70	42.4	56.9
2R-2, 138–141	3.21	—	—
2R-3, 101–104	0.15 (A)	37.2	62.7
4R-2, 27–30	0.70	45.8	53.5
5R-1, 10–14	0.20 (A)	—	—
6R-1, 0–5	0.28 (A)	42.4	57.3
6R-1, 26–28	0.06 (A)	43.5	56.5
6R-1, 116–120	0.40	—	—
6R-3, 0–4	0.44	—	—
7R-1, 67–70	0.13 (A)	33.3	66.6
9R-3, 0–5	0.06 (A)	—	—
9R-4, 84–88	0.31	—	—
11R-3, 43–45	0.13 (A)	42.7	57.2
12R-4, 37–40	0.36	46.2	53.4
13R-3, 101–103	0.15 (A)	66.0	33.9
17R-2, 9–13	0.16 (A)	43.9	55.9
20R-3, 95–97	1.36	49.5	49.1
Averages			
number	17 (16)**	10	
mean	0.52 (0.34)**	44.9	
s.d.	0.77 (0.33)**	8.7	

North Slope					
Dive	Sample	% oxides*	Mg#	TiO_2 (%)	Zr (ppm)
2213	1053	2.03	0.590	1.28	31
	1110	0.17 (A)	0.652	0.46	18
	1125	0.27 (A)	—	0.49	21
	1206	0.23 (A)	0.669	0.87	44
	1226	0.18 (A)	0.711	0.60	25
	1333	1.00	0.656	1.00	52
	1351	5.65	0.538	2.11	60
2218	1057	0.09 (A)	0.739	0.39	10
	1132	0.25 (A)	0.728	0.88	38
	1210–6	12.07	0.317	5.10	101
	1229	0.43	0.626	1.40	72
	1308	3.27	0.507	2.92	110
	1440	0.28 (A)	0.744	0.66	38

Notes: (A) = adcumulate with ≤0.3% oxides. * = calculated by difference. ** = excludes sample with 3.21% oxides. s.d. = standard deviation.

lyzed, but the analyses were accomplished in traverses with which we intended to establish core and rim (or grain edge) compositions. Additional data, obtained as part of a study on alteration mineralogy for this volume, were kindly provided by Dr. Kathryn Gillis. Average grain analyses of plagioclases, clinopyroxenes, orthopyroxenes, and olivines, with standard deviations, are listed in Tables 2–5. Ilmenite and magnetite were also analyzed in many samples, but the compositions are not reported here since they are revealing mainly of the extensive subsolidus reequilibration and oxidation exsolution (Buddington and Lindsley, 1964) of these minerals.

We also obtained trace-element data on clinopyroxenes and plagioclases using the ion microprobe in the laboratory of Dr. Nobu Shimizu at Woods Hole Oceanographic Institution. The data include a reconnaissance of several samples from Site 894, and one sample studied in considerable (some would say excruciating) detail. The ion-probe routine for plagioclases includes measurement of Al, which allows immediate transformation to the An contents of the feldspars. These correspond to within 1–2 mol% of An contents determined from electron-probe analyses of the same minerals obtained as nearly as possible at immediately adjacent spots. Since K, Fe, and Mg are also measured in an ion-probe analysis of plagioclase (along with Ti and Sr), the result actually provides the equivalent of a full electron probe analysis, but with minor and trace elements measured to much higher precision. Electron probe analyses corresponding to most points of the ion probe traverses on clinopyroxenes, and some of the points on plagioclases, were obtained on the detailed-study sample at Scripps Institution of Oceanography. The results of ion probe analyses, and corresponding electron probe end-member compositions of clinopyroxenes (WoEnFs) and plagioclases (An), are listed respectively in Tables 6 and 7.

LITHOLOGIC SUMMARY OF SITE 894

A lithostratigraphic summary of Hole 894G is presented in Figure 2. This is a more detailed version of the shipboard lithostratigraphy, in which 13 lithologic units were identified (here labelled A through M). In Figure 2, a total of 43 distinct lithologic intervals are indicated. An interval is defined by any significant detectable change in modal mineralogy or grain size (i.e., a change from coarse to fine grain size, or a change from poikilitic to granular textures). Similarly, the appearance of a significant amount of olivine in hand specimen, or the disappearance of orthopyroxene, is defined as an interval. Thus, igneous intervals represent the smallest conveniently divisible igneous "units" in the lithologic sequence. Two of the intervals are basaltic, leaving 41 gabbroic intervals. Summary descriptions of each interval, and the corresponding curated and expanded thicknesses (taking into account intervals of no core recovery), are given in the Appendix.

Almost all gabbroic rocks from Site 894 are olivine gabbronorites and gabbronorites, with orthopyroxene present in amounts >5% (Streckeisen, 1974). The average orthopyroxene mode measured by point counting of 13 samples on board ship is 12.0 ± 5.5% (Gillis, Mével, Allan, et al., 1993). The rocks may or may not contain olivine (up to about 4% of the mode), but they always contain two pyroxenes and plagioclase. In the shipboard lithostratigraphy, there are a few simple gabbros with very little or no orthopyroxene, but in our col-

Table 2. Hole 894G average plagioclase compositions.

Core, section, interval (cm)	Pc	Depth (mbsf)	Rock type	Pts.	AS	Gr.	Loc	Grain size (mm)		Na_2O	MgO	Al_2O_3	SiO_2	CaO	FeO	K_2O	Total	An	Ab	Or
147-894G-																				
1R-1, 8–10	2	22.60	Gabbronorite	5	HD	1e	B	1.90	0.70	4.14	0.05	30.1	53.2	12.6	0.51	0.08	100.7	62.4	37.2	0.5
1R-1, 8–10	2	22.60	Gabbronorite	sd	HD	1e	B	1.90	0.70	0.29	0.01	0.5	0.5	0.4	0.07	0.02	0.3	2.4	2.4	0.1
2R-3, 101–103	13	37.76	Olivine gabbro	5	HD	1e	B	5.20	1.10	3.45	0.06	30.4	48.5	13.8	0.31	0.14	96.6	68.2	30.9	0.8
2R-3, 101–103	13	37.76	Olivine gabbro	sd	HD	1e	B	5.20	1.10	0.50	0.03	0.5	5.1	0.9	0.09	0.04	4.6	4.5	4.4	0.2
2R-3, 101–103	13	37.76	Olivine gabbro	3	HD	2c	B	0.90	0.09	3.82	0.04	30.6	51.8	13.1	0.22	0.14	99.7	64.9	34.2	0.8
2R-3, 101–103	13	37.76	Olivine gabbro	sd	HD	2c	B	0.90	0.09	0.44	0.04	0.8	1.0	0.5	0.19	0.05	0.2	3.3	3.4	0.3
4R-2, 27–30	6	48.14	Gabbro?	5	HD	1e	B	4.70	1.80	4.36	0.05	29.7	53.6	12.2	0.53	0.06	100.4	60.5	39.2	0.4
4R-2, 27–30	6	48.14	Gabbro?	sd	HD	1e	B	4.70	1.80	0.37	0.04	0.5	0.8	0.6	0.09	0.02	0.3	3.1	3.2	0.1
4R-2, 27–30	6	48.14	Gabbro?	3	HD	2c	B	0.60	0.35	4.09	0.05	30.5	52.7	12.7	0.49	0.04	100.6	63.0	36.8	0.2
4R-2, 27–30	6	48.14	Gabbro?	sd	HD	2c	B	0.60	0.35	0.31	0.04	0.5	0.8	0.5	0.08	0.03	0.3	2.6	2.5	0.2
5R-1, 10–14	2	51.41	Olivine gabbronorite	5	HD	1e	B	1.70	2.50	4.10	0.05	30.2	53.2	12.5	0.42	0.07	100.5	62.5	37.1	0.4
5R-1, 10–14	2	51.41	Olivine gabbronorite	sd	HD	1e	B	1.70	2.50	0.34	0.01	0.4	0.7	0.5	0.04	0.02	0.4	2.9	2.8	0.1
5R-1, 10–14	2	51.41	Olivine gabbronorite	3	HD	2c	B	1.40	0.30	3.93	0.27	30.2	52.5	12.7	0.78	0.04	100.4	63.9	35.9	0.2
5R-1, 10–14	2	51.41	Olivine gabbronorite	sd	HD	2c	B	1.40	0.30	0.21	0.32	0.7	0.2	0.6	0.56	0.01	0.2	2.4	2.4	0.0
6R-1, 26–28	4	55.61	Olivine gabbronorite	5	HD	1e	B	4.20	1.40	4.31	0.07	29.7	52.8	12.2	0.34	0.21	99.6	60.2	38.6	1.2
6R-1, 26–28	4	55.61	Olivine gabbronorite	sd	HD	1e	B	4.20	1.40	0.21	0.03	0.4	0.7	0.5	0.06	0.04	0.3	2.1	2.2	0.2
6R-1, 26–28	4	55.61	Olivine gabbronorite	3	HD	2c	B	1.10	0.15	4.07	0.07	30.1	52.1	12.5	0.18	0.09	99.2	62.6	36.8	0.5
6R-1, 26–28	4	55.61	Olivine gabbronorite	sd	HD	2c	B	1.10	0.15	0.12	0.04	0.3	0.3	0.1	0.16	0.04	0.4	0.7	1.0	0.3
7R-1, 67–70	12	65.94	Olivine gabbro	5	HD	1e	B	2.80	1.30	3.89	0.06	30.2	52.6	13.0	0.46	0.06	100.3	64.6	35.0	0.4
7R-1, 67–70	12	65.94	Olivine gabbro	sd	HD	1e	B	2.80	1.30	0.49	0.04	0.7	1.3	0.9	0.08	0.02	0.6	4.5	4.5	0.1
7R-1, 67–70	12	65.94	Olivine gabbro	3	HD	2c	B	2.50	0.50	4.06	0.14	29.7	53.2	12.2	0.40	0.22	99.9	61.5	37.1	1.3
7R-1, 67–70	12	65.94	Olivine gabbro	sd	HD	2c	B	2.50	0.50	0.31	0.18	0.4	0.5	0.6	0.06	0.28	0.7	2.0	2.6	1.7
9R-4, 84–88	7	78.38	Gabbronorite	10	JN	1	C											90.0		
9R-4, 84–88	7	78.38	Gabbronorite	sd	JN	1	C											2.4		
9R-4, 84–88	7	78.38	Gabbronorite	7	JN	1	R											61.8		
9R-4, 84–88	7	78.38	Gabbronorite	sd	JN	1	R											1.7		
9R-4, 84–88	7	78.38	Gabbronorite	4	JN	2	B											75.5		
9R-4, 84–88	7	78.38	Gabbronorite	sd	JN	2	B											3.5		
9R-4, 84–88	7	78.38	Gabbronorite	6	JN	3	B											70.1		
9R-4, 84–88	7	78.38	Gabbronorite	sd	JN	3	B											2.5		
9R-4, 84–88	7	78.38	Gabbronorite	3	JN	5	B											67.4		
9R-4, 84–88	7	78.38	Gabbronorite	sd	JN	5	B											1.5		
11R-3, 43–45	6	92.90	Olivine gabbronorite	3	HD	1c	B	0.30	0.30	3.73	0.06	31.0	52.6	13.4	0.43	0.02	101.2	66.5	33.4	0.1
11R-3, 43–45	6	92.90	Olivine gabbronorite	sd	HD	1c	B	0.30	0.30	0.11	0.03	0.2	0.3	0.3	0.04	0.02	0.0	1.3	1.2	0.1
11R-3, 43–45	6	92.90	Olivine gabbronorite	5	HD	2e	B	3.00	1.50	4.10	0.04	30.3	52.9	12.9	0.51	0.05	100.8	63.3	36.5	0.3
11R-3, 43–45	6	92.90	Olivine gabbronorite	sd	HD	2e	B	3.00	1.50	0.42	0.03	0.6	0.9	0.7	0.07	0.02	0.1	3.6	3.6	0.1
12R-4, 37–40	4a	99.58	Gabbronorite	42	HD	2	B	2.40	1.50	3.46	0.05	31.1	51.4	13.7	0.46	0.05	100.2	68.4	31.3	0.3
12R-4, 37–40	4a	99.58	Gabbronorite	42	HD	sd	B	2.40	1.50	0.35	0.03	0.7	1.0	0.7	0.09	0.02	0.2	3.3	3.3	0.1
12R-4, 37–40	4a	99.58	Gabbronorite	3	HD	2c	C	0.45	0.20	4.38	0.07	30.1	53.5	12.2	0.50	0.03	100.8	60.5	39.3	0.2
12R-4, 37–40	4a	99.58	Gabbronorite	sd	HD	2c	C	0.45	0.20	0.42	0.06	0.6	0.8	0.7	0.09	0.01	0.3	3.6	3.6	0.0
13R-3, 101–103	11	112.31	Gabbronorite	3	HD	1	B	0.80	0.20	4.08	0.06	30.4	52.9	12.8	0.52	0.05	100.9	63.2	36.6	0.3
13R-3, 101–103	11	112.31	Gabbronorite	sd	HD	1	B	0.80	0.20	0.09	0.02	0.1	0.1	0.1	0.11	0.00	0.1	0.7	0.8	0.0
13R-3, 101–103	11	112.31	Gabbronorite	6	HD	2	I	2.70	0.75	4.40	0.05	30.1	53.7	12.3	0.49	0.06	101.0	60.4	39.2	0.4
13R-3, 101–103	11	112.31	Gabbronorite	sd	HD	2	I	2.70	0.75	0.53	0.02	0.8	1.0	0.8	0.09	0.01	0.2	4.4	4.4	0.1
17R-2, 9–13	1a	128.78	Olivine gabbronorite	5	HD	1e	B	2.30	1.30	4.33	0.04	30.0	53.7	12.3	0.43	0.06	100.9	60.9	38.7	0.3
17R-2, 9–13	1a	128.78	Olivine gabbronorite	sd	HD	1e	B	2.30	1.30	0.29	0.03	0.4	0.5	0.5	0.08	0.01	0.2	2.6	2.6	0.1
17R-2, 9–13	1a	128.78	Olivine gabbronorite	3	HD	2c	B	0.30	0.20	3.89	0.07	30.6	52.5	13.2	0.52	0.03	100.8	65.0	34.8	0.2
17R-2, 9–13	1a	128.78	Olivine gabbronorite	sd	HD	2c	B	0.30	0.20	0.07	0.04	0.2	0.1	0.0	0.10	0.01	0.2	0.4	0.5	0.1
20R-3, 95–97	14	153.55	Gabbronorite	5	HD	1e	B			4.09	0.03	30.3	53.2	12.6	0.42	0.06	100.7	62.8	36.8	0.3
20R-3, 95–97	14	153.55	Gabbronorite	sd	HD	1e	B			0.42	0.02	0.5	0.9	0.7	0.07	0.02	0.6	3.6	3.6	0.1
20R-3, 95–97	14	153.55	Gabbronorite	3	HD	2c	B	1.00	0.30	3.97	0.03	30.3	52.8	12.9	0.54	0.08	100.7	63.9	35.6	0.5
20R-3, 95–97	14	153.55	Gabbronorite	sd	HD	2c	B	1.00	0.30	0.73	0.02	0.9	1.6	1.2	0.00	0.03	0.3	6.3	6.5	0.2

Notes: Pc = piece number. Pts. = number of spots analyzed. sd = standard deviation. AS = analysis source: HD = H. Dick from the electron probe lab at MIT; JN = J. Natland using Woods Hole Ion Probe. Gr. = grain number. Loc = location: B = average of traverse across grain; C = core; R = rim; I = intermediate (between core and rim). Grain size = maximum length and width of grain in millimeters. Grain size gives largest and smallest long dimensions of grains used for averages.

Table 3. Hole 894G average clinopyroxene compositions.

Core, section, interval (cm)	Pc	Depth (mbsf)	Rock type	Pts.	AS	Gr.	Loc	Grain size (mm)		Morph.	Na_2O	MgO	Al_2O_3
147-894G-													
1R-1, 8–10		22.60	Gabbronorite	10	HD	1	B	0.77	0.67	anhed. gran.	0.33	14.57	1.89
				sd							0.02	0.09	0.08
4R-2, 27–30		48.14	Gabbronorite	10	HD	1	I				0.32	14.30	1.54
				sd							0.04	0.08	0.06
5R-1, 10–14		51.41	Olivine gabbronorite	10	HD	1	B				0.34	14.88	2.02
				sd							0.04	0.08	0.05
7R-1, 67–70		65.94	Olivine gabbro	10	HD	1	B				0.41	15.08	2.88
				sd							0.03	0.06	0.25
9R-1, 75–79	11	75.05	Gabbronorite	10	JN	1–4	B				0.29	15.67	1.58
				sd							0.02	0.34	0.17
9R-4, 84–88	7	78.38	Olivine gabbronorite	19	JN	1	I			oikocryst	0.31	16.39	2.23
				sd							0.02	0.58	0.55
11R-3, 43–44		92.90	Olivine gabbronorite	11	HD	1	I				0.32	15.65	2.16
				sd							0.03	0.14	0.04
12R-4, 37–40		99.58	Gabbronorite	10	HD	1	C				0.33	14.90	2.06
				sd							0.02	0.22	0.03
13R-3, 101–103		112.30	Gabbronorite	10	HD	1	R	2.00	1.50		0.38	15.80	2.56
				sd							0.06	0.69	0.14
17R-2, 9–13		128.78	Olivine gabbronorite	10	HD	1	R	2.50	2.00		0.34	15.19	2.24
				sd							0.01	0.27	0.06
20R-3, 95–97		153.55	Gabbronorite	10	HD	1	C	1.00	0.60	sub.eq.pr.gr.	0.36	14.43	2.25
				sd							0.02	0.10	0.06
North Wall Dive/Sample													
2213/1053			Gabbronorite	4	JN		B				0.28	13.78	1.64
				sd							0.02	0.16	0.28
2213/1226			Gabbronorite	8	JN		B				0.27	14.53	2.02
				sd							0.04	0.33	0.30
2213/1316			Gabbronorite	2	JN		B				0.28	14.73	2.19
				sd							0.02	0.27	0.22
2218/1111			Gabbronorite	2	JN		B				0.29	15.07	2.12
				sd							0.07	0.45	0.11
2218/1210–3			Oxide gabbronorite	3	JN		B				0.22	13.37	1.36
				sd							0.05	0.17	0.55
2218/1337			Gabbronorite	3	JN		B				0.23	14.18	0.85
				sd							0.03	0.35	0.04
2218/1434			Gabbronorite	2	JN		B				0.65	12.86	3.04
2213/1110			Gabbronorite	4	JN		B				0.28	15.83	1.84
				sd							0.04	0.68	0.57

Notes: Abbreviations and column headings are the same as in Table 2. Morph. = grain morphology. Mg#, Wo, En, and Fs are the molecular ratios of Mg/(Mg+Fe), wollastonite, enstatite, and ferrosilite. Grain size gives largest and smallest long dimensions of grains used for averages.

lection of thin sections, this mineral is always present. Similarly, oxide minerals are not always evident in hand specimen, but among our thin sections there is no sample completely without oxide minerals (mainly ilmenite with some magnetite, usually intergrown), and in a few samples there are several per cent of oxide minerals. Interval 26 in Figure 2, which is very thin (1 cm in recovery; 0.16 m in expanded recovery), has sufficient oxide (>8%) to be termed oxide gabbronorite.

Most interval boundaries correspond to variations in grain size. The 41 lithologic units in the gabbros so identified thus plausibly represent individual crystallization units, with boundaries defining magma bodies which cooled as individual entities, or portions of such bodies which were later cut by others. From the Appendix, the average interval thickness of the gabbroic rocks defined by mineralogical contrasts is 3.6 m, with the largest (in expanded recovery) being 8.5 m thick. Some variations in grain size are too small to record individually. One such, shown in oversized thin section in Figure 3, is a 2-cm vein of coarse gabbronorite which penetrated a deformable, probably partly molten, fine-grained gabbronorite, twisting an original preferred orientation of plagioclases differently on either side. The vein extends almost vertically for nearly 30 cm in the core (Gillis, Mével, Allan, et al., 1993).

As this example demonstrates, the rocks may vary considerably in grain size on the scale of a few centimeters. But marked grain-size variations more usually occur several tens of centimeters apart. These are evidenced mainly by size variations in plagioclases, with individual grains ranging from less than a millimeter to a half-centimeter or more. Some of the grain size variations occur abruptly across sharp contacts. Where orientations of these with respect to magnetic inclination can be reconstructed, they are fairly steeply dipping and lie within about 20° of north-south (MacLeod, Manning, et al., this volume). Although the contacts are sharp, they are not planar in the manner of quickly chilled margins. In thin sections, there is always some interpenetration of coarse and fine-grained materials at these boundaries (Figs. 3, 4). But the consistency of the north-south orientation and the overall steepness of reconstructed dips suggests that at this high level in the gabbros, individual crystallization units are dike-like in general aspect, and not very wide.

PETROGRAPHY AND TEXTURES

Crystallization Sequence

Idiomorphic relations and mineral compositions in all Site 894 gabbroic rocks point to a crystallization sequence in the following order: plagioclase, plagioclase with olivine, plagioclase with clinopyroxene, orthopyroxene, and the two oxide minerals, ilmenite and magnetite. This is typical of abyssal tholeiites through a wide range of crystallization (e.g., Walker et al., 1979). Indeed, the abundance of orthopyroxene, and the overall compositions of the minerals (to be discussed) indicate that the rocks crystallized from strongly fractionated ferrobasaltic to ferroandesitic liquids of the type described from the Galapagos Spreading Center by Perfit et al. (1983) and Juster et al. (1989). Rocks with this mineralogy would follow dunites, troctolites, olivine gabbros, and gabbros in a standard crystallization sequence from parental abyssal tholeiite, and precede ferrodiorites.

Table 3 (continued).

Core, section, interval (cm)	SiO_2	CaO	TiO_2	Cr_2O_3	MnO	FeO	Total	Mg#	Wo	En	Fs
147-894G-											
1R-1, 8–10	51.53	20.38	0.82	0.13	0.24	9.77	99.66	72.7	42.2	42.0	15.8
	0.19	0.25	0.05	0.04	0.03	0.16	0.18	0.3	0.5	0.2	0.3
4R-2, 27–30	51.25	20.06	0.59	0.09	0.27	10.71	99.12	70.4	41.5	41.2	17.3
	0.22	0.22	0.04	0.02	0.01	0.16	0.28	0.2	0.4	0.2	0.2
5R-1, 10–14	51.10	20.60	0.76	0.15	0.23	9.21	99.31	74.2	42.5	42.7	14.8
	0.16	0.25	0.03	0.05	0.03	0.20	0.29	0.3	0.5	0.2	0.3
7R-1, 67–70	50.71	20.31	0.70	0.73	0.23	8.56	99.62	75.9	42.3	43.7	13.9
	0.11	0.26	0.06	0.06	0.02	0.26	0.11	0.6	0.4	0.2	0.4
9R-1, 75–79	52.10	19.29	0.57	0.03	0.29	10.48	100.29	72.7	39.2	44.2	16.6
	0.44	0.62	0.09	0.02	0.02	0.63	1.21	1.1	1.2	0.9	0.9
9R-4, 84–88	51.80	19.19	0.56	0.15	0.20	8.19	99.58	76.9	39.3	46.7	14.0
	1.12	1.25	0.08	0.04	0.02	0.41	0.62	1.0	2.3	1.9	0.8
11R-3, 43–44	52.15	20.99	0.61	0.24	0.22	8.24	100.59	77.2	42.7	44.2	13.1
	0.19	0.11	0.02	0.03	0.02	0.12	0.22	0.4	0.2	0.3	0.2
12R-4, 37–40	51.79	19.91	0.87	0.13	0.30	10.45	100.75	71.8	40.8	42.5	16.7
	0.27	0.66	0.03	0.03	0.03	0.48	0.34	0.7	1.4	0.6	0.8
13R-3, 101–103	51.96	20.29	0.61	0.48	0.19	8.21	100.47	77.5	41.7	45.2	13.2
	0.24	1.38	0.04	0.02	0.05	0.73	0.33	0.7	2.9	1.8	1.1
17R-2, 9–13	51.49	20.01	0.95	0.20	0.27	9.85	100.54	73.3	41.0	43.3	15.7
	0.26	0.60	0.04	0.03	0.02	0.38	0.26	0.4	1.3	0.7	0.6
20R-3, 95–97	51.64	20.65	0.74	0.26	0.26	9.74	100.33	72.5	42.7	41.5	15.7
	0.21	0.28	0.03	0.03	0.03	0.14	0.28	0.2	0.5	0.3	0.2
North Wall Dive/Sample											
2213/1053	51.86	20.73	0.69	0.02	0.31	11.36	100.67	68.4	42.5	39.3	18.2
	0.67	0.24	0.13	0.02	0.05	0.47	0.56	0.9	0.7	0.3	0.7
2213/1226	52.36	22.04	0.74	0.18	0.25	8.84	101.23	74.5	44.8	41.1	14.0
	0.46	0.51	0.21	0.14	0.06	0.55	0.61	1.4	0.9	0.6	0.9
2213/1316	51.84	20.90	0.76	0.03	0.34	9.82	100.87	72.8	42.6	41.8	15.6
	0.31	0.21	0.07	0.03	0.06	0.21	0.63	0.4	0.6	0.4	0.3
2218/1111	51.36	21.05	0.81	0.08	0.24	8.88	99.89	75.2	43.0	42.8	14.2
	0.23	1.47	0.03	0.05	0.08	1.28	0.38	2.0	3.1	1.1	2.0
2218/1210–3	52.46	21.32	0.54	0.15	0.23	11.19	100.84	68.1	43.8	38.2	18.0
	0.72	0.93	0.34	0.20	0.20	0.91	0.33	1.6	1.8	0.5	1.5
2218/1337	52.37	22.09	0.23	0.03	0.26	9.98	100.22	71.7	44.5	39.8	15.7
	0.06	0.21	0.07	0.01	0.04	0.43	0.42	0.8	0.8	0.7	0.5
2218/1434	52.09	10.15	0.13	0.04	0.44	19.17	98.54	54.4	23.6	41.6	34.8
2213/1110	52.39	20.31	0.58	0.09	0.23	9.44	100.99	74.9	40.9	44.3	14.8
	1.05	1.30	0.13	0.04	0.00	0.64	0.83	1.0	2.6	1.7	1.1

Subsolidus Reequilibration and Alteration

Crystallization from the melt was followed by extensive subsolidus recrystallization of plagioclase, clinopyroxene, and oxide minerals. Exsolution phenomena are optically resolvable in all of these phases. Exsolution of orthopyroxene from clinopyroxene occurs on an extremely fine scale, thus individual lamellae are rarely wide enough to distinguish colors under crossed nichols. Instead, lamellae show up as cleavage-like traces across the centers, but not the mantles, of many crystals.

Exsolution in plagioclases is compositionally dependent (e.g., Ribbe, 1975). In these samples, fine intertwining exsolution lamellae are evident optically in some orientations of plagioclase. The lamellae are orthogonal or strongly oblique to Carlsbad twin planes (Fig. 5A, -B). Some of the plagioclases are also kinked (Figs. 5B, 11B) and many of them have irregular extinction resulting from crystal deformation.

Oxide recrystallization in some samples is quite extreme, depending on the extent and intensity of metamorphic transformation of surrounding minerals to amphiboles. In strongly altered rocks, the oxides are now trellises and cross-trellises of various minerals (ilmenite, magnetite, hematite, rutile) produced during extensive oxidation exsolution (Fig. 6). In many cases, the magnetite has been partially removed by dissolution or reaction, leaving behind a more resistant grid of ilmenite lamellae.

Oxide recrystallization largely overlapped partial transformation of pyroxenes and olivine to amphiboles. Some of the amphibole appears to have formed from hydrous late-magmatic liquids (Gillis, this volume). There are no primary sulfides remaining in these gabbros, but secondary sulfides, usually associated with green amphiboles, abound. The site report in Gillis, Mével, Allan, et al. (1993) notes topotaxial transformation of oxides to titanate (sphene), and the presence of accessory zircon and apatite in gabbros from Core 147-894G-12R, about 80 mbsf.

One consequence of recrystallization is that, in most cases, there were changes in the chemical compositions of primary silicates as well as the oxide minerals. There were effects on both major oxides and trace elements. These effects, which are discussed further in a later section, are important when trying to reconstruct the compositions of melts from which the minerals, particularly the silicates, originally crystallized.

General Textural Attributes

Most textures in the gabbros result from crystallization along a plagioclase-clinopyroxene cotectic. Thus in thin section the rocks are dominated by intergrowths of these two minerals. That is, even though plagioclase crystallized first, and in particular samples may include some quite large and strongly zoned crystals, most specimens still consist predominantly of plagioclase-clinopyroxene intergrowths in various forms. The majority of rocks are either fine- to medium-grained and equigranular, or they have large, coarse clumps of plagioclase with finer grained intergrowths of plagioclase and pyroxenes in between (Fig. 7). A smaller percentage of rocks consist predominantly of coarse plagioclase and pyroxene, with rare intergranular oxide minerals large enough to be visible in hand specimen.

The most eye-catching form of plagioclase-pyroxene intergrowth in many samples is the oikocryst, up to 1 cm in longest dimension, wherein large domains of optically uniform clinopyroxene or orthopyroxene enclose small and tabular, as well as quite angular plagioclases. In olivine gabbronorites, clinopyroxene oikocrysts enclose rounded ovoids of olivine (Fig. 8A) and both tabular and angular,

Table 4. Hole 894G orthopyroxene compositions.

Core, section, interval (cm)	Pts.	Na_2O	MgO	Al_2O_3	SiO_2	CaO	TiO_2	Cr_2O_3	MnO	FeO	Total	Mg#	Wo	En	Fs
147-894G-															
Gabbronorite															
1R-1, 8–10	10	0.03	23.4	1.16	53.5	2.03	0.47	0.08	0.41	18.7	99.8	69.1	4.1	66.2	29.6
	sd	0.02	0.1	0.02	0.3	0.22	0.02	0.02	0.04	0.1	0.3	0.1	0.4	0.3	0.2
12R-4, 37–40	10	0.03	23.5	1.04	53.3	2.26	0.39	0.09	0.39	18.6	99.5	69.3	4.6	66.1	29.3
	sd	0.02	0.1	0.02	0.2	0.20	0.01	0.01	0.03	0.2	0.3	0.2	0.4	0.3	0.2
13R-3, 101–103	10	0.03	23.1	1.03	52.7	2.07	0.37	0.06	0.41	19.7	99.5	67.6	4.2	64.8	31.1
	sd	0.03	0.3	0.07	0.4	0.21	0.03	0.01	0.03	0.3	0.4	0.6	0.4	0.5	0.6
20R-3, 95–97	10	0.01	23.5	1.09	53.1	1.83	0.48	0.07	0.40	19.1	99.7	68.7	3.7	66.1	30.2
	sd	0.01	0.1	0.03	0.2	0.12	0.02	0.02	0.03	0.1	0.3	0.1	0.2	0.1	0.2
Olivine gabbronorite															
5R-1, 10–14	10	0.03	24.0	1.16	52.8	2.12	0.41	0.11	0.40	18.4	99.4	70.0	4.3	67.0	28.8
	sd	0.04	0.1	0.05	0.2	0.18	0.02	0.04	0.03	0.2	0.3	0.1	0.4	0.3	0.2
11R-3, 43–45	10	0.00	24.4	1.24	53.2	2.02	0.50	0.07	0.39	18.0	99.8	70.8	4.0	67.9	28.0
	sd	0.01	0.1	0.03	0.2	0.14	0.01	0.02	0.03	0.1	0.3	0.2	0.3	0.2	0.2
17R-2, 9–13	10	0.00	24.7	1.11	53.4	2.02	0.44	0.08	0.38	17.5	99.7	71.5	4.0	68.6	27.3
	sd	0.00	0.1	0.03	0.1	0.28	0.03	0.02	0.04	0.2	0.3	0.2	0.6	0.4	0.3
Olivine gabbro															
7R-1, 67–70	10	0.03	25.1	1.17	53.3	1.81	0.52	0.08	0.35	17.3	99.7	72.1	3.6	69.5	26.9
	sd	0.02	0.2	0.04	0.3	0.05	0.01	0.02	0.02	0.1	0.3	0.2	0.1	0.2	0.2

Notes: Abbreviations and column headings as in Tables 2 and 3. All analyses represent the average of 10 points along an approximately 100-µm traverse using a 10-µm traverse spot in the interior of each grain.

Table 5. Hole 894G olivine analyses.

Core, section, interval (cm)	Pc	Rock type	Pts.	MgO	Al_2O_3	SiO_2	CaO	TiO_2	Cr_2O_3	MnO	FeO	NiO	Total	Mg#
147-894G-														
2R-3, 101–103	13	Olivine gabbro	5	33.5	0.03	36.4	0.05	0.06	0.03	0.50	28.94	0.11	99.6	67.3
			sd	0.8	0.01	0.2	0.04	0.01	0.02	0.01	0.91	0.02	0.4	1.2
5R-1, 10–14	9	Olivine gabbronorite	5	31.1	0.03	36.3	0.07	0.07	0.07	0.54	32.18	0.10	100.5	63.3
			sd	0.7	0.01	0.3	0.04	0.02	0.01	0.05	0.81	0.01	0.3	1.1
6R-1, 26–28	4a	Olivine gabbronorite	4	24.4	1.02	52.5	2.02	0.40	0.04	0.49	18.93	0.04	99.8	69.6
			sd	0.0	0.03	0.1	0.09	0.03	0.02	0.03	0.15	0.00	0.2	0.2
7R-1, 67–70	12	Olivine gabbro	3	31.8	0.04	36.7	0.07	0.07	0.07	0.51	31.81	0.10	101.2	64.0
			sd	0.9	0.01	0.3	0.03	0.01	0.01	0.02	1.03	0.01	0.4	1.4
11R-3, 43–45	6	Olivine gabbronorite	3	31.8	0.05	36.6	0.29	0.07	0.08	0.51	31.30	0.09	100.8	64.4
			sd	0.4	0.03	0.2	0.53	0.01	0.02	0.04	0.40	0.01	0.4	0.2

Notes: Same as for Tables 2–4.

broken, or embayed crystals of plagioclase (Figs. 8A, 11B). Most oikocrysts are quite irregular in shape, as for example the one shown in Figure 9. In this sample, the plagioclase chadacrysts have a preferred orientation which also exists in the surrounding rock. The pattern of the oikocryst suggests the filling of an irregular crack, with plagioclases simultaneously growing inward from the walls of the crack. In some thin sections, oikocrysts are the most abundant form of clinopyroxene, but all samples contain at least a significant percentage of individual clinopyroxene crystals arrayed between and intergrown with plagioclases. Usually, but not always, plagioclases outside of oikocrysts are larger than the plagioclase chadacrysts within them, and they have less regular shapes.

Orthopyroxene also forms prominent oikocrysts, and is always an interstitial phase between portions of thin sections which have intergrowths of individual clinopyroxenes and plagioclases. In gabbronorites, orthopyroxene oikocrysts contain chadacrysts only of plagioclase, again usually smaller than in surrounding portions of the rocks. As in clinopyroxene oikocrysts, these feldspars may either be tabular and euhedral or angular and irregular, sometimes embayed (Fig. 8B). Both tabular and angular plagioclase chadacrysts can be zoned. Broken and zoned chadacrysts obviously do not represent plagioclase intergrowths. Instead, they are xenocrysts which were either broken from the sides of the cavities into which the oikocrysts grew (e.g., Figure 9), or they were carried in from some distance away.

In olivine gabbronorites, olivines touching or within orthopyroxene oikocrysts have irregular (not ovoidal) shapes. This suggests a reaction relationship, but the details of this are hard to see since much of the olivine and some of the orthopyroxene are invariably replaced by secondary amphibole at the grain contacts.

At the other end of the grain-size scale are very fine-grained equigranular mosaics of anhedral plagioclase and clinopyroxene. These typically occur as small patches or sectors in samples otherwise dominated by tabular or coarse plagioclases intergrown with equally coarse anhedral or oikocrystic pyroxenes (Fig. 10). In many respects the fine-grained intergrowths resemble neoblastic aggregates in some of the deformed and highly recrystallized gabbros of ODP Hole 735B (Robinson, Von Herzen, et al., 1989), but the phenomenon here occurs on an extremely local scale. In Figure 10C, partial recrystallization is responsible for the present grain shapes in the interior of the fine-grained patch, but some euhedral plagioclases are preserved at the margins. Thus the original aggregate was a fine-grained intergrowth of clinopyroxene with acicular plagioclases. Individual gabbros consisting of both coarse and fine-grained patches, and containing oikocrysts, thus experienced varying conditions of crystal nucleation and growth on the scale of a few centimeters or less.

One consequence of cotectic crystallization and evidently of crystal growth in small magma bodies, is that the proportion of plagioclase in the rocks is not highly variable. All but three of the 10 fine- to medium-grained samples we examined using image-analysis techniques have between 40% and 50% plagioclase (Table 1). The average plagioclase mode in these plus 13 additional samples point counted on board ship is 49.7 ± 7.7% (Gillis, Mével, Allan, et al., 1993).

Table 6. Ion microprobe trace element concentrations in clinopyroxenes, Sample 147-894G-9R-1, 75–79 cm.

Traverse ID		Wo	En	Fs	Ti	Cr	V	Sr	Y	Zr
Clinopyroxene 1 Traverse 1 Adjacent to Plagioclase 2										
Edge	44	40.1	46.3	13.5	3856	440	805	8.2	37.3	45.9
	45	37.3	49.2	13.5	3050	446	957	6.7	24.5	15.8
	46	33.0	53.3	13.7	5199	339	857	3.7	11.1	6.3
	47	40.9	46.5	12.6	5115	601	1882	12.6	23.9	13.8
	43	38.8	48.1	13.1	3768	425	1278	8.5	16.8	12.1
Center	48	41.4	46.8	11.8	3114	367	1043	8.2	15.6	10.8
	53	41.2	47.0	11.8	3562	397	715	9.3	18.2	14.2
	52	35.8	49.5	14.7	3555	402	743	8.9	18.0	16.7
	51	41.3	46.0	12.7	3485	398	817	8.5	20.1	20.9
	50	41.1	46.3	12.6	3461	398	816	8.5	22.5	25.0
Edge Adjacent to Plagioclase 3	49	40.6	46.2	13.2	3849	357	1013	7.1	26.8	45.9
Clinopyroxene 1 Traverse 2										
	59				2164	290	776	5.9	17.8	15.0
	58				3673	411	1326	8.9	22.8	20.4
	57				3142	394	1133	7.8	19.9	21.3
	56				3315	403	739	5.6	23.9	32.9
Edge Adjacent to Plagioclase 3	55				3505	420	792	6.3	24.6	43.4
Clinopyroxene 1 Traverse 3 (near Plagioclase 3)										
	60	40.5	46.5	13.1	3302	392	1142	8.2	26.8	36.7
	61	40.6	46.2	13.2	3306	399	1598	8.5	20.9	18.8
	62	40.9	46.1	13.0	3477	389	741	8.5	19.2	15.0
	63	41.3	46.2	12.5	3244	395	693	7.0	16.8	15.0
	64	37.5	48.5	14.0	3389	413	1489	9.3	17.1	8.3
Clinopyroxene 2										
	39				2540	168	343	1.5	4.7	—
	40				3040	250	409	2.6	5.5	—
	41				2873	438	778	7.8	37.0	—
	42				3428	397	919	6.7	29.1	47.1
Others (SIO electron probe)					TiO_2(%)		Cr_2O_3(%)			
	41)	41.2	45.4	13.4	0.68	—	0.17	—	—	—
	43)	40.6	45.8	13.6	0.62	—	0.18	—	—	—
	45)	43.0	45.2	11.8	0.41	—	0.11	—	—	—
	50)	43.0	44.2	12.8	0.46	—	0.02	—	—	—

Averages		Wo	En	Fs	Ti	V	Cr	Sr	Y	Zr
CPX-1	mean	39.5	47.4	13.1	3551	404	1017	7.9	21.5	22.5
(n = 21)	s.d	2.4	1.9	0.8	647	57	331	1.8	5.9	12.8
CPX-2	mean				2968	313	612	4.7	19.1	47.1
(n = 4)	s.d.				365	126	280	3.1	16.5	—
Others					TiO_2(%)		Cr_2O_3(%)			
(n = 4)	mean	42.0	45.1	12.9	0.54		0.12			
	s.d.	1.2	0.7	0.8	0.13		0.07			
All					TiO_2(%)		Cr_2O_3(%)			
(n = 5)	mean	41.5	45.6	12.9	0.51		0.12			
	s.d.	1.5	1.2	0.7	0.12		0.06			

Calculated concentrations in liquids

D's (Hart and Dunn, 1993)	Ti	V	Cr	Sr	Y	Zr
	0.384	3.1	3.8	0.1283	0.415	0.1234

Liquid compositions		Mg#	TiO_2(%)	V	Cr	Sr	Y	Zr
CPX-1	Max	46.4	1.86	194	495	98	90	372
	Min	40.9	0.77	61	188	29	27	51
	Average	43.2	1.16	130	267	62	52	182
CPX-2	Max	—	1.23	141	242	61	89	382
	Min	—	0.91	54	90	12	11	382
	Average	—	0.97	101	167	37	46	382
Others		42.1						
All		42.5						

Note: Except where stated, concentrations in parts per million.

Table 7. Ion-microprobe trace element concentrations in plagioclases, Sample 147-894G-9R-1, 75–79 cm.

	Traverse ID	An (mol%)	Mg	K	Ti	Fe	Sr
Plagioclase 1 Calcic core							
Near core rim	1	89.9	296	104	201	3845	168
	3	89.4	347	169	173	3769	168
	4	92.1	198	9	184	3484	172
	5	87.6	194	110	177	3462	163
	6	90.3	250	131	189	3715	172
	8	88.1	186	120	223	3747	186
	7	89.1	234	223	213	3880	177
	32	86.8	263	148	232	3934	190
	37	95.0	405	218	180	3836	163
Core center	38	91.3	186	45	180	3868	158
Zoned mantle							
Nearest core	9	82.5	575	234	257	3658	177
	10	74.8	367	267	156	3244	181
	11	70.5	446	381	187	3378	181
	12	65.9	461	532	229	3022	163
	13	62.9	257	346	287	2888	158
	14	67.2	621	494	281	3876	163
	15	65.8	481	288	278	3475	172
	16*	62.8	373	332	296	3271	158
	2*	61.1	256	245	335	3093	172
	30*	60.0	361	375	390	2248	172
Rim	31*	59.8	445	207	407	2247	186
Plagioclase 2							
	17	72.9	439	332	280	3707	177
	29	76.6	368	402	279	2968	190
	19	80.0	1130	760	260	4321	177
	18	72.6	504	424	300	3814	172
Rim	20*	64.8	413	261	281	3391	168
Plagioclase 3							
Rim	24*	61.1	268	242	345	3195	177
	25*	61.5	242	1990	239	2652	149
	26	72.6	350	315	281	3934	190
	27	73.1	434	305	305	3965	190
	21	70.3	318	418	309	3814	190
	22	69.0	434	375	308	3987	186
	23	66.3	504	435	302	3720	186
	54	69.2	488	261	296	3698	177
Plagioclase 4							
	33	67.8	509	207	300	3898	199
	34	68.6	263	216	314	3876	204
	35	65.7	323	250	315	2982	190
Averages							
Plagioclase 1 Calcic core	Mean	90.0	256	136	195	3754	172
	s.d.	2.4	74	56	21	162	10
Plagioclase 2	Mean	75.5	610	480	280	3702	179
	s.d.	3.5	351	191	16	558	8
Plagioclase 3	Mean	70.1	421	352	300	3853	187
	s.d.	2.5	74	69	10	127	5
Plagioclase 4	Mean	67.4	364	224	310	3585	198
	s.d.	1.5	127	23	8	127	7
Rims (*)	Mean	61.8	338	277	328	2871	169
	s.d.	1.7	84	63	60	485	12

Calculated concentrations in liquids

			Mg	K	Ti	Fe	Sr
D's (Meyer and Shibata, 1990)			0.03	0.15	0.028	0.05	1.32
	An (mol%)	Mg#	MgO(%)	K_2O (%)	TiO_2 (%)	FeO (%)	Sr
Plagioclase 1	90.0	23.4	1.42	0.11	0.87	9.66	130
Plagioclase 2	75.5	42.3	3.37	0.39	1.25	9.53	136
Plagioclase 3	70.1	32.8	2.33	0.28	1.34	9.91	142
Plagioclase 4	67.4	31.1	2.01	0.18	1.38	9.22	150
Rims	61.8	34.3	1.86	0.22	1.46	7.39	128

Notes: Except where stated, concentrations in parts per million.

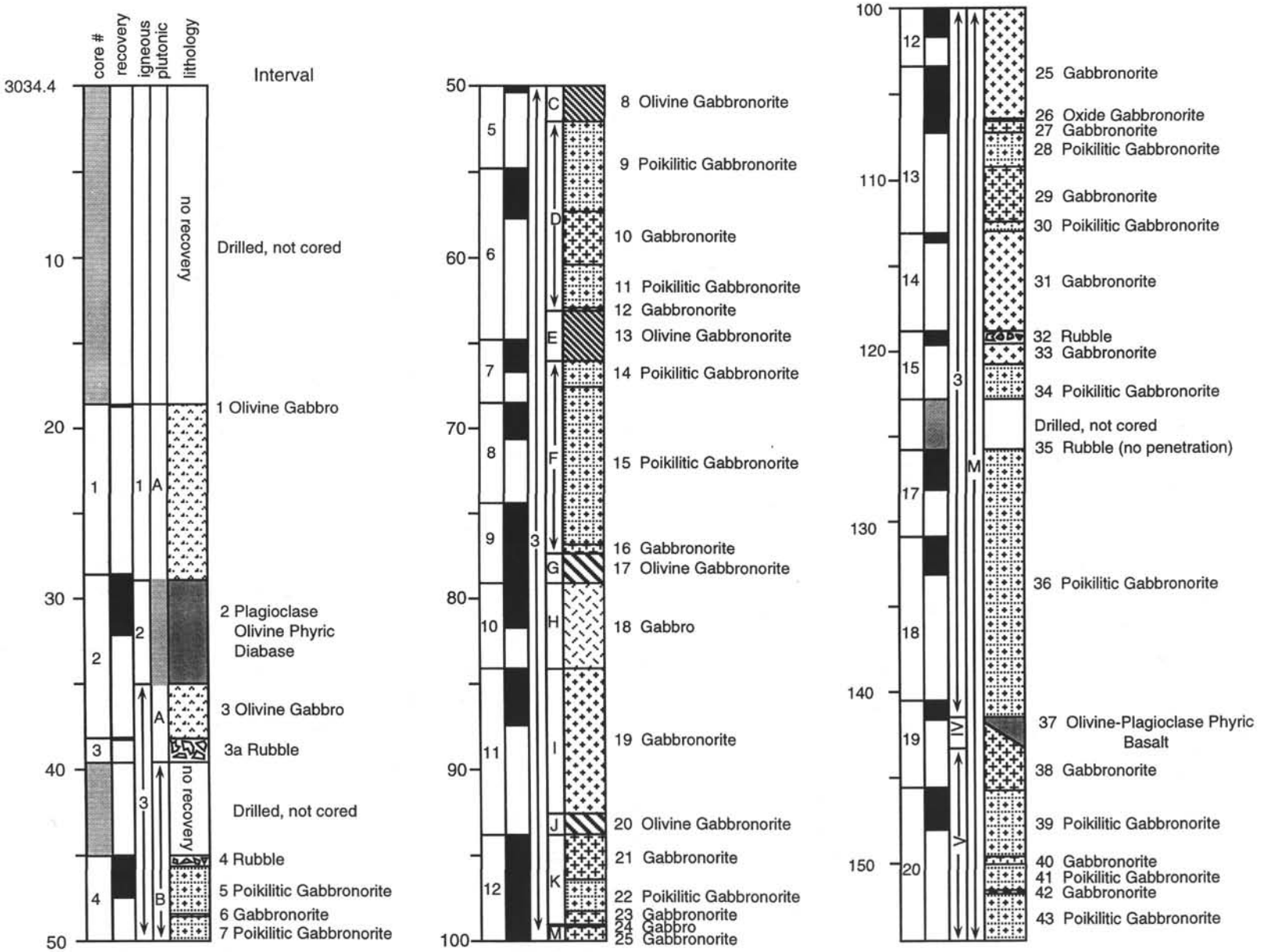

Figure 2. Hole 894G igneous lithostratigraphy. Columns give core recovery, major igneous units, and lithologic intervals, as defined in the text. There are five major igneous units. Three of them are gabbroic and are separated by two basaltic dikes. Within the gabbros there are 13 plutonic units (labelled A through M) representing mineralogical changes, which correspond to the units in the site report (Gillis, Mével, Allan, et al., 1993). There are 43 igneous intervals, two of them the basaltic dikes, and 41 of them gabbroic rocks. The latter are defined by both mineralogical and textural changes, as discussed in the text and Appendix. The intervals are graphically expanded to fill core recovery gaps according to their proportion in each core, except where no coring was attempted.

Figure 3. Photomicrograph in cross-polarized light of an igneous contact between fine-grained gabbro with preferred orientation of plagioclase and coarse-grained gabbronorite. Sample 147-894G-12R-2, Piece 9, 87–107 cm. The coarse-grained gabbronorite is about 2 cm wide. The preferred orientation at the bottom is oblique and cut by the gabbronorite. The contact at the bottom is sharper than the one at the top. Upcore is to the left.

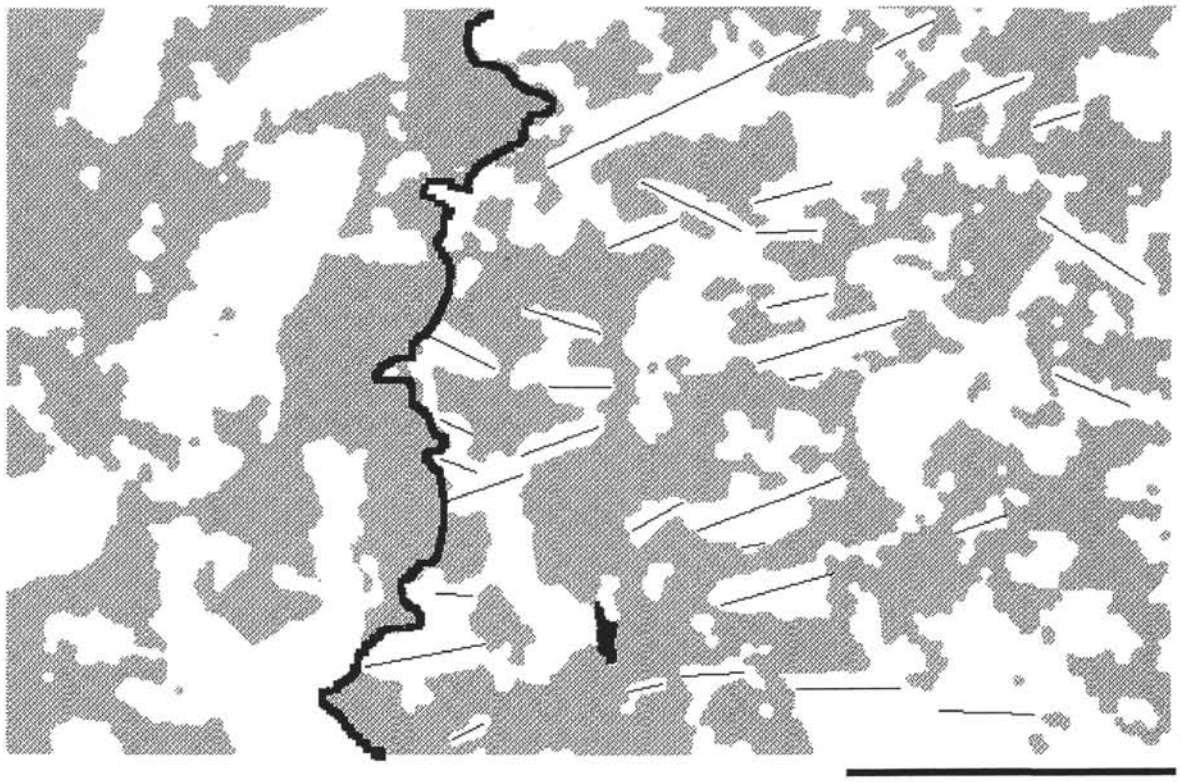

Figure 4. Image-analysis micrograph of Sample 147-894G-11R-3, 70–77 cm, showing an irregular contact (black line) between coarse- and medium-grained gabbronorite, the latter having preferred orientation of plagioclases (short narrow lines), subhorizontal in the orientation of the micrograph. White = plagioclase; gray = mafic silicates; small black patch = oxide minerals. The scale bar is 0.5 cm.

Higher proportions of plagioclase are found only among coarse-grained rocks (e.g., Sample 147-894G-13R-3, 101–103 cm, in Table 1) for which thin sections of standard size are rarely representative of the mode. Site 894 gabbronorites thus not only lack the primary rhythmic layering of classical cumulates, but crystal sorting under the influence either of gravity or flotation was not an important process.

Mineral Zoning

Many plagioclases are moderately to strongly normally zoned (Figs. 5, 11, 12). Most zoned plagioclases are large crystals in otherwise finer grained rocks (Figs. 5A, -B, 11A) but some are also tabular euhedra within or at the edges of clinopyroxene oikocrysts, as well as broken crystal fragments within them (Fig. 11B). Faint oscillatory zoning is preserved in the centers of many of these crystals. In cumulate theory, zoning of primocrysts is traditionally interpreted to result from post-cumulus crystallization of trapped melt (Wager et al., 1960). Thus among layered intrusions, a hallmark of adcumulates—rocks from which almost all intercumulus melt has been expelled—is the absence of strongly zoned minerals. Zoning of plagioclases in Site 894 rocks notwithstanding, there are other indications that they did not crystallize with substantial proportions of trapped melt.

Optically obvious zoning is rare in pyroxenes and there is none in olivines. Evidently plagioclases reacted far more sluggishly with intergranular melts than did ferromagnesian silicates. Incomplete reequilibration of plagioclases indicates that there was no prolonged contact with intergranular melts, either because of rapid crystallization, or because reduction of melt porosity proceeded sufficiently quickly that there was not enough intergranular melt to react entirely with surrounding crystals. Crystallization of these rocks did not necessarily trap much melt; instead, porosity reduction trapped zoned crystals before they could reequilibrate.

Grain Boundaries

A common attribute of intergrowths of plagioclase and pyroxenes is irregular, embayed, and interpenetrating grain boundaries (Fig. 12). Grain boundaries between plagioclases are of two types. Where one crystal penetrates the side of another orthogonally or highly obliquely, it often has curved terminations (Fig. 5A) or preserves protruding, partially faceted terminations (Fig. 12A). Where crystals are side-by-side, the crystals are not precisely parallel, with one crystal laid precisely against another (synneusis). Instead, the crystals are usually partially penetrate each other at slightly oblique angles. The long-axis grain boundaries tend to be slightly kinked, and their orientations are not parallel either to Carlsbad twin planes or the euhedral zoning patterns in the adjacent crystals. Where three plagioclases come together at odd angles, grain boundaries nevertheless curve to approximately 120° triple junctions (Figs. 5B and 12B, lower right). This is a characteristic of textural equilibrium which Hunter (1987) considers to be the culmination of a process of grain-boundary dissolution and reprecipitation in the development of adcumulates.

Intergrowths between plagioclase and clinopyroxene can be quite extraordinary, with deep embayments involving up to half of the grain widths, in a manner resembling the pieces of jigsaw puzzle. In Figure 12C, the original outlines of the large plagioclase crystal are still preserved where it is in contact with other plagioclases at the upper and lower left. The embayments with clinopyroxene cut deeply into the rest of the crystal. More precisely, the plagioclase and clinopyroxene are mutually embayed. This is aptly termed puzzle-piece texture (J. Dieu, pers. comm., 1994). Other contacts of plagioclase with clinopyroxene are curved and they sometimes cut across euhedral zoning patterns in the plagioclases (Fig. 12D). Indeed, both zoning and albite twinning are often truncated at such grain contacts.

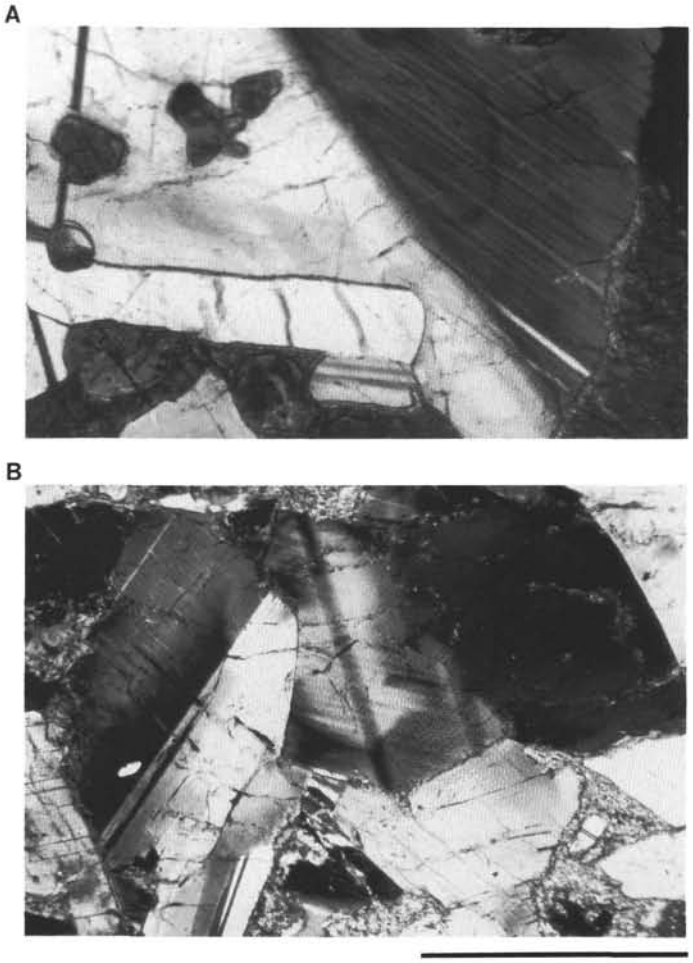

Figure 5. Photomicrographs in cross-polarized light, showing exsolution of normally zoned plagioclases. The scale bar is 1 mm. **A.** Sample 147-894G-2R-2, 83–86 cm, Piece 8. **B.** Sample 147-894G-6R-1, 0–3 cm, Piece 1.

In fact, all of these varieties of grain contacts suggest some extent of removal, or dissolution, of one crystal at the expense of another, or both at the expense of each other, and an approach to textural equilibrium. The plagioclases, in particular, are not euhedral primocrysts with post-cumulus overgrowths. Instead, they were originally euhedral crystals which have been partially, or extensively, eaten away. Hunter (1987) argues that dissolution of small crystals, and reprecipitation on the surfaces of adjacent larger crystals of the same mineral phase as they grow, is an important mechanism of porosity reduction during adcumulus growth. But this does not produce embayed crystals. The most usual and distinctive petrographic attribute of these rocks is embayed dissolution grain boundaries which are not obviously accompanied by overgrowths on adjacent crystals. Intergranular melt was not all that was removed from between these crystals; significant portions of the crystals themselves also disappeared.

If embayments in broken plagioclase chadacrysts were also produced by dissolution along grain boundaries, then the mineral grains originally in contact had to be separated (the puzzle-pieces were pulled apart), and the plagioclases transported to their present locations, before becoming surrounded by oikocrystic pyroxene. Despite the presence of interpenetrating embayments, the grain boundaries were weak, as they would be, for example, in the presence of a film of melt. The embayments in the chadacrysts are now filled with pyroxenes in optical continuity with the greater parts of surrounding oikocrysts. That such pyroxene did not itself produce the embayments is evident, since the oikocrysts surround a greater number of broken and zoned euhedral plagioclases without having produced embayments in them.

Figure 6. Reflected light photomicrograph of magnetite with ilmenite exsolution lamellae; Sample 147-894G-2R-4, 16–19 cm, Piece 3. The oxide intergrowth is 1.1 mm wide. Some of the magnetite has been eaten away during hydrothermal alteration.

Preferred Orientation of Plagioclases

In a number of samples, plagioclases define a weak to moderate preferred orientation. This was termed magmatic foliation in the site report (Gillis, Mével, Allan, et al., 1993), but since the rocks are not really foliated, and the origin of the texture is uncertain, we prefer the simply descriptive "preferred orientation." Where the direction of this can be reconstructed, it is more nearly vertical than anything else, thus does not constitute gravitational layering. In the example of Figure 3, some of the current preferred orientation can be attributed to a ductile deformation which accompanied a nearly vertical injection of magma which crystallized to coarse grain size. In several other thin sections of ours, preferred orientation of plagioclases exists in patches, as if crystallization domains were often chaotically broken, mixed, and annealed on quite a small scale (Fig. 4). In some samples there are even quasi-xenolithic clumps of rock with completely different mineral proportions than their surroundings (Fig. 13). Thus there is no evidence that preferred orientation results from gravity-driven cumulus processes, and only rarely is it produced by varieties of crescumulate growth (Fig. 9). Instead the rocks appear to be an amalgam of crystallization domains, somewhat coherent on the scale of lithologic units, but ofttimes quite chaotic on the scale of individual samples and thin sections. The simplest interpretation is that most preferred orientation resulted from stretching of pre-existent crystal mush, or from continued crystal growth in a semi-rigid matrix undergoing deformation under some (but not all) of the prevailing stress conditions. As those varied spatially or in time, and generally as the deformable mass was repeatedly intruded, the rocks were disrupted, and fine-scale channelized flow of melt was changed. All of this caused complex textural and grain-size variations on the scale of centimeters.

Distribution of Oxide Minerals

Oxide minerals in Site 894 gabbros are always interstitial, and most rocks have very low modal proportions (Table 1). That is, whole sectors of many thin sections lack oxide minerals altogether, and ilmenite or ilmenite-magnetite intergrowths are both rare and scattered (Fig. 14A). The sectors without oxide minerals are always characterized by the various types of dissolution grain boundaries between pla-

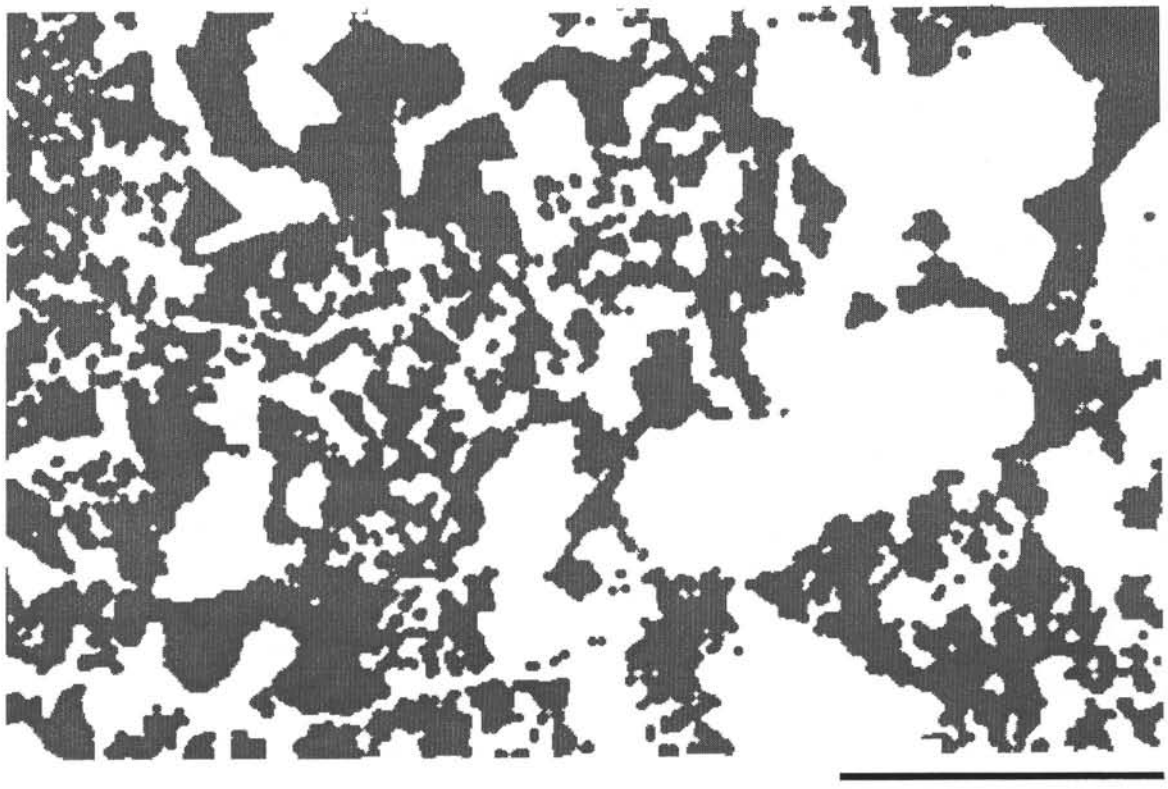

Figure 7. Image-analysis micrograph of gabbronorite with coarse- and fine-grained crystallization domains. Sample 147-894G-4R-2, 27–30 cm. White = plagioclase. Gray = ferromagnesian silicates. The scale bar is 0.5 cm.

gioclases and pyroxenes described above, and an approach to textural equilibrium. In those samples in which oxide proportions approach or exceed 1%, one still sees entire sectors of thin sections without oxides, and with dissolution grain boundaries between silicate minerals. But in concentrated local patches, the oxide minerals occur along silicate grain boundaries, and may nearly surround individual plagioclase euhedra (Fig. 14B, -C). We term these "wrap-around" oxides.

The very low modal proportions of oxide minerals in many of these rocks are a critical indication that a low percentage of trapped melt crystallized within the rocks (Wager et al., 1960). If an original aggregate of closely packed, yet uncompacted cumulus minerals on the floor of a magma chamber contains about 50% of melt between crystals (Jackson, 1961), and if all of that melt was basaltic and crystallized in situ, the resulting cumulates should contain about half of the proportion of oxide minerals that would normally crystallize from the basalt. If the residual melt porosity is quite low, however, say 10%, then the cumulate will have only 10% of the percentage of oxide minerals latent in the basaltic liquid. Given that typical holocrystalline ferrobasalts may crystallize 2%–3% of oxides, then modal proportions of oxides of only a few tenths of a per cent suggest that residual melt was quite efficiently expelled from many Site 894 gabbronorites. Below, we explore these estimates more quantitatively. However, this contradicts the indication from zoned plagioclases in the same samples that there was substantial "post-cumulus" crystallization from trapped melt. Nevertheless, it is in accord with the inference from extensive grain boundary dissolution between silicate mineral grains, and indications of textural equilibrium, that intercrystalline melt was effectively removed from most of these rocks.

What of the samples with more abundant oxides? In samples with 1% or more of modal oxides, ilmenite and magnetite still occur in patches between whole sectors of the thin sections without oxides. These sectors have all the features of grain dissolution described above. Thus melt expulsion was actually as efficient in those parts of the rocks as in entire rocks almost wholly lacking oxides. Oxide minerals are thus an indication of *where* small quantities of melt may have remained trapped in individual specimens. They provide a picture of the final, or nearly final, porosity structure of the rock, at the point just prior to its final freezing. They also indicate that melt which may still have been mobile within that porosity structure was extremely fractionated, to the extent that ilmenite and magnetite were on the liquidus. As intimated by Wager et al. (1960) in their discussion of post-cumulus crystallization, gabbro cumulates may carry a substantial history of crystallization differentiation, even if the proportions of late-crystallizing oxides within them are extremely low.

Figure 15 is an image-analysis micrograph of a full thin section including the one thin oxide gabbronorite recovered from Hole 894G (lithologic interval 26 of Fig. 2). The oxide minerals (black) were selected by image analysis to contrast with all the silicate minerals combined (gray). Most of the section is virtually devoid of oxide minerals. In the oxide gabbronorite (lower third of the micrograph), which has a similar grain size, oxide minerals compose 8.7% of the rock, and show a distinct oblique preferred orientation parallel to the inclination of a basal fracture. Several plagioclases in the interval and just adjacent to it, which are not shown, also have a similar preferred orientation. The diagonal base of the micrograph represents the true maximum inclination of the fracture, since the thin section slab was cut orthogonal to the fracture surface at the base of an oriented piece of core.

Overall, the section suggests that a concentration of shear stresses acted to produce a faint preferred (oblique) orientation of pre-existing silicate minerals in a nearly crystalline gabbronorite. The shear concentration enhanced the dilatancy of the same zone of rock, allowing it to collect highly fractionated iron-rich intercumulus melts from surrounding partially molten rock, and perhaps elsewhere, from which the oxide minerals precipitated. The pattern of oxide minerals thus effectively provides a map of late-stage intergranular porous

flow in these rocks, now frozen in place. The flow was concentrated by shear into a narrow channel perhaps already about 90% crystalline. This is now the oxide gabbronorite.

THE NORTH SLOPE

Briefly, the North Slope gabbroic rocks sampled by submersible differ from those of Site 894 in the following ways. First, there are no olivine gabbros or olivine gabbronorites among the dive samples. A trace amount of olivine occurs in only one sample. Second, there are both fine-grained and coarse-grained oxide-gabbronorites and ferrodiorites from the two dives which extended deepest into the gabbros. These occur as pods or pockets in a matrix of gabbronorite which is virtually oxide free. Modal oxide proportions in the oxide gabbronorites and ferrogabbros range from nearly 4% to more than 12% (Table 1). Finally, there are several narrow dikelets, or veins, of quartz-bearing felsic material, and a variety of quartzose patches and intergrowths. One of the dikelets was sufficient for a chemical analysis. The fairly calcic composition is that of a tonalite, one of the variants of the plagiogranite suite defined for ophiolites by Coleman and Peterman (1975).

A photograph of the sawn surface of the rock cut by this veinlet is shown in Figure 16. Based on dive notes of observer Peter Lonsdale (pers. comm., 1990), the long dimension of the rock is the way it was sampled from the outcrop, although it may be inverted here. The outcrop tilt of the specimen is also uncertain. With the specimen held precisely vertically, the tonalite dikelet is horizontal, as is the contact between a coarse oxide ferrogabbro and the fine-grained oxide gabbronorite at the bottom of the specimen.

There is yet a third medium-grained gabbro at the top of the sample in the photo, the contact of which is cut by the tonalite. This one sample thus provides a fragile indication that magma injection at the very top of the gabbros, at the level of the melt lens, is horizontal, or nearly so, and is a contrast to the high-angle crosscutting relationships observed at Site 894.

Figure 17 shows oxide-mineral distributions in some of the more fractionated North Slope samples. In one thin section, from the sample just described (Fig. 17A), oxides are concentrated in small patches in modal proportions up to about 10%, but the patches are so scattered that the overall oxide mode is only about 1%. The oxides are associated with a coarse anastomosing patch of strongly zoned sodic plagioclase which is intergrown with quartz. This may represent an irregular offshoot of the tonalite dikelet which was only a few centimeters away. The oxides, and green amphiboles next to them, partially enclose euhedral crystals of apatite. The sodic plagioclase ($\sim An_{21}$) actually abruptly mantles a pre-existing intermediate plagioclase (An_{48}). The mantles of sodic feldspar, too, enclose euhedral apatite.

Two liquids may have been involved in the crystallization of this rock. One of them clearly was tonalitic (rhyodacitic). The other was extremely iron rich, and precipitated both apatite and oxide minerals, perhaps also amphibole. We speculate that the two liquids, which were so intimately associated in space, separated immiscibly from an iron-rich ferroandesite (e.g., Dixon and Rutherford, 1979), although we have not yet explored this by trace-element study of all the associated minerals. On the same dive track and quite nearby, a fine-grained ferroandesite dike, which is appropriately iron-rich, intrudes these same gabbros. It has 18% iron as Fe_2O_3 (Nilsson, 1993).

The tonalite dikelet in the rock shown in Figure 16 is one of several recovered in both cumulates (whether oxide gabbros or gabbronorites) and coarse diabases across the gabbro-dike transition. In addition, some oxide-poor gabbronorite adcumulates have rare, tiny patches of quartz immediately adjacent to oxide minerals. These must have resulted from very late-stage intergranular flow of high-silica melts. Even the diabases at the very base of the dikes are sufficiently coarse-grained to have distinctive quartz-oligoclase myrmekitic intergrowths, despite the rocks having the bulk compositions of

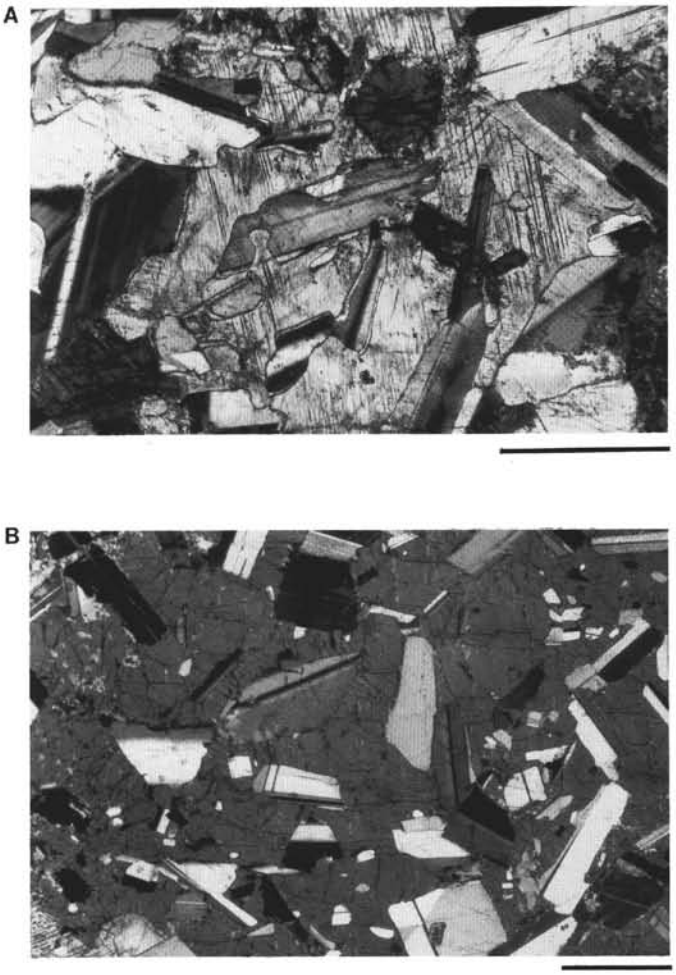

Figure 8. Photomicrographs in cross-polarized light of pyroxene oikocrysts enclosing angular or embayed broken plagioclase chadacrysts, as well as tabular euhedra. The scale bars are 1 mm. **A.** Sample 147-894G-9R-4, 84–88 cm, Piece 7, olivine gabbronorite. The oikocryst is clinopyroxene. The gray, rounded crystal at top center is olivine. **B.** North Slope Sample 2213-1152, gabbronorite. The oikocryst is orthopyroxene. Note that many of the chadacrysts appear to be completely suspended in the oikocryst, and the grain sizes are quite variable.

basalts and ferrobasalts (Natland et al., 1991). These various occurrences of quartzose patches, small tonalite dikelets, and quartz-plagioclase myrmekitic intergrowths are distinctive features of the North Slope rocks, and have no counterparts at Site 894.

Figure 18 is another image-analysis micrograph contrasting the distribution of oxide minerals with silicates in a North Slope gabbronorite. The sample contains 3.27% modal oxide minerals rather evenly distributed throughout the rock overall, but in detail being concentrated in numerous irregular patches. Some of the patches enclose, or nearly enclose, small islets of intergrown euhedral silicate minerals, mainly plagioclase. They are all "wrap-around" oxides, as previously described. But there are several portions of the rock, measuring about ½ × 1 cm, without oxide minerals at all. From these portions of rock, intercumulus melt has been almost completely expelled, producing what are effectively very small-scale adcumulates. The concentrated patches of oxide minerals tell us where that melt must have gone. They are a map of the porosity structure of the nearly crystalline rock after oxide minerals began to crystallize. In three dimensions, the oxide patches might be linked in complex ways, to de-

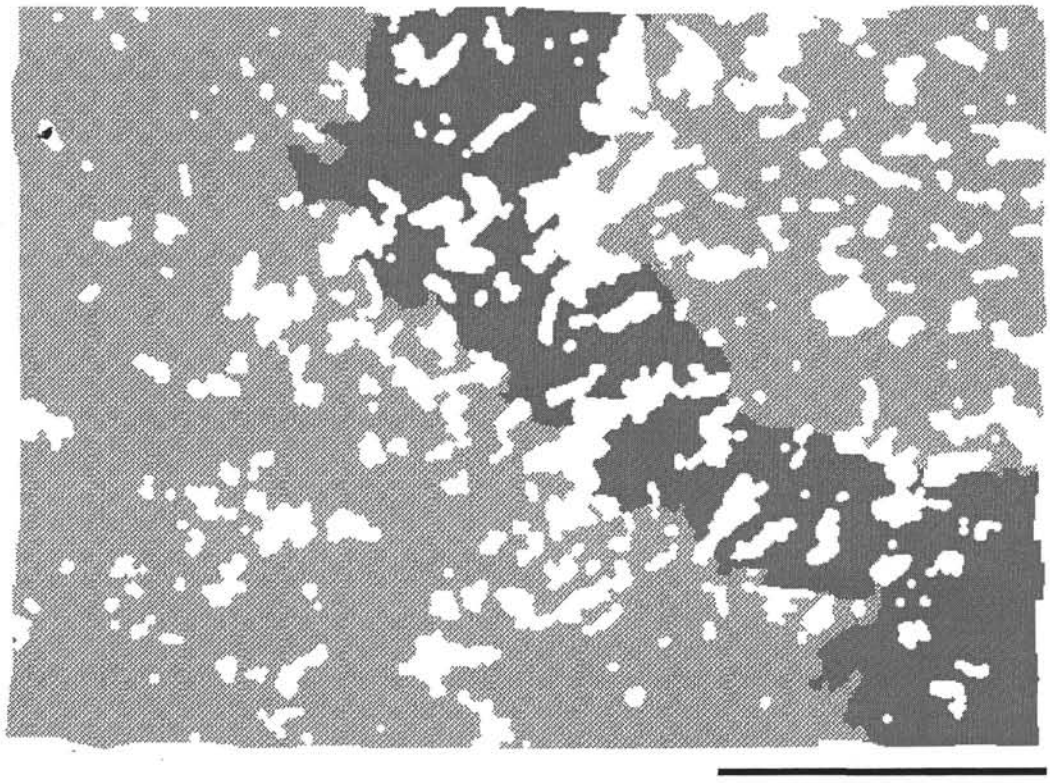

Figure 9. Image-analysis micrograph of a large, irregular clinopyroxene oikocryst in gabbronorite. Sample 147-894G-12R-3, 60–64 cm. The oikocryst is black, plagioclases are white, and ferromagnesian silicates are gray. The scale bar is 0.5 cm.

fine a network of centimeter-scale channelized porous flow of late stage melts through this rock.

Finally, Figure 19 is a photomicrograph of a narrow pyroxenite veinlet in another North Slope oxide gabbronorite. The rock is a cumulate screen within, but near the base of, the sheeted dikes. The host rock (Sample 2213-1351) is very fine grained, nearly equigranular, and contains 5.65% oxide minerals (Table 1). The veinlet is one of three crossing the section, two of which are subparallel, being 0.3 and 0.7 mm wide, respectively. A third, 1.0 mm wide, obliquely intersects the larger of the two subparallel veinlets. The principal mineral in the veinlets is orthopyroxene, with about 10% clinopyroxene and 2–3% plagioclase. Oxides are nearly absent in the veinlets, in contrast to their abundance in the host rock. Orthopyroxenes in the veinlets have the same composition as those in the host rock (hypersthene with Mg/[Mg + Fe] = 0.592–0.607).

The veinlets are clearly crack fillings, and the minerals in them apparently crystallized from interstitial melts derived from the host rock which infiltrated the veinlets as the cracks widened. The situation perhaps was similar to the process which produced the crack-filling pyroxene oikocryst in the gabbronorite sample from Site 894 shown in Figure 11, except that here, at the very top of the gabbros, high cooling rates allowed only small minerals to form. Nonetheless, on the very tiny scale of the veinlets, there are no minerals precipitated from "trapped" liquids. They are the closest approach to monomineralic crystallization among any of the samples we have studied.

In a composite crustal stratigraphy, the North Slope rocks, which were literally sampled just below the base of sheeted dikes, would have to be placed slightly higher than the rocks of Site 894. Of course one might imagine that the distribution of oxide-rich, tonalite-veined gabbroic rocks such as those from the North Slope is simply a local phenomenon, and that the two locations might occupy the same structural level, with only one containing the oxide-rich and quartz-bearing rocks. But the North Slope oxide gabbronorites, ferrodiorites, and tonalites clearly represent an extension of the processes which are evident mainly on the scale of thin sections at Site 894. The local pooling, or concentration, of fractionated liquids which precipitated wrap-around oxides in small patches in gabbronorites at Site 894, led either laterally or vertically to a larger scale of pooling and concentration of highly fractionated liquids, and still further fractionation, to produce high-silica differentiates, at the North Slope.

QUANTITATIVE ESTIMATES OF RESIDUAL MELT POROSITY

The percentages of trapped melt which crystallize in cumulates have been estimated both petrographically and using bulk compositions of rocks. Petrographic approaches utilize modes, and have their basis in classical cumulate theory. It is absolutely required that primocrysts be distinguishable from post-cumulus overgrowths, and this has to be done on the basis of mineral zoning (Wager et al., 1960). Such estimates may be imprecise, since zoning is not as readily apparent on, say, pyroxenes, as it is on plagioclases. Modal estimates are usually most useful for cumulates with a fair percentage (more than 10%) of material which crystallized from trapped melt.

Gabbroic rocks from Hess Deep are not good candidates for modal estimates of residual melt porosity based on mineral zoning. They are texturally complex and many are fairly fine-grained, or contain fine-grained sectors; what should be termed a primocryst is uncertain. Many zoned plagioclases themselves are effectively xenocrysts trapped in unzoned pyroxenes, including oikocrysts. Grain-boundary dissolution has been extensive. Some intergrowths of plagioclase with clinopyroxene may result from recrystallization. The rocks have experienced extensive greenschist facies alteration. We provide two means of estimating residual melt porosities in such rocks, one based on geochemistry, the other on percentages of oxide minerals.

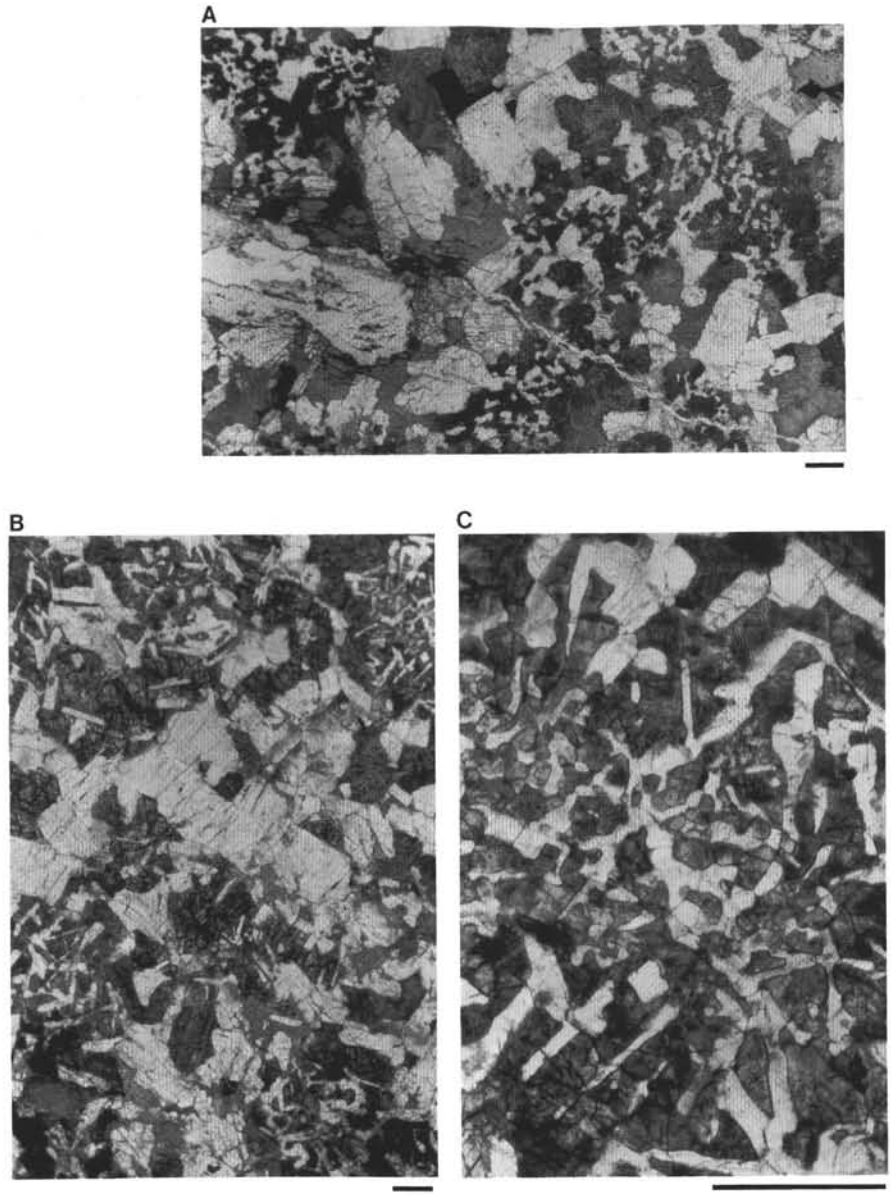

Figure 10. Plagioclase-pyroxene intergrowths in plane-polarized light. Gabbronorites with coarse- and fine-grained crystallization domains. The scale bars = 1 mm. **A.** Sample 147-894G-4R-2, 27–30 cm. **B, C.** Sample 147-894G-6R-1, 0–3 cm, Piece 1. (C) is a blow-up of the fine-grained patch at the upper right in (B). The mosaic-like intergrowth in the center of the patch probably recrystallized from a texture originally more like that at the margins of the photograph.

The geochemical procedure is from Natland et al. (1991), who proposed a geochemical definition for adcumulates. The procedure is based on the approach of Wager (1963) who showed that the concentration of a highly incompatible element (e.g., phosphorus) in a cumulate is nearly ideally proportional to the percentage of material which crystallized from trapped melt. For very low residual melt porosities, the incompatible element has to be measured to high precision. Natland et al. (1991) used Zr, since it usually can be measured by XRF procedures to three significant figures. But Zr does not have as low a bulk partition coefficient (K_D) as phosphorus, because of its tendency to partition moderately (D = 0.123; Hart and Dunn, 1993) into clinopyroxene.

The general procedure, which can be visualized using Figure 20, is to consider that gabbroic clinopyroxene, which takes in some Zr, is simply diluted in a perfect adcumulate (residual melt porosity = 0) by plagioclase, olivine, and possibly orthopyroxene, for which Ds for Zr are very low. Almost all Zr in such a rock is thus tied up in the clinopyroxene.

Therefore, the bulk Zr content of a cumulate is, for all practical purposes, divided between that in clinopyroxene and that which crystallized from trapped intercumulus melt. If we know the composition of the liquid which produced the cumulate, and can determine the extent of clinopyroxene dilution, we can first calculate what Zr should be in the ideal adcumulate, and assign the remainder to the portion of the rock which crystallized from trapped melt. That remainder, divided by the amount estimated for the liquid, gives the *maximum* fractional melt porosity. If the liquid finally trapped was actually more fractionated than that which produced the bulk of the pyroxenes in the rock (for example, by displacement of some or all of the original intercrystalline liquid), then the actual residual melt porosity is less than calculated here. This is probably the case for these samples.

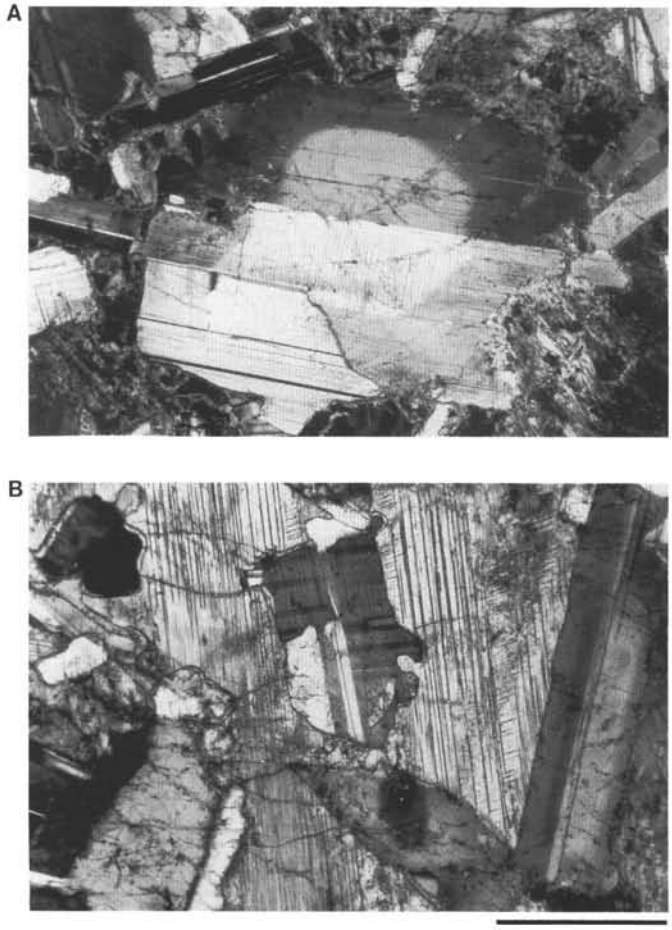

Figure 11. Strongly zoned plagioclases in cross-polarized light. Sample 147-894G-9R-4, 84–88 cm, Piece #7. The scale bar is 1 mm. **A.** Plagioclase with a highly calcic core, analyzed as Plagioclase 1 in Table 7. **B.** Plagioclases at the edge and in the center of an oikocryst. The zoned plagioclase at the right is Plagioclase 2 of Table 7. Ion probe traverse 1 of clinopyroxene was between this crystal and the irregular crystal with the embayment in the center of the photomicrograph (Plagioclase 3). Note the kinking in this plagioclase.

To estimate the liquid compositions, one needs the Mg# (= Mg/(Mg + Fe^{2+}) of the bulk rock (assumed to a first approximation to be equal to that of the most abundant mafic silicate in the rock, clinopyroxene), and knowledge of the covariation of Zr and TiO_2 with Mg# of glasses or aphyric basalts dredged or drilled from the vicinity. These data are available for Hess Deep (Nilsson, 1993). Basalt compositions were also used to estimate compositions of trapped melts in dredged gabbros from the Southwest Indian Ridge (Meyer et al., 1989).

Figure 21 shows estimated percentage residual melt porosities, calculated in this fashion, plotted vs. depth for Hole 894G, using shipboard X-ray fluorescence data from the site report (Gillis, Mével, Allan, et al., 1993). Irvine (1982) defines adcumulates as having residual melt porosities of 7% or less. Rocks with more than this are termed mesocumulates. On this basis, most of the rocks analyzed from Hole 894G are indeed adcumulates. The average estimated residual melt porosity for 21 samples is 4.4%. Only four samples are not adcumulates, and five samples have less than 2% of material which crystallized from tapped residual melt.

Individual estimates of residual melt porosity are given for North Slope samples listed in Table 1, calculated from values of Mg#, TiO_2 content, and Zr concentrations. The maximum Zr concentrations of adcumulates are 44 ppm; maximum TiO_2 contents are 0.88%. The most ideal bulk adcumulate (Sample 2218-1057) has 10 ppm Zr and 0.39% TiO_2, slightly more than the average contents in clinopyroxene diluted by about 50% plagioclase, as estimated earlier.

The second procedure for estimation of residual melt porosities is petrographic, but also depends to an extent on the bulk compositions of the rocks. If the liquids which produced a given gabbroic rock were generally basaltic, and did not have oxide minerals on the liquidus, then the percentage of oxide minerals in a cumulate is a measure only of the proportion of liquid which was trapped in the rock when it froze. The lower the mode of oxides, the lower the percentage of that trapped melt. But this is dependent on composition.

Figure 22 shows that there is a significant correlation between the percentage of oxides in fine- to medium-grained aphyric abyssal tholeiites of the East Pacific Rise from the vicinity of Hess Deep, measured by image-analysis procedures, and their TiO_2 contents. The TiO_2 contents correlate with iron enrichment, and decreasing Mg#. The coincidental relationship between modal oxides and TiO_2 contents is surprisingly convenient. With each percentage of TiO_2 contents, there is almost the same percentage of oxides in the mode. The maximum TiO_2 contents among the basalts is about 3%, in a ferrobasalt with Mg# ≈ 0.4. This is approximately the average composition of liquids which produced the gabbroic rocks of Hole 894G (see below). On this basis, any of those rocks with modal oxides of about 0.21% or less should be an adcumulate with <7% residual melt porosity. However, this assumes that all of the oxides crystallized from trapped melt, and none before.

Texturally, wrap-around oxides do not appear to have coprecipitated with a greater abundance of silicate minerals from grain-boundary pockets of trapped melt. Melt was still being expelled from the rocks while those oxides precipitated. By comparing modal and geochemical estimates for North Slope samples, we estimate that a safe petrographic criterion for identification of a gabbronorite adcumulate from Hess Deep is an oxide modal proportion of 0.3% or less. Each tenth of a percent of oxides represents slightly more than 2% residual melt porosity. On this basis, 9 of the 17 samples we examined from Hole 894G (Table 1) are adcumulates, with an average oxide mode of 0.15 ± 0.07% (approximately 3.5% trapped residual melt). Another 7 of the 13 samples from the North Slope listed in Table 1 are adcumulates, with an average oxide mode of 0.21 ± 0.7% (approximately 5% trapped residual melt).

Higher oxide percentages do not preclude a rock from being an adcumulate. North Slope Sample 2213-1053 has 2.03% modal oxides, and 1.28% TiO_2 contents, but only 31 ppm Zr. In this rock, oxide precipitation preceded the last stages of reduction of melt porosity. Ilmenite and magnetite are mainly wrap-around oxides occurring in concentrated patches (Fig. 19A). The simple petrographic criterion of 0.3% oxides thus is a conservative means of identifying adcumulates. It recovers about two-thirds of the number of adcumulates identified by geochemistry.

Figure 23 shows a summary sketch of the outcrop distribution of residual melt porosity for the North Slope dive samples. The vertical axis is water depth, the horizontal axis is in meters relative to transponder reference used to navigate the dives. Gabbro cumulates are all samples below "gabbros of basaltic composition" which in fact are the coarse-grained base of the dike complex. These rocks have the compositions of aphyric basalts, not cumulates. The diagram is derived from the geochemical definition of adcumulates, based on basaltic compositions of dikes and pillows sampled from other North Slope exposures located upslope (Nilsson, 1993). The diagram is intended to show that there are pockets of gabbro just below the dikes which crystallized with >20% trapped melt, but within a matrix of gabbronorite mesocumulates having considerably lower residual melt porosity. Adcumulates with <7% residual melt porosity occur from 200 m to 500 m below the coarse-grained base of the dikes. These gabbronorites are the rocks most comparable to those of Site 894.

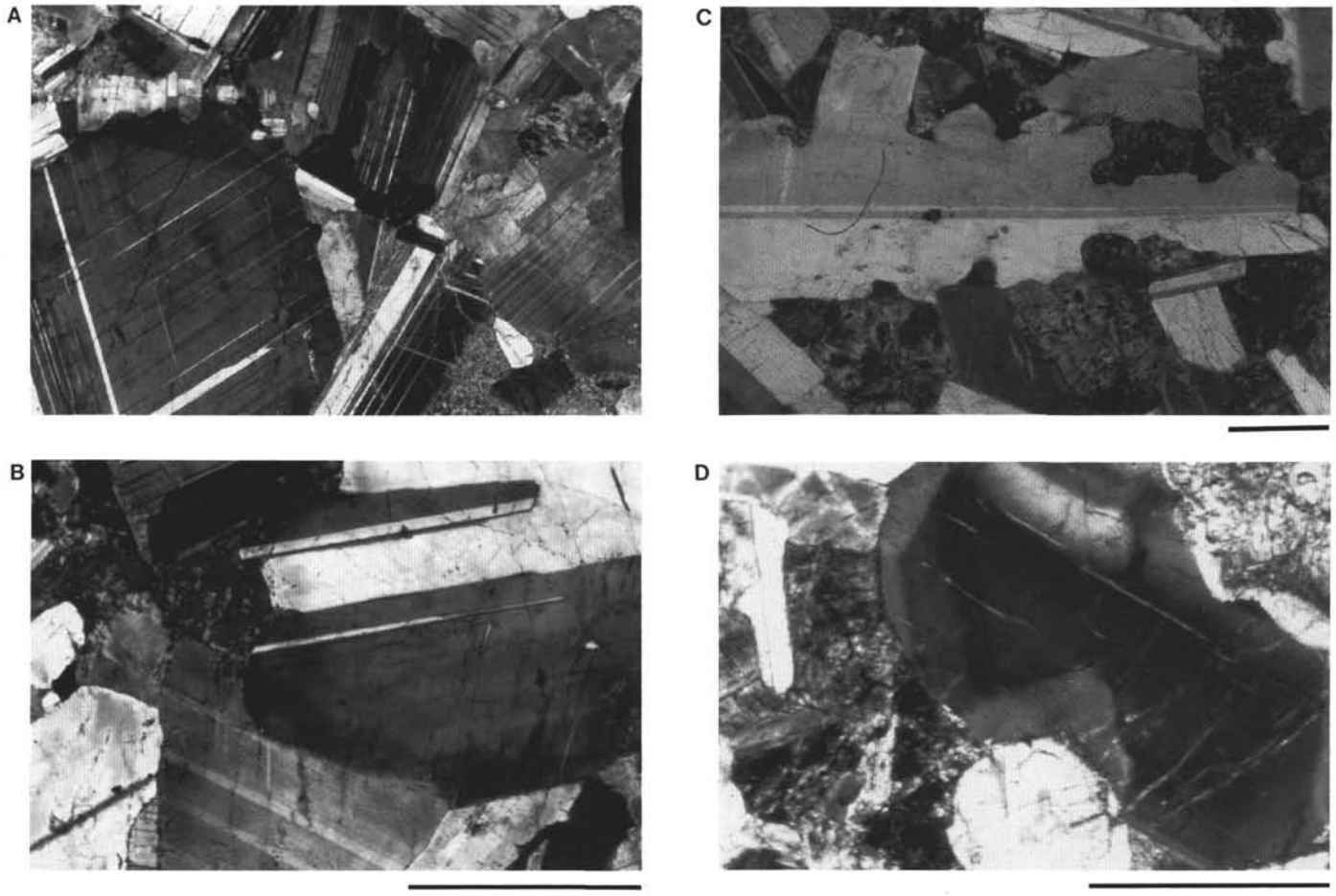

Figure 12. Photomicrographs in cross-polarized light showing grain-boundary relationships between plagioclases and pyroxenes. **A, B.** Sample 147-894G-16WS, 136–144 cm, Piece 7. In (A), plagioclases protrude into each other at various orientations. In (B), a portion of the zoned outer mantle of the large crystal at the upper right has been removed. The boundary between it and the crystal on the lower left twists to meet a 120° triple junction where three crystals join at the lower right. **C.** Sample 147-894G-8R–2, 83–86 cm, Piece 8. The plagioclase is highly embayed where in contact with clinopyroxene (some of it replaced by amphibole). Where in contact with plagioclases, edges are straight (top left) and faceted (lower left). **D.** Sample 147-894G-6R-1, 0–3 cm, Piece 1. A strongly zoned plagioclase with a section of the outer mantle and a portion of the inner core removed by grain-boundary dissolution in contact with an altered clinopyroxene, at center left. All scale bars are 1 mm. The one below (B) applies to both (A) and (B).

MINERAL COMPOSITIONS

Compositions of olivine and clinopyroxene from samples of Hole 894G are very similar with depth in average compositions, and in the limited range found for each sample (e.g., Fig. 24). The overall average by sample of olivine composition is an iron-rich $Fo_{65.3 \pm 2.6}$.

Pyroxenes experienced extensive subsolidus reequilibration. The temperature grid of Lindsley and Andersen (1983) superimposed on the pyroxene quadrilateral (Fig. 25) suggests that clinopyroxenes were particularly susceptible. Those from both Site 894 and the North Slope show a broad band of reequilibration temperatures, from about 1000° to 650°C. The effect is obviously primarily in the Wo component, with Mg# being little changed. Thus despite reequilibration, both pyroxenes are confined to narrow and similar ranges in Mg# at both Site 894 and the North Slope. The average Mg# by sample of orthopyroxenes is 69.9 ± 1.5 and of clinopyroxenes it is 74.1 ± 2.4. These are substantially iron-rich compositions, and indicate crystallization from highly fractionated liquids. This is considered in more detail in the following section.

Plagioclase shows nothing like the same consistency (Fig. 26). The strong plagioclase zoning observed in thin section results from a substantial range in compositions in most samples ($An_{76–55}$) and a remarkable range ($An_{95–60}$) in the one olivine gabbronorite selected for detailed study. The most calcic composition (An_{95}) was determined by ion microprobe within the dark core of the large plagioclase shown in Figure 9A. The core has an average composition of An_{90}, and the mantle of the grain grades to a rim of $An_{59.8}$.

Two plagioclases enclosed in a nearby clinopyroxene oikocryst (plagioclases 2 and 3, identified in the caption of Fig. 11B) have different most-calcic core compositions ($An_{80.0}$ and $An_{73.2}$, respectively). These occur in a rock in which the average plagioclase rim composition, including very narrow rims on the two grains within the oikocryst, is $An_{61.8}$. The disparate core compositions support the interpretation that the two grains, one of them tabular, the other angular and embayed, are transported xenocrysts now trapped within the oikocryst. Individual plagioclases more calcic than An_{80} were found in two other samples by Dr. Kathryn Gillis (Table 2) in connection with her alteration studies.

The fairly common labradorite-bytownite cores to zoned plagioclases in gabbroic rocks of Site 894 must have precipitated from only moderately fractionated basaltic liquids not very different from average eruptives at the East Pacific Rise. Those liquids either reached this

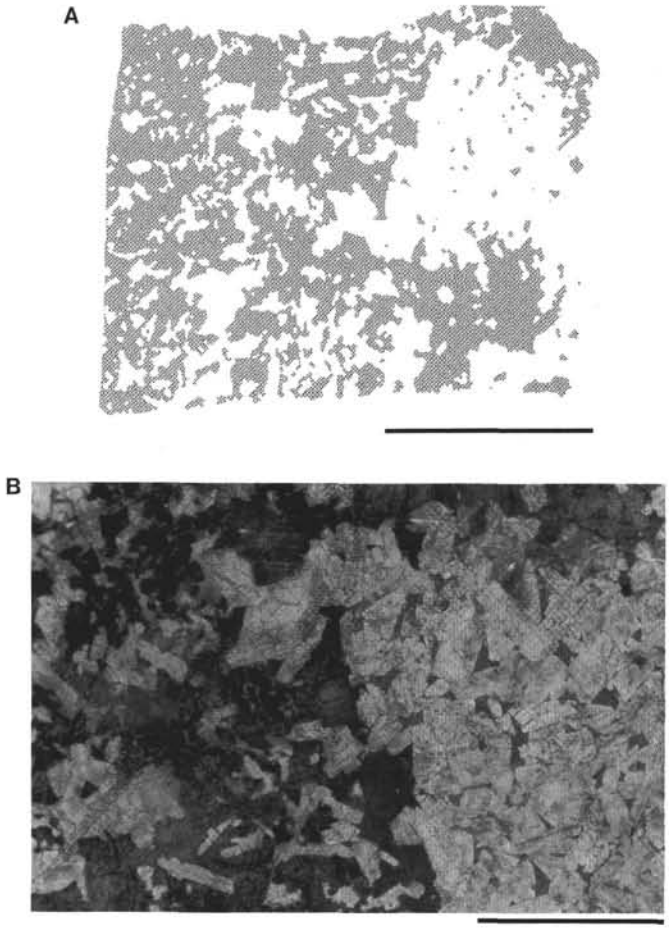

Figure 13. Two views of an anorthositic xenolith in gabbronorite. Sample 147-894G-14R-1, 35–40 cm. The scale bars are 0.5 cm. **A.** Image-analysis micrograph showing the distribution of plagioclase (white) and ferromagnesian silicates (gray). **B.** Photomicrograph in plane-polarized light. The cloudiness in the plagioclases results from alteration. The mafic minerals in the plagioclase clot are secondary amphiboles.

level in the crust, or the mineral cores are all fundamentally xenocrysts which were transported to their present location from somewhere else. Since moderately fractionated basalts commonly erupt at the East Pacific Rise, there is no reason why some of them should not precipitate minerals all the way to the top of the gabbros, and that is our preferred interpretation. Subsequently these rocks were penetrated by substantial quantities of much more fractionated melt, and an original matrix of fairly primitive minerals was made over into gabbronorite. Whatever olivines and pyroxenes originally may have precipitated are now almost entirely transformed, but not the plagioclases.

The identification of anorthite zoned to andesine in an olivine gabbronorite presents quite another problem. Plagioclases as calcic as An_{88-95} do not represent the compositions of minerals that can precipitate on the liquidus of any known erupted primitive abyssal tholeiite (Fisk, 1984). The most calcic plagioclase phenocrysts we know of in any basalt from the vicinity of the East Pacific Rise is $An_{90.5}$, and these crystals enclose unusually refractory basaltic melt inclusions which have no eruptive counterparts (Natland, 1989). However, even more calcic plagioclases evidently do form in reaction zones between primitive mafic liquids and refractory abyssal peridotites, and a number of such rocks were cored during Leg 147 in the mantle transition at Site 895 (Dick and Natland, this volume).

The overlap in calcic plagioclase compositions between Sites 894 and 895 is shown in histograms in Figure 27. The occurrence of such plagioclases at or just beneath crustal levels postulated for a magma lens shows that refractory crystals which more than likely originated at the top of the mantle can survive transport, presumably in quite primitive liquids, through the entire gabbroic layer. Reequilibration of olivine and clinopyroxene, but not plagioclase, is also observed in abyssal gabbros from the Southwest Indian Ridge (Meyer et al., 1989). Transport and preservation of xenocrystic calcic plagioclase in crustal gabbros was suggested by those authors and by Meyer and Shibata (1990).

A number of authors have noted that basalts of the East Pacific Rise, which typically are moderately to strongly fractionated, are usually almost entirely aphyric (e.g., Morel and Hekinian, 1980; Bryan, 1983), in contrast to more primitive, often plagioclase-phyric, basalts from fracture zones such as Siqueiros (Natland and Melson, 1980; Natland, 1989), and most basalts from slowly spreading ridges. The lost phenocrysts have now been found, tied up in high-level gabbronorites which precipitated at or just beneath the melt lens once present at this location on the East Pacific Rise.

The histograms of Figure 27 also provide a comparison to the North Slope. This simply shows that plagioclases in gabbronorites there are no different from the typical intermediate plagioclases at Site 894. Oxide gabbronorites, ferrodiorites and the one tonalite contain more sodic plagioclase. Data for clinopyroxene-plagioclase pairs again show the fundamental resemblance of gabbronorites, with the contrast at the North Slope of one more sodic, less magnesian outlier, an oxide gabbronorite (Fig. 26).

Figure 28 also shows the wide range of plagioclase compositions that coexist in samples from Site 894 and the North Slope with only a limited range of clinopyroxene compositions. As discussed earlier, the more calcic plagioclases are relics which crystallized from primitive liquids, some of them of the type which produced gabbros and troctolites in the mantle transition drilled nearby at Site 895. This is indicated by the horizontal arrows in Figure 28. The gabbroic rocks of Site 894 thus are hybrids resulting from incomplete reequilibration between crystals precipitated from primitive, high-temperature melts and highly fractionated, cooler melts which were introduced later during episodes of channelized porous flow.

In contrast, gabbros from slowly spreading ridges (ODP Hole 735B, Southwest Indian Ridge; Cayman Trough), have more limited ranges in plagioclase composition in association with given clinopyroxenes, thus more ideally represent a crystal-fractionation line of descent. Since many eruptive basalts at slowly spreading ridges, including those in the Indian Ocean (Natland, 1991a), are strongly porphyritic, some "xenocrystic" minerals, shed along the path of transport, should initially be present throughout the gabbroic crustal column. But such minerals are not present in the rocks of Hole 735B. The restricted fractionation trend for Hole 735B gabbros in Figure 28 thus probably is the result of nearly complete reequilibration of those rocks during their history of crystallization and development into adcumulates. That process was carried more nearly to completion than at Hess Deep, resulting, for example, in an average residual melt porosity for 300-m of olivine gabbros of only 1.4% (calculated for 30 chemical analyses in the site report; Robinson, Von Herzen, et al., 1989). It was probably strongly assisted by the marked deformation which resulted in the occurrence of porphyroclastic to gneissic rocks in more than 40% of the cored section (Natland et al., 1991).

ESTIMATED LIQUID COMPOSITIONS

One objective of mineral studies on gabbros is to be able to relate crystalline phase compositions to those of the liquids which produced them. This can become difficult if the rocks have experienced extensive subsolidus reequilibration, as these rocks have. An assumption

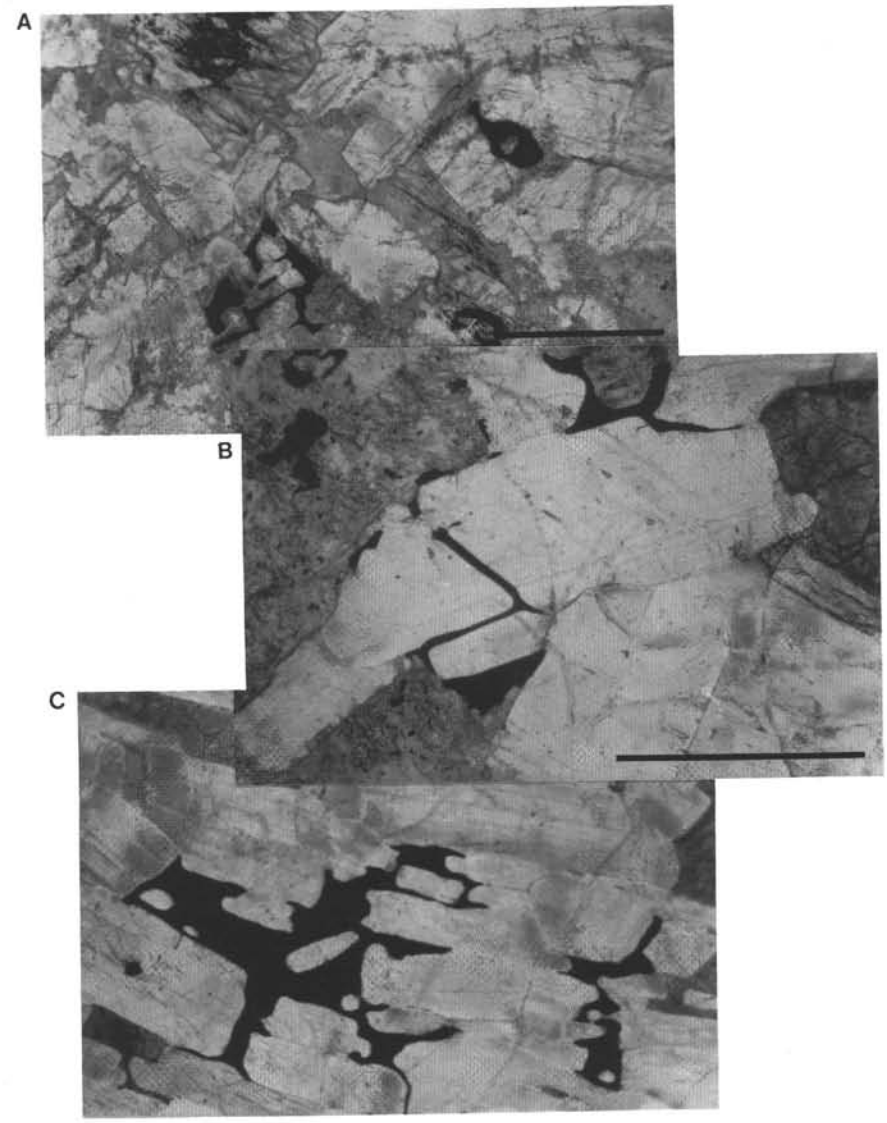

Figure 14. Photomicrographs in plane-polarized light showing oxide-mineral distributions. Scale bars = 1 mm. **A.** Sample 147-894G-9R-4, 84–88 cm, Piece 7. The three irregular oxides represent most of the total oxides found in the mode of the entire thin section of this sample. **B.** Sample 147-894G-9R-1, 110–114 cm, Piece 10. Wrap-around oxides filling interstices between plagioclase crystals. **C.** Sample 147-894G-12R-2, 25–27 cm, Piece 4. A coarse patch of oxides completely filling intergranular spaces between side-plated plagioclases with preferred orientation. Note the 120° triple junction where three plagioclases join.

of the procedure for evaluating residual melt porosity using bulk-rock compositions is that the Mg#s are nearly the same as those of average clinopyroxenes, the most abundant ferromagnesian silicate in the rocks. A first test of this is to compare liquid Mg#s estimated from minerals and bulk-rock compositions.

Table 8 lists the Mg#s of average clinopyroxene and olivines in the samples we have studied from Hole 894G and the North Slope. Estimated liquid Mg#s, calculated by the procedures of Duke (1976), as slightly modified by Natland et al. (1991), are also listed by sample, and the averages and standard deviations over all samples are given at the bottoms of the columns. The overall results for clinopyroxenes and olivines are extremely consistent. The liquid from which those minerals crystallized had an average Mg# of 36, as estimated using both clinopyroxenes and olivines. This is a modest victory for the consistency of the procedures to recover liquid Mg#s from the compositions of different minerals. The most magnesian liquid that can be inferred from the composition of any average mineral had a Mg# of 41.6. From any individual mineral analysis, the most magnesian liquid had Mg# = 46.4. This is the composition of a strongly fractionated ferrobasalt. Even for the East Pacific Rise, this is an uncommon eruptive (Sinton and Detrick, 1992). The average composition of Site 894 gabbroic rocks crystallized from liquids which only very rarely erupt at this fast-spreading ridge.

Bulk rock analyses, which are influenced in the average by the presence of both oxide minerals and secondary amphibole, indicate an even more iron-rich parental liquid for Site 894 gabbroic rocks, with an average Mg# = 31.5. Use of bulk analyses therefore tends to underestimate residual melt porosities slightly compared with bulk mineral analyses, because it overestimates liquid Zr and TiO_2 contents, assuming that both increase with fractionation in basaltic liquids. If oxides have already joined the liquidus, however, then liquid TiO_2 contents will be overestimated, and the extent of dilution of clinopyroxene with other silicate minerals will be underestimated.

This appears to be the case with these rocks. Figure 29 compares inferred liquid Mg#s and TiO_2 contents for sample averages of Site 894 and North Slope clinopyroxenes (Ti partition coefficient = 0.384; Hart and Dunn, 1993) with those of basalts and ferroandesites from the East Pacific Rise (Nilsson, 1993, and J. Natland, unpubl. data).

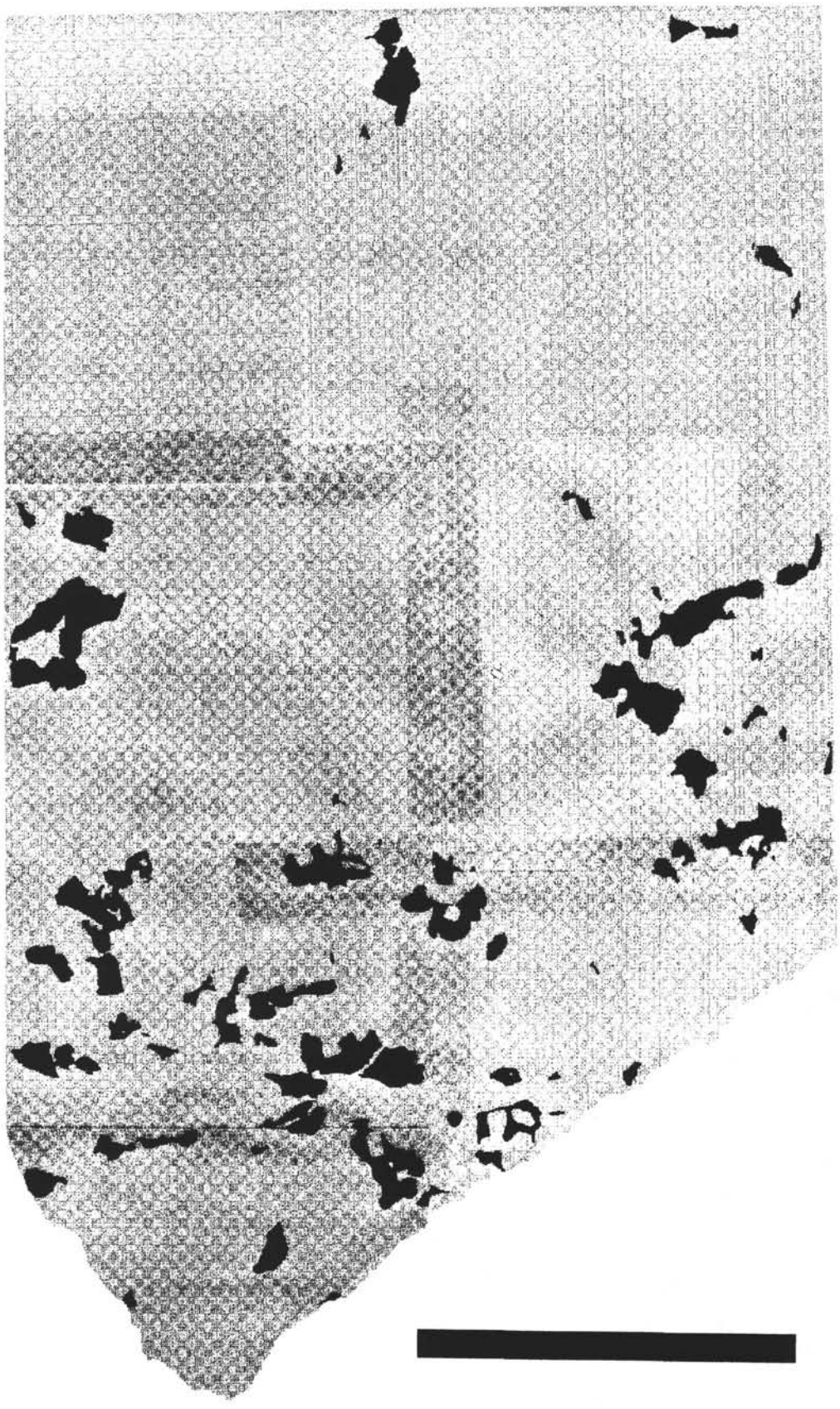

Figure 15. Image-analysis micrograph showing the distribution of oxides (black) and silicates (gray) in a full thin section of Sample 147-894G-13R-1, 132–136 cm. The obliquely trending zone in the lower third of the micrograph is an oxide gabbronorite (lithologic interval 26 of Fig. 2). The section is oriented to correspond with its orientation in the core (top is up). The scale bar is 1 cm.

Those rocks have a maximum TiO_2 contents of 3.19% at Mg# = 43.5. The corresponding sample is a fine-grained ilmenite-bearing ferrobasalt. Less magnesian lava compositions are ferroandesites and andesites with high SiO_2 contents (54%–60%). The low Mg#s and TiO_2 contents of liquids inferred for Site 894 and North Slope clinopyroxenes thus show a trend compatible with crystallization from successively more fractionated, and less titanian, high-SiO_2 liquids.

These comparisons indicate that the earliest detectable crystallization of ferromagnesian silicates (not plagioclases) in gabbroic rocks at Site 894 began from ferrobasaltic liquids. Those liquids soon reached a peak in contents of iron and titania, whence oxides joined the liquidus, reducing liquid contents of both these oxides, and increasing silica. The rocks probably originally contained more magnesian pyroxenes and presumably olivines, based on the calcic compositions of cores to many plagioclase crystals. But there are no relics of these ferromagnesian silicates remaining in the rocks.

More complete evaluation of liquid compositions, including estimates based on trace-element measurements of individual minerals (Table 6) is problematic. Estimates of liquid concentrations of Ti, V, Cr, Sr, Y, and Zr for clinopyroxenes of given Mg#, based on partition coefficients of Hart and Dunn (1993), bear little resemblance to actual ferroandesitic and andesitic lavas which have been dredged from this vicinity, or the North Slope tonalite, sampled by submersible. The pyroxenes are strongly enriched in Cr, have about the right levels of V, and are increasingly depleted in Zr, Y, and Sr, relative to natural lavas of appropriate Mg#. The best that can be said is that, apart from the high Cr, the average pyroxenes appear to have crystallized from lavas more like ferroandesites than ferrobasalts. That is, both V and TiO_2 contents are low enough, and Y and Zr concentrations high enough, that the pyroxenes do not look as though they crystallized from a simple basaltic liquid.

One complication is that Zr and Y are strongly concentrated precisely at edges adjoining plagioclases of all three traverses of the clinopyroxene oikocrysts examined. But there is no corresponding zoning of V, Cr, Sr, TiO_2, or Mg# (Table 6). This distribution may have to do with diffusion processes acting at the boundaries of grains which crystallized in very confined spaces, but it is clear that there is no simple way to reconstruct liquid compositions for all these elements based on clinopyroxene compositions.

The high Cr contents of the clinopyroxenes are consistent with the high Cr contents of bulk-rock analyses of Site 894 gabbroic rocks (average 329 ± 175 ppm) which are also quite variable (maximum 714 ppm; minimum 67 ppm), as given in the site report (Gillis, Mével, Allan, et al., 1993). If the rocks consist roughly of 50% clinopyroxene, then their average Cr contents are roughly 650 ppm, with a maximum of 1400 ppm and a minimum of 130 ppm. These specify average Cr contents of about 170 ppm for the melts which produced the average bulk clinopyroxenes from Site 894, with a maximum concentration greater than 350 ppm and a minimum of about 35 ppm. Only the latter value is similar to the low Cr contents of the highly fractionated ferroandesitic liquids which set the Mg#s of the pyroxenes in the rocks. The higher values are those of much more primitive basaltic liquids.

There seems little choice but to presume that many of the rocks, but not all, once contained far more magnesian, and Cr-rich, clinopyroxenes than they now do. These were the ferromagnesian counterparts of the calcic cores to zoned plagioclases. Perhaps the rocks also contained Cr-spinels. But the clinopyroxenes, at least, have been almost completely made over, transformed, into the minerals now in the rocks by reaction with fractionated liquids. The present clinopyroxenes contain high concentrations of what can be termed cryptic Cr, their one distinctive sign of an initial stage of crystallization from primitive liquids.

Average trace and minor element compositions of plagioclases in the one sample studied in detail (Table 7) are similarly complicated. Plagioclase phenocrysts in a fairly primitive abyssal tholeiite from the Mid-Atlantic Ridge gave results that are reasonably consistent

Figure 16. Photograph of the sawn surface of tonalite-veined oxide-rich gabbronorite, North Slope Sample 2218-1210. The scale bar is 5 cm. Note the variations in grain size across the rock. Rock just above the contact with coarse gabbroic material at the bottom is oxide-rich (12% oxides in the mode; Table 1).

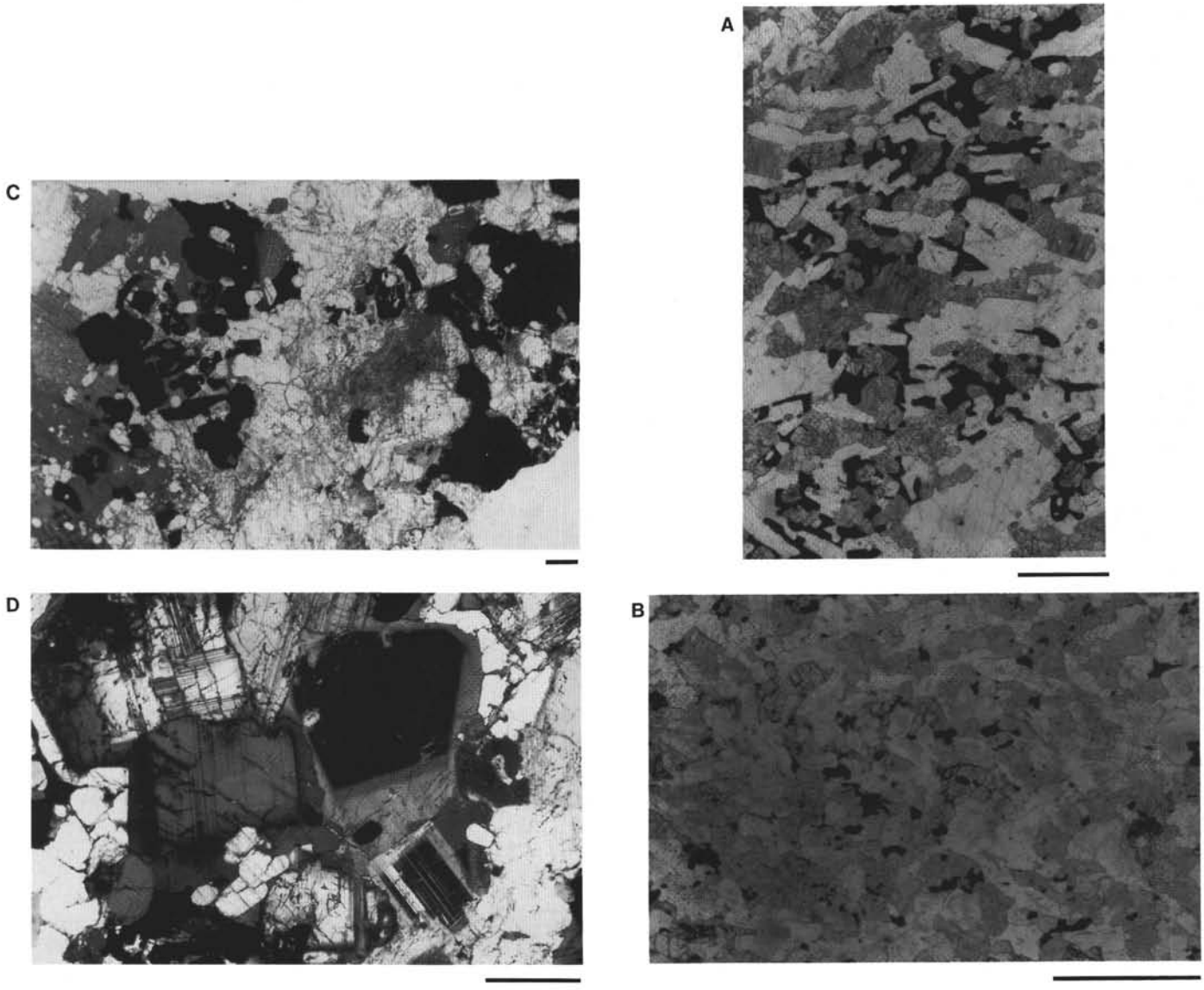

Figure 17. Photomicrographs showing aspects of oxide-bearing gabbroic rocks from the North Slope of Hess Deep. The scale bars are 1 mm. **A.** North Slope Sample 2213-1053. Plane-polarized light. A portion of an oxide-rich patch. Wrap-around oxides fill interstices between plagioclases and clinopyroxenes. The plagioclases show a preferred orientation, arbitrarily placed horizontally in this photomicrograph. **B.** North Slope Sample 2218-1221. Plane-polarized light. Fine-grained gabbronorite with uniformly distributed oxides, some of them with euhedral grain boundaries, others irregularly filling intergranular space. The mineral with high relief is orthopyroxene. **C, D.** North Slope Sample 2218-1210, oxide-rich portion of the rock. (C), in plane-polarized light, shows euhedral to skeletal oxide minerals associated with dark green amphibole to the left and right, separated by an irregular felsic patch. The clear subhedral crystals in oxides and amphibole on the left are apatite. The overexposed patch on the lower right is quartz. (D), in cross-polarized light, shows abrupt mantles of unzoned sodic plagioclase surrounding large zoned plagioclases. Oxides occur at bottom left, with rounded crystals of apatite just above them, and partly enclosed in the sodic plagioclase.

with published partition coefficients (Meyer and Shibata, 1990). However, the plagioclases in this sample have considerably less MgO than the natural liquids which can have produced them, their Mg#s are too low for their range of An contents (anorthite to sodic labradorite), and their K_2O and TiO_2 contents are too low for their Mg#s.

Concentrations of these elements and oxides appear to have been reset to proportions consistent with the highly fractionated liquids which produced the immediately surrounding pyroxenes (Fig. 23), but their levels were almost certainly influenced by subsolidus re-equilibration. However, none of the few pyroxenes or plagioclases studied in detail in the one sample are fully representative of the range of mineral compositions observed in all the rocks.

DISCUSSION

We may now stand back to view the portrait. Here we summarize the manner in which the rocks crystallized, and consider how their melt porosity was so efficiently reduced.

An obvious comment is that the portrait is not complete. Various complex processes have been established, but—as the last section suggests—their geochemical consequences are not fully understood, let alone adequately documented. Precise inferences about liquid lines of descent may not be possible to reconstruct using extensively recrystallized minerals. Comparisons to relevant highly fractionated natural compositions suffer from the rarity of appropriate eruptive rocks, and uncertainty about the conditions (especially oxygen fugac-

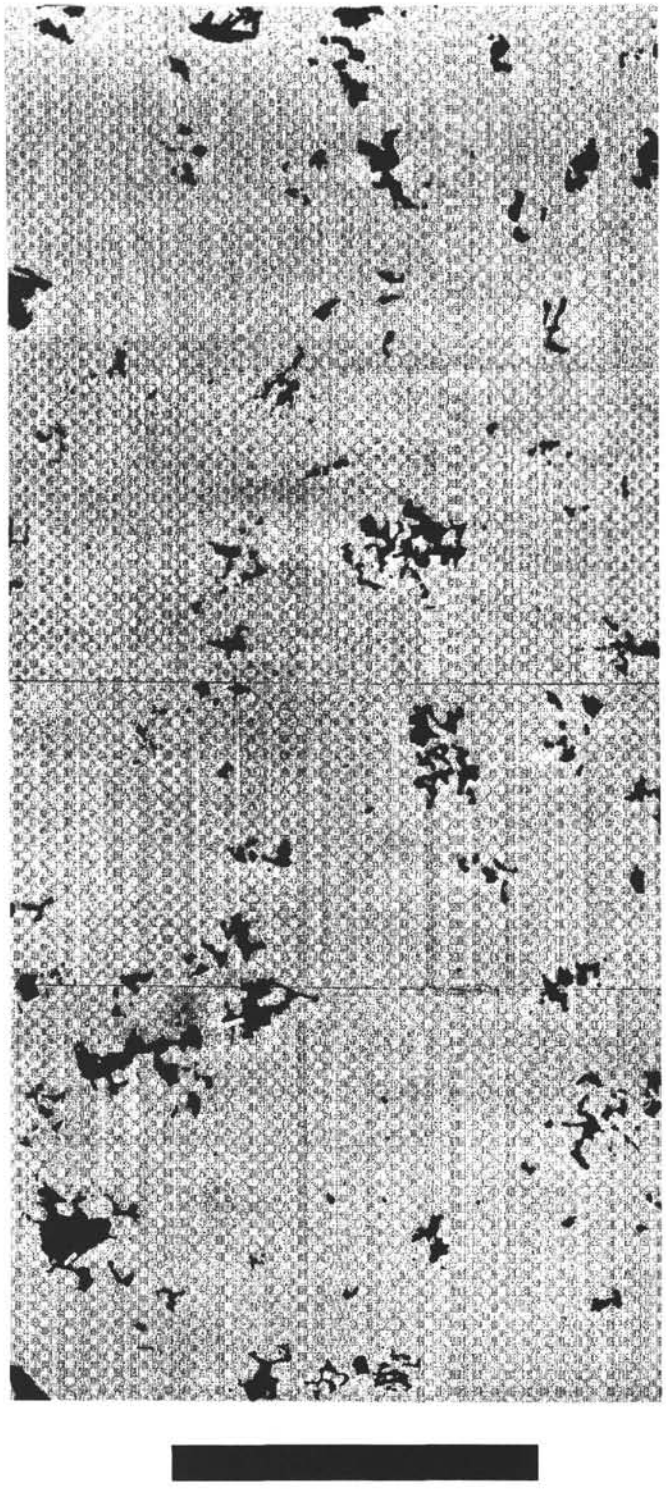

Figure 18. Image-analysis micrograph of a full thin section of North Slope Sample 2218-1308, showing the distribution of oxide minerals (black) vs. all silicate minerals (gray). Scale bar is 1 cm.

ities) and petrogenetic processes (fractionation, mixing, liquid immiscibility) which may have produced them (Juster et al., 1989; Natland, 1991b).

The rocks are also not conventional cumulates, although we have adopted a chemical definition for adcumulates which seems useful and does not depend on any particular mechanism of adcumulus

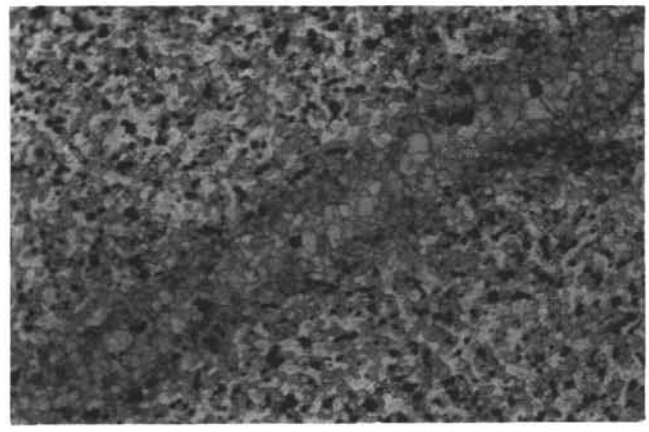

Figure 19. Transmitted light photomicrograph of a 0.7-mm-wide orthopyroxenite veinlet in an oxide gabbronorite, North Slope Sample 2213-1351.

growth. But how these adcumulates formed must be assessed in part from the fact that they are not layered, nor graded, nor modally sorted, nor is there any obvious means of rigorously distinguishing primocrysts from post-cumulus minerals or overgrowths. The rocks contain xenocrystic calcic plagioclase, and most have high cryptic Cr in clinopyroxenes, both evidently relics of some earlier stage of crystallization from more primitive magmas. The possibility exists that these are evidence for an original collection of primary precipitate minerals (the nearly nongenetic term of Jackson, 1961) which are now almost wholly transformed. Most of the conventions of cumulate theory thus do not apply to these rocks. Their bulk compositions, however, are clearly not those of liquids. This is sufficient reason to consider that they formed by some process of concentration of minerals, thus that they must be considered cumulates in the broadest sense.

The outstanding impression given by the rocks is that of textural variability on a very fine scale. Principal crystallization units, corresponding to shipboard lithologic units, are only centimeters to a few meters wide, and probably are dike-like in overall aspect. But even individual thin sections are texturally variable. Some of them are chaotic amalgams of coarse- and fine-grained, modally variable material. If we assume that these diverse crystallization sectors required different conditions of nucleation and crystal growth, then each of them represents a distinctive body of liquid from which that particular material crystallized. Either most of those bodies were very small, and crystallization occurred in situ, or the rocks represent mélanges of material mixed together and annealed after most crystallization had taken place. Oikocrysts appear to be a particular type of space which opened in the rocks and within which extremely coarse pyroxenes could grow. The spaces, or at least some of them, were cracks, and the melt that flowed into them and through them transported xenocrysts of broken, embayed, and tabular plagioclases having varying compositions. These are now chadacrysts.

We have seized on the modal proportions and distribution of oxide minerals to evaluate residual melt porosities, and as a means of outlining the final porosity structure of the nearly crystalline rocks. But there was a porosity structure before oxides began to crystallize, and its traces must be marked by the various zones of differing grain size and texture exhibited by the principal silicate minerals. Oikocrysts in cracks are one example. Pockets of very fine-grained plagioclase-pyroxene intergrowths in otherwise coarser grained rocks are another. Narrow dike-like bodies of coarse-grained gabbronorite crosscutting finer grained rocks are yet another. These are all evidence for localized flow of magma in successively larger channels or ducts.

As the ductwork formed, persisted, was modified, clogged up, and finally was closed off, the flowing magmas differentiated and residual melt was expelled from between the crystals which eventually

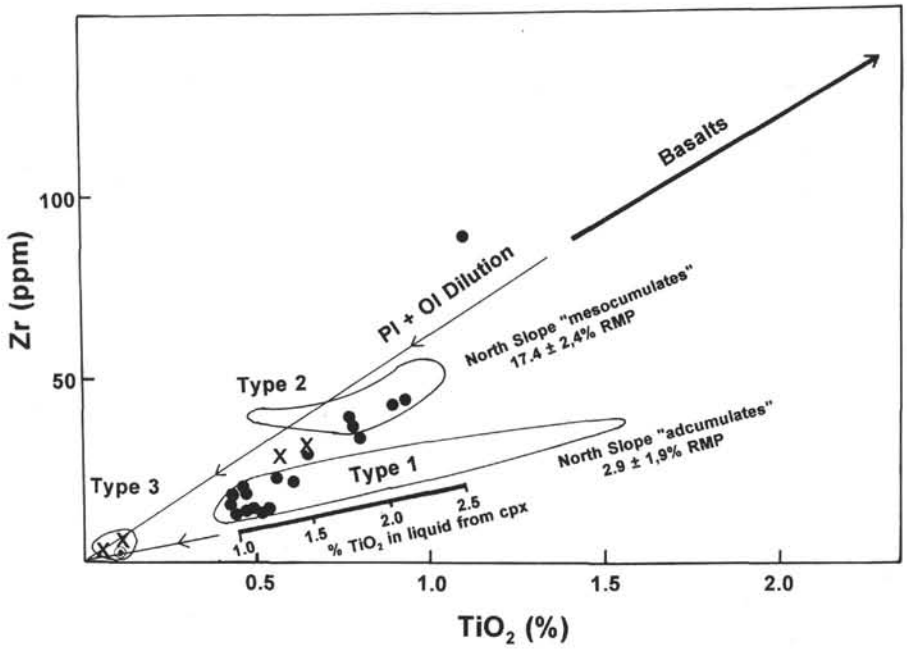

Figure 20. TiO_2 vs. Zr for Site 894 gabbroic rocks (dots) compared with two data fields for North Slope gabbronorites. Data are from Gillis, Mével, Allan, et al., 1993. The steeper diagonal line pointing toward the origin represents the effect of plagioclase and olivine accumulation on basaltic liquids. The less-steep line with tick marks shows estimated compositions of clinopyroxenes that would precipitate from liquids having the TiO_2 contents shown, based on partition coefficients. Pure gabbroic adcumulates would lie somewhere on this line or toward the origin. Compositions plotting between the two lines contain some percentage of material crystallized from trapped melt. Type 1 North Slope gabbronorite adcumulates with less than 3% estimated residual melt porosity (RMP) fall parallel to the clinopyroxene trend line. North Slope Type 2 gabbronorite mesocumulates (average 17% RMP) are in the upper field. The Type 3 data field includes one Site 895 olivine gabbro (circled dot) and two samples of cumulate gabbro (X's) from *Nautile* samples downslope from Hole 894G reported by Hekinian et al. (1993). These have <1% RMP.

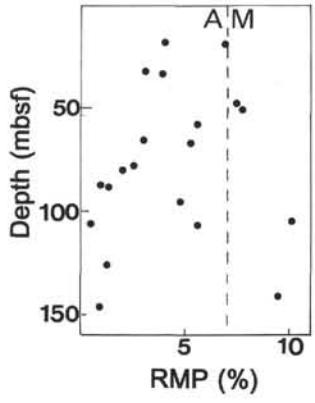

Figure 21. Residual melt porosity (RMP), calculated as described in the text, vs. depth for Site 894 gabbroic rocks. The dashed line separates adcumulates (A, <7% RMP) from mesocumulates (M).

choked the ducts. Many of the ducts probably only ever carried squeezed-out intergranular melt. That the melt was squeezed out is indicated by the considerable evidence for grain-boundary dissolution and embayment in most of the rocks.

We also need a mechanism of formation of adcumulates which can operate in confined space and throughout nearly the entire gabbroic column in the dynamic region of crustal dilation and spreading beneath the ridge axis. Models based on large magma bodies, such as all those derived from consideration of layered intrusions, are not appropriate. Some details of those models, particularly at the stage of grain dissolution and reprecipitation, are relevant, but not the connection to a major magma body. Instead, we are dealing with fluid-grain interactions and porosity reduction in a thick compacting medium, much like that of sedimentary rocks. And here, the literature on formation of quartzites and sandstones provides some guidance.

Mutual interpenetration of grains is one characteristic of pressure solution, which in sedimentary rocks is known to be quite efficient in reducing porosity through hundreds, even thousands of meters of compacting rock (e.g., Thompson, 1959; Tada and Siever, 1989). By analogy to sedimentary formations, the main requirement for pressure solution is vertically directed stress, which in the case of spreading ridges is supplied by the thick mass of crystallizing gabbroic rock, material in the melt lens, and the body of dikes and pillow basalts making up the upper portion of the ocean crust.

A second requirement for the ocean crust is a positive temperature gradient above the solidus from the melt lens all the way into the mantle. Crystallization is driven by heat loss only from the top of the body of rocks. This provides the potential for melt to exist anywhere in the crust, and assures that solidified rock below the magma lens throughout the crust must be concentrated from the melt.

The third requirement for grain dissolution by pressure solution is the existence of grain-coating films of fluid (Weyl, 1959), in this case melt. This is the only way for material to be transported away from the surfaces of mineral grains in contact. We have suggested that rare embayments in xenocrystic plagioclase chadacrysts are evidence for such films, since they were so cleanly separated from the phase (presumably pyroxene) which originally was in the embayments. Wrap-around oxides in some samples are also evidence for the nearly complete permeation of a melt phase around silicate grain boundaries.

All other mechanisms for formation of adcumulates require the presence of a body of melt, probably substantial, probably convect-

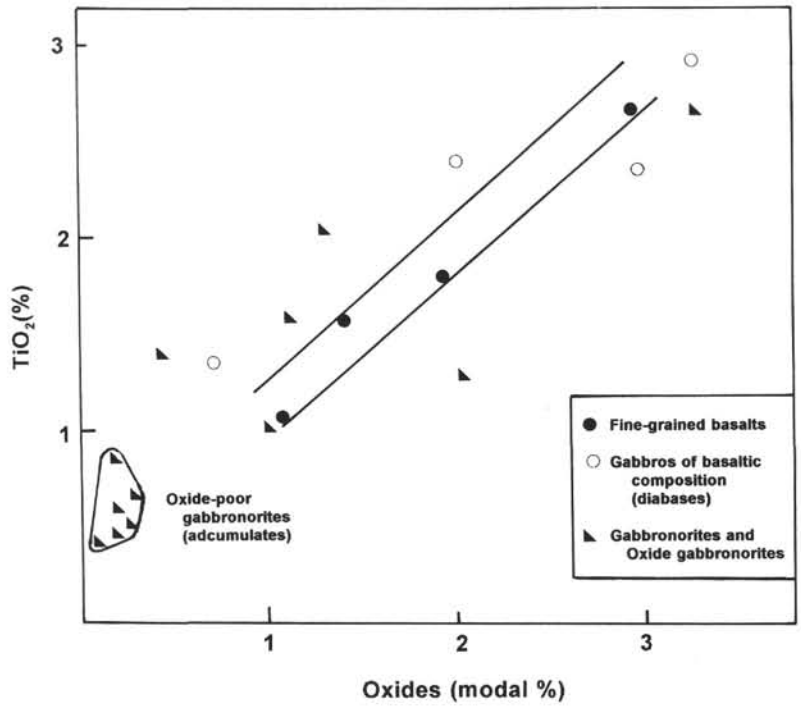

Figure 22. TiO_2 vs. modal percentages of oxides for abyssal tholeiites from the north and south rift margins of Hess Deep, compared with some North Slope gabbronorites and oxide gabbros. Parallel lines bound data points for fine-grained basalts. Data are from Nilsson (1993) and J. Natland (unpubl. data).

ing, very nearby (e.g., Morse, 1986). At the East Pacific Rise, there is no substantial magma chamber, and all crystallization throughout a column of nearly solidified gabbro several kilometers thick must be accomplished within a few thousand years, despite repeated introduction of new magma at the base of the column, passage of melt through that column, and frequent eruptions off the top. What is necessary in the end is a mechanism for extremely efficient expression of intergranular melt from the walls of nearly crystalline rock surrounding small, pipe-like, anastomosing melt channels (Natland and Dick, 1993) which probably extend in some disconnected fashion all the way into the mantle. In fact, those channels are the complement of porosity reduction, as are the numerous veins in stylolitic limestones. In this milieu, pressure solution provides a plausible and simple explanation for formation of massive adcumulates in the ocean crust.

Given that the rocks which crystallized under these conditions were subject to sudden rapid changes resulting from crustal dilation and magma inflation, the patterns of channelized flow and of pressure solution must have fluctuated constantly. For this reason, we term the overall process of crystallization, porosity reduction, and extensive transformation of crystals by reaction with melt *dynamic crystallization* (homologous to the term *dynamic partial melting* of Langmuir et al., 1977). To the extent that porosity reduction was sufficiently efficient to produce a thick column of adcumulates, the effect of dynamic crystallization on melt compositions is best described as that of nearly ideal fractional crystallization. This is one end-member of in situ crystallization differentiation described by Langmuir (1989).

By this means, virtually all highly incompatible elements introduced by primitive basaltic magmas into the base of the crust no longer reside in the gabbroic portion of the crust. They are concentrated in the basalts and dikes, and are enriched on average by factors of 2–3 above concentrations in original parental basalt. The locus of transfer of incompatible elements into the basalts must be the melt lens, since they are not present in significant abundances in the rocks below it. The mechanism of transfer has to be mixing, between whatever volumes of basalt are injected into and past the lens during an inflation-eruption cycle, and highly fractionated liquids, including andesites and dacites, which episodically reside in the lens itself. An example of the type of mixing is that of a composite basalt-ferroandesite lava flow dredged from the axis of the East Pacific Rise near 9°N (Natland, 1991b). The andesite itself is a hybrid of a very iron-rich ferrobasalt (Mg# = 0.42 with 16.3% iron as FeO*) and rhyodacite, which is found as isolated blebs in the quenched margin of the rock. These two compositions, as molten material, had to be present just below the ridge axis, when they were entrained in the more primitive basalt (Mg# = 0.543) which carried them to the surface. They are prima facie evidence for nearly complete crystallization of gabbroic rocks in the underlying crust, and of mixing. Are such compositions generally representative of material in the melt lens? The evidence from North Slope and Site 894 is that the gabbronorite substrate of the melt lens crystallized mainly from extremely fractionated liquids, with two pyroxenes and oxide minerals near or on the liquidus; in other words, ferrobasalts and ferroandesites. The North Slope at Hess Deep suggests that even more radically fractionated melts, including those with high SiO_2, occupy the melt lens, at least from time to time. An extremely small proportion of eruptive rocks along the East Pacific Rise, perhaps only 2%–3%, are actually this fractionated. To be sure, Site 894 gabbroic rocks carry zoned plagioclases, which are evidence for the crystallization of more typical basalts in their histories. Many of the zoned minerals may have crystallized in situ, but others are clearly xenocrysts. Thus although this high level of the gabbroic crust must have been invaded frequently by fairly primitive basaltic magmas (since they do erupt), the time-averaged composition of melts in the lens, and in porosity structure below it, was very fractionated (iron rich, interlaced with minor high-silica magma). It was quite dense.

Why are there melt lenses? Models for melt lenses must distinguish their condition *at rest,* that is, between eruptions, and *at the*

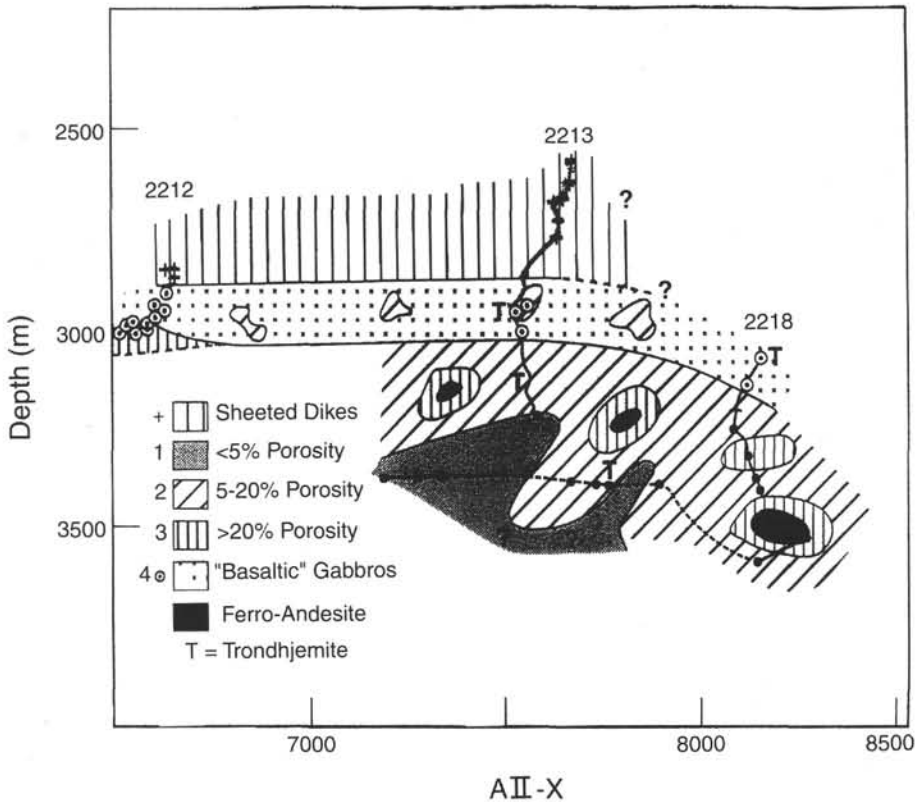

Figure 23. A sketch map of the face of the steep scarp at the North Slope of Hess Deep, across the dike gabbro transition. The vertical axis is water depth, the horizontal axis is in meters from a reference in the transponder array used to navigate the *Alvin* dives. Dives are 2212, 2213, and 2218. The sketch is precise for the dive tracks, but schematic elsewhere. In upward succession, the dive tracks crossed outcrops of gabbronorite with low residual melt porosity (adcumulates), then gabbronorites with moderate residual melt porosity (mesocumulates), locally interspersed with oxide-rich gabbro and tonalite/trondhjemite dikelets. Above these abruptly at almost the same depth on three dives are coarse-grained diabases, or gabbros of basaltic composition. Above these at precisely the same depth on the tracks of Dives 2212 and 2213 are fine-grained basaltic rocks of the sheeted dike complex. Dike contacts were not seen in the interval of "gabbros of basaltic composition." These are interspersed with mesocumulate gabbronorites on the track Dive 2213. There was also one interval where fine-grained quenched dikes of ferrobasalt and ferroandesite were sampled on track 2218.

eruptive stage. Almost certainly, the dimensions of melt lenses inferred from multichannel seismic observations, and the persistence of their characteristics along axis, reflect the condition *at rest.* The rocks we have described were also produced *at rest.* The two processes of channelized flow and pressure-solution porosity reduction are features of rocks which crystallized beneath the melt lens *at rest.* To the extent that melt lenses are steady-state features (mappable almost everywhere, thus never completely frozen), they must be supplied with melt on a continuous basis, in addition to being sporadically charged with primitive magma at the eruptive stage. But those are exceptional conditions, disturbances in the main and more persistent pattern of channelized flow which is driven by porosity reduction and formation of adcumulates throughout the lower crust. Channelized flow is what keeps melt lenses alive, and it is driven in turn by persistent channelized flow of magma from the mantle into the base of the crust (Dick and Natland, this volume). One feeds into the other, sometimes allowing highly calcic, refractory plagioclases derived from reaction of basalts with mantle peridotites to be carried nearly to the magma lens.

The magma lens itself resides below the brittle rocks of the basaltic layer. It is a pool of melt that collects at or just below a freezing front. It may simply be a place where melt bleeds from confined flow channels in hot, relatively impermeable adcumulate rock into a looser porosity structure created by cold, cracked rock. Neutral buoyancy (Ryan, 1993) does not necessarily have anything to do with it. Certainly, the very iron-rich melts that are present are too dense ($\rho = 2.7$–2.9) to do much else but sink through any loose body of crystals or network of fractures that might open up and remain opened for any period of time, as they do, for example, in the formation of discordant iron-rich pegmatites in layered intrusions (Bateman, 1951; Scoon and Mitchell, 1994). Such liquids need a nearly impermeable mat on which to sit. The mat is gabbronorite adcumulates.

The general model of formation of the gabbroic portion of the crust at a fast-spreading ridge which can be gleaned from the rocks is that of crystallization in a vertical network of fractures, repetitively opening and closing. The magma lens does not act in the manner of a stratiform intrusion, with the bulk of minerals precipitating on a steadily subsiding floor (Phipps Morgan and Chen, 1993). Strictly speaking, that mechanism should produce a major cyclic variation in the compositions of minerals in the crust. Instead, a base-level steady-state temperature gradient, to which the column of crust must return after an eruptive event (cold at the top; hot at the bottom), imposes a strict large-scale cryptic variation on the column of crystallizing rock. This column has to undergo major reequilibration in response to melts continually permeating upward in response to deep adcumulus growth and pressure solution. As those melts cool in their upward migration, they will precipitate minerals appropriate only to the ambient temperature conditions at a given level in the crust. For those liquids to continue to crystallize, they must migrate upward, to cooler levels. Only the most fractionated liquids will reach the top of the column, where a downward-reaching cracking front in the brittle basaltic carapace causes a sharp change in the temperature gradient.

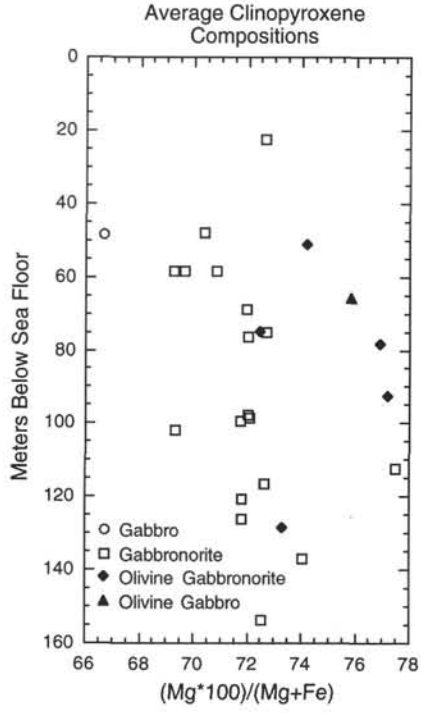

Figure 24. Average Mg# of clinopyroxene grains vs. depth, and by lithology, for samples of Hole 894G used in this study. There is no trend with depth, and no consistent differences in clinopyroxene compositions between lithologies. Data are from Table 3 and Gillis (this volume).

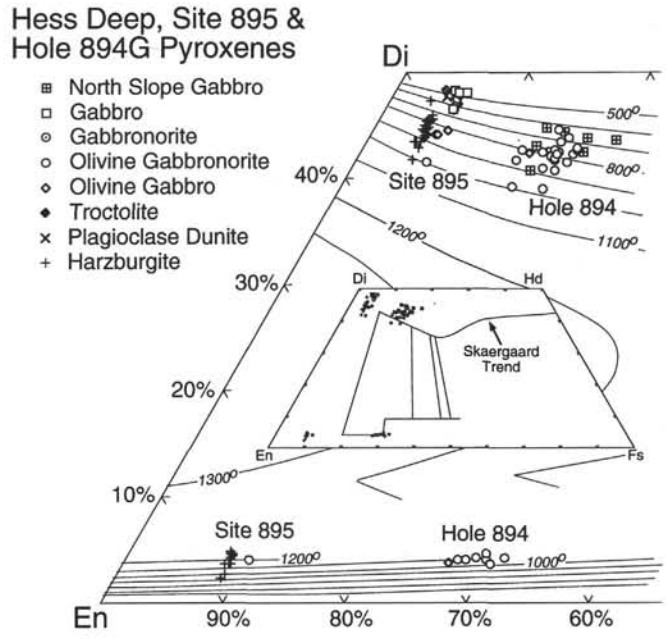

Figure 25. A portion of the pyroxene quadrilateral (Wo-En-Fs), showing the compositions of pyroxenes in gabbroic and ultramafic rocks sampled from Hess Deep, by lithology as indicated. The temperature grid is that of Lindsley and Andersen (1983). Wo has not been corrected for minor components, thus the projected temperatures for clinopyroxenes are probably systematically about 50° too low.

This is in the region of the melt lens. Below this, gabbroic rocks should become steadily more magnesian and calcic with depth, in accord with the liquidus mineralogy dictated by the average temperature gradient. Most of the crust, except perhaps where primitive magmas may pond near the base (Garmany, 1989), will not be gravitationally layered.

This is admittedly a partial picture, made with reference to rock textures and mineral compositions mainly near the top of the gabbro column. Nevertheless, the rocks of Hole 894G, which present a short but critical cored sequence, provide a firm impression of a major petrogenetic and fluid-dynamical process acting on a global scale. Channelized flow accompanied by adcumulus growth beneath spreading ridges is as commonplace as the circulation of the atmosphere or the oceans. It directly affects the structure of the ocean crust and the composition of every rock within it.

ACKNOWLEDGMENTS

Leg 147 post-cruise studies were sponsored by the JOI-USSAC United States Science Support Program. Studies on *Alvin* samples from the North Slope were supported by the U.S. National Science Foundation Ocean Sciences Program, Division of Marine Geology and Geophysics. We thank Kristen Nilsson Farley, Jeff Gee, Peter Schiffman, Chris Roudin, and Kathy Gillis for their contributions to the set of electron probe mineral analyses. Nobu Shimizu was, as usual, indispensable in the ion probe lab. Many of the ideas presented here were originally conceived and debated during many pleasant discussions with members of the Leg 147 scientific party as the rocks were brought on board. John Bender, Chip Lesher, and Peter Meyer provided thoughtful and encouraging reviews of the manuscript.

REFERENCES

Barth, G.A., 1994. Plate boundary geometry to Moho depths within the 9°30′N and 12°54′N overlapping spreading centers of the East Pacific Rise. *Earth Planet. Sci. Lett.*, 128:99–112.

Bateman, A.M., 1951. The formation of late magmatic oxide ores. *Econ. Geol.*, 46:404–426.

Bloomer, S.H., Meyer, P.S., Dick, H.J.B., Ozawa, K., and Natland, J.H., 1991. Textural and mineralogic variations in gabbroic rocks from Hole 735B. *In* Von Herzen, R.P., Robinson, P.T., et al., *Proc. ODP, Sci. Results,* 118: College Station, TX (Ocean Drilling Program), 21–39.

Bryan, W.B., 1983. Systematics of modal phenocryst assemblages in submarine basalts: petrologic implications. *Contrib. Mineral. Petrol.*, 83:62–74.

Buddington, A.F., and Lindsley, D.H., 1964. Iron-titanium oxides minerals and synthetic equivalents. *J. Petrol.*, 5:310–357.

Burnett, M.S., Caress, D.W., and Orcutt, J.A., 1989. Tomographic image of the magma chamber at 12°50′N on the East Pacific Rise. *Nature*, 339:206–208.

Chalokwu, C.L., and Grant, N.K., 1990. Petrology of the Partridge River Intrusion, Duluth Complex, Minnesota, I. Relationships between mineral compositions, density, and trapped liquid abundance. *J. Petrol.*, 31:265–293.

Clarke, D.B., and Loubat, H., 1977. Mineral analyses from the peridotite-gabbro-basalt complex at Site 334, DSDP Leg 37. *In* Aumento, F., Melson, W.G., et al., *Init. Repts. DSDP,* 37: Washington (U.S. Govt. Printing Office), 847–855.

Coleman, R.G., and Peterman, Z.E., 1975. Oceanic plagiogranite. *J. Geophys. Res.*, 10:1099–1108.

Dixon, S., and Rutherford, M.J., 1979. Plagiogranites as late-stage immiscible liquids in ophiolite and mid-ocean ridge suites: an experimental study. *Earth Planet. Sci. Lett.*, 45:45–60.

Duke, J.M., 1976. Distribution of the period four transition elements among olivine, calcic clinopyroxene and mafic silicate liquid: experimental results. *J. Petrol.*, 17:499–521.

Elthon, D., 1987. Petrology of gabbroic rocks from the Mid-Cayman Rise spreading center. *J. Geophys. Res.*, 92:658–682.

Fisk, M.R., 1984. Depths and temperatures of mid-ocean ridge magma chambers and the composition of their source magmas. *In* Gass, I.G., Lippard, S.J., and Shelton, A.W. (Eds.), *Ophiolites and Oceanic Lithosphere.* Geol. Soc. Spec. Publ. London, 13:17–23.

Francheteau, J., Armijo, R., Cheminée, J.L., Hekinian, R., Lonsdale, P.F., and Blum, N., 1990. 1 Ma East Pacific Rise oceanic crust and uppermost mantle exposed by rifting in Hess Deep (equatorial Pacific Ocean). *Earth Planet. Sci. Lett.,* 101:281–295.

————, 1992. Dyke complex of the East Pacific Rise exposed in the walls of Hess Deep and the structure of the upper oceanic crust. *Earth Planet. Sci. Lett.,* 111:109–121.

Garmany, J., 1989. Accumulations of melt at the base of the young oceanic crust. *Nature,* 340:628–632.

Gee, J., Natland, J.H., Hurst, S., and Nilsson, K., 1992. Magnetic properties of ocean crust samples from Hess Deep: implications for marine magnetic anomalies. *Eos,* 73:490.

Gillis, K., Mével, C., Allan, J., et al., 1993. *Proc. ODP, Init. Repts.,* 147: College Station, TX (Ocean Drilling Program).

Harding, A.J., Orcutt, J.A., Kappus, M.E., Vera, E.E., Mutter, J.C., Buhl, P., Detrick, R.S., and Brocher, T.M., 1989. Structure of young oceanic crust at 13°N on the East Pacific Rise from expanding spread profiles. *J. Geophys. Res.,* 94:12163–12196.

Hart, S.R., and Dunn, T., 1993. Experimental CPX/melt partitioning of 24 trace elements. *Contrib. Mineral. Petrol.,* 113:1–8.

Hekinian, R., Bideau, D., Francheteau, J., Cheminée, J.L., Armijo, R., Lonsdale, P., and Blum, N., 1993. Petrology of the East Pacific Rise crust and upper mantle exposed in the Hess Deep (eastern equatorial Pacific). *J. Geophys. Res.,* 98:8069–8094.

Hodges, F.N., and Papike, J.J., 1976. DSDP Site 334: magmatic cumulates from oceanic layer 3. *J. Geophys. Res.,* 81:4135–4151.

Hunter, R.H., 1987. Textural equilibrium in layered igneous rocks. *In* Parsons, I. (Ed.), *Origins of Igneous Layering:* Dordrecht (D. Reidel), 473–503.

Irvine, T.N., 1982. Terminology for layered intrusions. *J. Petrol.,* 23:127–162.

Jackson, E.D., 1961. Primary textures and mineral associations in the ultramafic zone of the Stillwater complex, Montana. *Geol. Surv. Prof. Pap. U.S.,* 358.

Juster, T.C., Grove, T.L., and Perfit, M.R., 1989. Experimental constraints on the generation of FeTi basalts, andesites, and rhyodacites at the Galapagos Spreading Center, 85°W and 95°W. *J. Geophys. Res.,* 94:9251–9274.

Karson, J.A., Hurst, S.D., and Lonsdale, P.F., 1992. Tectonic rotations of dikes in fast-spread oceanic crust exposed near Hess Deep. *Geology,* 20:685–688.

Kent, G.M., Harding, A.J., and Orcutt, J.A., 1990. Evidence for a smaller magma chamber beneath the East Pacific Rise at 9°30′N. *Nature,* 344:650–653.

————, 1993. Distribution of magma beneath the East Pacific Rise between the Clipperton Transform and the 9°17′N Deval from forward modeling of common depth point data. *J. Geophys. Res.,* 98:13945–13969.

Klitgord, K.D., and Mudie, J.D., 1974. The Galapagos spreading centre: a near-bottom geophysical survey. *Geophys. J. R. Astron. Soc.,* 38:563–586.

Langmuir, C.H., 1989. Geochemical consequences of in situ crystallization. *Nature,* 340:199–205.

Langmuir, C.H., Bender, J.F., Bence, A.E., and Hanson, G.N., 1977. Petrogenesis of basalts from the FAMOUS area: Mid-Atlantic Ridge. *Earth Planet. Sci. Lett.,* 36:133–156.

Lindsley, D.H., and Andersen, D.J., 1983. A two-pyroxene thermometer. *J. Geophys. Res.,* 88 (Suppl.):A887–A906.

Lonsdale, P., 1988. Structural pattern of the Galapagos microplate and evolution of the Galapagos triple junctions. *J. Geophys. Res.,* 93:13551–13574.

McBirney, A.R., 1993. Is the cumulate paradigm worth saving? *Eos,* 74 (Suppl.):622.

Meyer, P.S., Dick, H.J.B., and Thompson, G., 1989. Cumulate gabbros from the Southwest Indian Ridge, 54°S–7°16′E; implications for magmatic processes at a slow spreading ridge. *Mineral. Petrol.,* 103:44–63.

Meyer, P.S., and Shibata, T., 1990. Complex zoning in plagioclase feldspars from ODP Site 648. *In* Detrick, R., Honnorez, J., Bryan, W.B., Juteau, T., et al., *Proc. ODP, Sci. Results,* 106/109: College Station, TX (Ocean Drilling Program), 123–142.

Morel, J.M., and Hekinian, R., 1980. Compositional variations of volcanics along segments of recent spreading ridges. *Contrib. Mineral. Petrol.,* 72:425–436.

Morse, S.A., 1986. Convection in aid of adcumulus growth. *J. Petrol.,* 27:1183–1214.

Natland, J.H., 1989. Partial melting of a lithologically heterogeneous mantle: inferences from crystallization histories of magnesian abyssal tholeiites from the Siqueiros Fracture Zone. *In* Saunders, A.D., and Norry, M.J. (Eds.), *Magmatism in the Ocean Basins.* Geol. Soc. Spec. Publ. London, 42:41–70.

————, 1991a. Indian Ocean crust. *In* Floyd, P.A. (Ed.), *Oceanic Basalts:* Glasgow (Blackie), 288–310.

————, 1991b. Mineralogy and crystallization of oceanic basalts. *In* Floyd, P.A. (Ed.), *Oceanic Basalts:* Glasgow (Blackie), 63–93.

————, 1991c. Secret life of a magma chamber: East Pacific Rise exposé at Hess Deep. *Eos,* 72 (Suppl.):526.

Natland, J.H., and Dick, H.J.B., 1993. Formation of cumulates at spreading ridges. *Eos,* 74 (Suppl.): 653.

Natland, J.H., Lonsdale, P., Karson, J., and Sims, D., 1990. High-level gabbros of the East Pacific Rise sampled by submersible at fault exposures in Hess Deep, Eastern Equatorial Pacific. *Eos,* 71:1647.

Natland, J.H., and Melson, W.G., 1980. Compositions of basaltic glasses from the East Pacific Rise and Siqueiros fracture zone, near 9°N. *In* Rosendahl, B.R., Hekinian, R., et al., *Init. Repts. DSDP,* 54: Washington (U.S. Govt. Printing Office), 705–723.

Natland, J.H., Meyer, P.S., Dick, H.J.B., and Bloomer, S.H., 1991. Magmatic oxides and sulfides in gabbroic rocks from Hole 735B and the later development of the liquid line of descent. *In* Von Herzen, R.P., Robinson, P.T., et al., *Proc. ODP, Sci. Results,* 118: College Station, TX (Ocean Drilling Program), 75–111.

Nilsson, K., 1993. Oxidation state, sulfur speciation, and sulfur concentration in basaltic magmas: examples from Hess Deep and the Lau Basin [Ph.D. dissert.]. Univ. California–San Diego.

Nilsson, K., and Natland, J.H., 1991. Oxide crystallization and fO_2 during differentiation of abyssal tholeiites and gabbros at Hess Deep, E. Pacific. *Eos,* 72 (Suppl.):526.

Orcutt, J.A., Kennett, B., and Dorman, L., 1976. Structure of the East Pacific Rise from an ocean bottom seismometer survey. *Geophys. J. R. Astron. Soc.,* 45:305–320.

Ozawa, K., Meyer, P.S., and Bloomer, S.H., 1991. Mineralogy and textures of iron-titanium oxide gabbros and associated olivine gabbros from Hole 735B. *In* Von Herzen, R.P., Robinson, P.T., et al., *Proc. ODP, Sci. Results,* 118: College Station, TX (Ocean Drilling Program), 41–73.

Perfit, M.R., Fornari, D.J., Malahoff, A., and Embley, R.W., 1983. Geochemical studies of abyssal lavas recovered by DSRV Alvin from eastern Galapagos Rift, Inca Transform and Ecuador Rift, 3. Trace element abundances and petrogenesis. *J. Geophy. Res.,* 88:10551–10572.

Phipps Morgan, J., and Chen, Y.J., 1993. The genesis of oceanic crust: magma injection, hydrothermal circulation, and crustal flow. *J. Geophys. Res.,* 98:6283–6297.

Ribbe, P.H., 1975. Exsolution textures in ternary and plagioclase feldspars: interference colors. *In* Ribbe, P.H. (Ed.), *Rev. Mineral.,* 2:241–270.

Robinson, P.T., Von Herzen, R., et al., 1989. *Proc. ODP, Init. Repts.,* 118: College Station, TX (Ocean Drilling Program).

Rosendahl, B.R., 1976. Evolution of oceanic crust, 2. Constraints, implications, and inferences. *J. Geophys. Res.,* 81:5305–5314.

Ryan, M.P., 1993. Neutral buoyancy and the structure of mid-ocean ridge magma reservoirs. *J. Geophys. Res.,* 98:22321–22338.

Scoon, R.N., and Mitchell, A.A., 1994. Discordant iron-rich ultramafic pegmatites in the Bushveld Complex and their relationship to iron-rich intercumulus and residual liquids. *J. Petrol.,* 35:881–917.

Sinton, J.M., and Detrick, R.S., 1992. Mid-ocean ridge magma chambers. *J. Geophys. Res.,* 97:197–216.

Streckeisen, A., 1974. Classification and nomenclature of plutonic rocks. *Geol. Rundsch.,* 63:773–786.

Symes, R.F., Bevan, J.C., and Hutchinson, R., 1977. Phase chemistry studies on gabbro and peridotite rocks from Site 334, DSDP Leg 37. *In* Aumento, F., Melson, W.G., et al., *Init. Repts. DSDP,* 37: Washington (U.S. Govt. Printing Office), 841–844.

Tada, R., and Siever, R., 1989. Pressure solution during diagenesis. *Ann. Rev. Earth Planet. Sci.,* 17:89–118.

Thompson, R.A., 1959. Pressure solution and porosity. *In* Ireland, H.A. (Ed.), *Silica in Sediments.* Spec. Publ.—Soc. Econ. Paleontol. Mineral., 7:92–110.

Wager, L.R., 1963. The mechanism of adcumulus growth in the layered series of the Skaergaard intrusion. *Min. Soc. Am., Spec. Pap.*, 1:1–19.
Wager, L.R., and Brown, G.M., 1968. *Layered Igneous Rocks:* London (Oliver and Boyd).
Wager, L.R., Brown, G.M., and Wadsworth, W.J., 1960. Types of igneous cumulates. *J. Petrol.*, 1:73–85.
Walker, D., Shibata, T., and Delong, S.E., 1979. Abyssal tholeiites from the Oceanographer fracture zone, II. Phase equilibria and mixing. *Contrib. Mineral. Petrol.*, 70:111–125.
Weyl, P.K., 1959. Pressure solution and the force of crystallization—a phenomenological theory. *J. Geophys. Res.*, 64:2001–2025.

Date of initial receipt: 2 August 1994
Date of acceptance: 15 June 1995
Ms 147SR-002

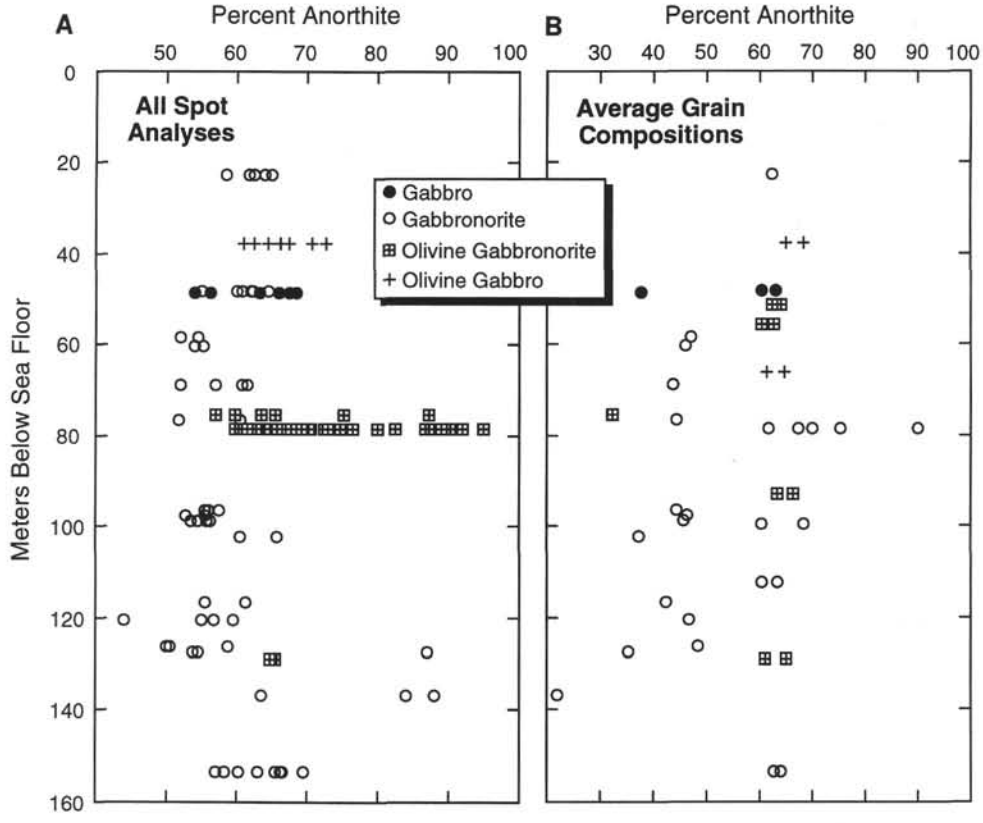

Figure 26. An contents of plagioclases vs. depth for samples used in this study. All spot analyses are plotted. Most plagioclases lie between An_{70-55}, except for more calcic plagioclase in one sample studied in detail from the middle of the section cored, and spot analyses of two samples farther down. Probably similarly calcic plagioclases occur in the centers of zoned crystals in other samples.

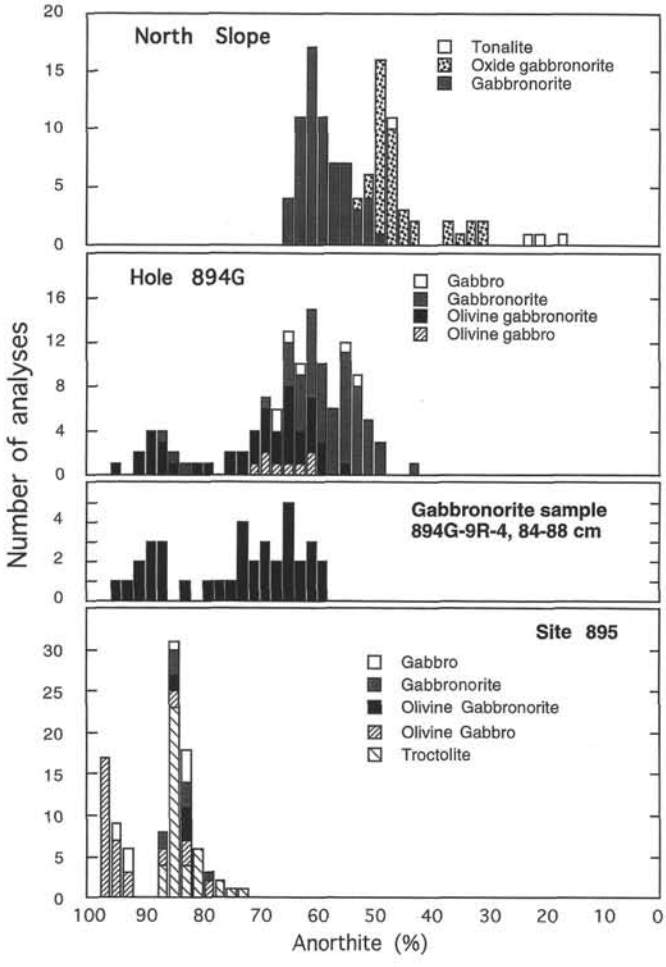

Figure 27. Histograms of all analyzed plagioclases, with analyses identified by lithology, for samples from the North Slope, Hole 894G, and the several holes of Site 895. An additional histogram is provided for the one sample (147-894G-9R-4, 84–88 cm, Piece 7) studied in detail, which provides a fair overlap at very calcic plagioclase compositions with Site 895.

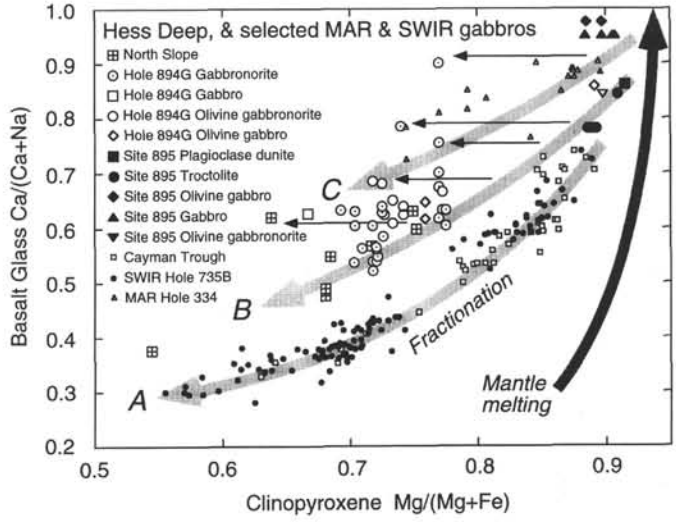

Figure 28. Compositions of coexisting plagioclases (An, mol%) vs. Mg/(Mg + Fe) of coexisting clinopyroxenes from gabbroic rocks of Hess Deep (ODP Sites 894 and 895; plus North Slope), compared with trends from other locales. The dark upward-pointing arrow indicates mineralogical relations expected in initial precipitates from primary magmas related by partial melting. The shaded arrows curving downward and to the left are three hypothetical trends for precipitates of the differentiation products of, from A to C, successively more refractory primary melts. The middle fractionation trend corresponds to Hess Deep. Cores of calcic plagioclases in Site 894 and North Slope gabbros, carried in by more primitive magmas than those that produce the clinopyroxenes, fall above this trend. The horizontal arrows suggest how far they are deflected from the idealized Hess Deep trend by hybridization. Data sources are: Hess Deep = this report and Dick and Natland (this volume); Hole 735B = Ozawa et al. (1991) and Bloomer et al. (1991); DSDP Site 334 = Hodges and Papike (1976), Symes et al. (1977), and Clarke and Loubat (1977); Cayman Trough = Elthon (1987).

Table 8. Melt Mg#s calculated from average clinopyroxene and olivine compositions.[a]

Sample	Calculated Mg# (cpx)	Mg# (L)	Mg# (ol)	Mg# (L)
147-894G-				
1R-1, 8–10 cm	72.7	33.7	—	—
2R-3, 101–103 cm	—	—	67.3	38.2
4R-2, 27–30 cm	70.4	30.4	—	—
5R-1, 10–14 cm	74.2	36.0	63.3	34.1
6R-1, 26–28 cm	—	—	69.6	40.7
7R-1, 67–70 cm	75.9	38.8	64.0	34.8
9R-1, 75–79 cm	72.7	33.7	—	—
9R-4, 84–88 cm	76.9	40.6	63.0	33.8
11R-3, 43–45 cm	77.2	41.1	64.4	35.2
12R-4, 37–40 cm	71.8	32.4	—	—
13R-3, 101–103 cm	77.5	41.6	—	—
17R-2, 9–11 cm	73.3	34.6	—	—
20R-3, 95–98 cm	72.5	33.4	—	—
Mean	74.1	36.0	65.3	36.1
s.d.	2.4	3.9	2.6	2.7
North Slope				
2213–1053	68.4	27.8	—	—
2213–1110	74.9	37.1	66.0	36.8
2213–1226	74.5	36.5	—	—
2213–1316	72.8	33.8	—	—
2218–1111	75.2	37.6	—	—
2218–1210–3	68.1	27.5	—	—
2218–1337	71.7	32.2	—	—
2218–1434	54.4	14.9	—	—
Mean	70.0	30.9	66.0	36.8
s.d.	6.9	7.6		

Summary:[b]		Hole 894G	North Slope
	Clinopyroxene	36.0 (11)	30.9 (7)
	Olivine	36.1 (6)	36.8 (1)
	Bulk rock[c]	31.5 (23)	26.0 (18)[d]

[a]Method of Duke (1976), modified by Natland et al. (1991).
[b] Number of samples in parentheses.
[c] Assumes bulk rock Mg# = clinopyroxene Mg#.
[d] Based on J. Natland, unpublished data.

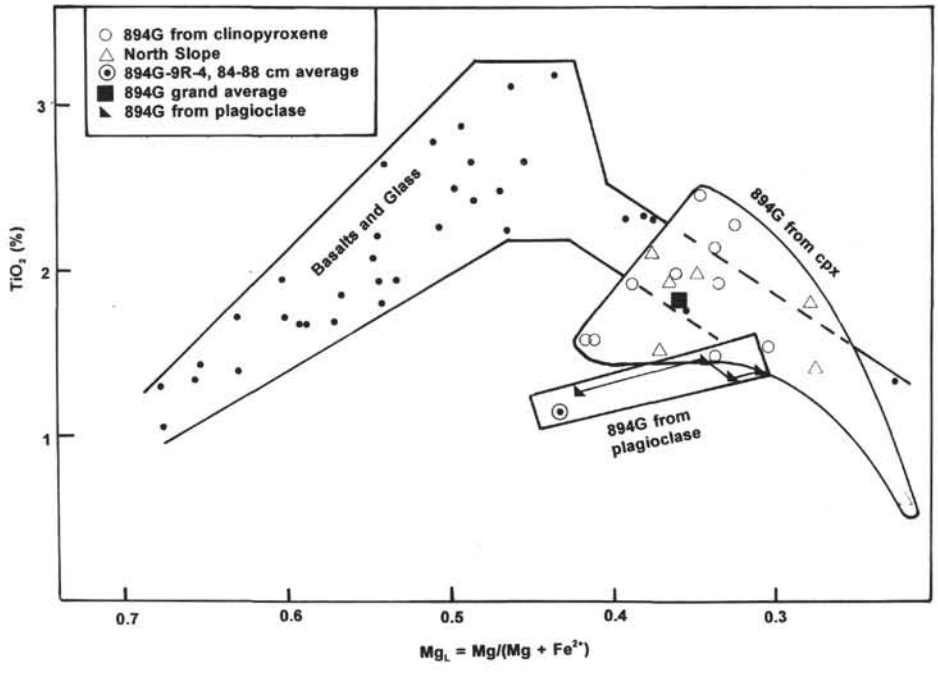

Figure 29. Mg# vs. TiO_2 for liquids reconstructed from mineral data compared with basalts and basalt glasses sampled by *Alvin* from crust of the East Pacific Rise on both the northern and southern marginal rifts of Hess Deep (Nilsson, 1993; J. Natland, unpubl. data). The irregular field at the right encloses data points for average clinopyroxene grain analyses from Hole 894G and the North Slope. The box encloses points estimated from average plagioclase compositions (filled triangles linked by dashed lines) of the sample studied in detail, and one point from the average composition of the immediately adjacent clinopyroxene. The only lava/glass analyses matching inferred liquid compositions for the gabbroic rocks are several ferroandesites and one andesite. See the text for additional discussion.

Leg 147 Igneous Contacts Log — Hole:894G

Ign. Inter.	Ign. Unit	Plut. Unit	Top C	Top S	Top Pc	Top cm	expan. Depth	Bottom C	Bottom S	Bottom Pc	Bottom Cm	Curat. Depth	Exp. Depth	Lithology	Expan. Thick.	Description Type	Nat.	Asp.	Mor.	Def.	Notes
Drilled							0.00						18.60		18.60						No Recovery
1	1	A	1	1	1	0.0	18.60	2	1	2	13.5	28.60	28.91	Olivine Gabbro	10.31	M					Medium-grained poikilitic olivine gabbro with 2.5% orthopyroxene oikocrysts, 7% olivine, and 0.25% oxide in thin
2	2		2	1	3	13.5	28.91	2	2	17	127.0	30.10	35.01	Plagioclase-Olivine Phyric Diabase	6.10	M					Fine-grained basaltic dike. Contains variable amounts of chrome spinel, large zoned plagioclase and large olivine phenocrysts.
3	3	A	2	2	18	127.0	35.01	2	3	14	120.0	31.55	38.20	Olivine Gabbro	3.19	M					Medium-grained olivine gabbro with variable olivine content ranging from 1 to 12% in thin section and a trace of orthopyroxene seen in one 5 thin sections.
3a	3	A	3	1	1	0.0	38.20	3	1	2b	14.0	38.20	39.60	Rubble	1.40						Piece 1 is an eight cm piece of plagioclase porphyritic diabase from interval 2 with a concave drilled surface, and is clearly a piece of breakout from the wall of the hole. Pc. 2 is two small pebbles of olivine gabbro rubble.
Drilled							39.60						45.00		5.40						No Recovery
4	3	B	4	1	1	0.0	45.00	4	1	6	32.5	45.00	45.63	Rubble	0.63	M					Two pebbles of diabase, one weathered, plus a heavily weathered baked-looking piece of gabbronorite and three other pebbles of fine and medium-grained gabbronorite.
5	3	B	4	1	7	32.5	45.63	4	2	7	41.0	46.34	48.42	Poikilitic Gabbronorite	2.79	M	GS				Medium grained poikilitic gabbronorite with 15% orthopyroxene oikocrysts, 0.8% oxide and no olivine in thin section.
6	3	B	4	2	8	41.0	48.42	4	2	9	49.0	46.34	48.57	Gabbronorite	0.15	S	SI	GS	I	N	Coarse grained pegmatitic gabbronorite interval with coarse orthopyroxene subhedra.
7	3	B	4	2	9	49.0	48.57	4	2	14	122.0	46.34	50.00	Poikilitic Gabbronorite	1.43	M					Medium grained gabbronorite with 7.2% orthopyroxene oikocrysts, no olivine, and 0.3% oxide in thin section.
8	3	C	5	1	1	0.0	50.00	5	1	2	14.5	50.00	52.05	Olivine Gabbronorite	2.05	M					Identified in hand specimen, the rock is medium-grained, with about 10% black olivine pseudomorphs in pc.1 and partly altered olivine in pc 2 (Core 5). Texture appears to be hypidiomorphic granular without oikocrysts under the hand lens.
9	3	D	5	1	3	14.5	52.05	6	1	7	80.0	54.80	57.30	Poikilitic Gabbronorite	5.25	G	SI	GS		N	Fine to medium-grained poikilitic gabbronorite with about 5% orthopyroxene oikocrysts and 0.5% oxide. Grades into interval 10 below with patches of coarse-grained granular gabbronorite interspersed with finer-grained poikilitic gabbronorite.
10	3	D	6	1	8	80.0	57.30	6	2	3	38.0	56.22	60.40	Gabbronorite	3.10	F			P	W	Medium to coarse-grained gabbronorite. Interval coarsens downward from 1-3 mm to 3-8 mm at bottom. Coarse interval has stubby subhedral and anhedral granular pseudomorphs apparently after orthopyroxene, 2% oxides, and <1% possible small olivine pseudomorphs. Medium-grained interval has about 8% orthopyroxene oikocrysts and 0.5% oxides. Next interval begins with a 1 cm. zone of weakly foliated fault breccia with hydrothermal clasts suggesting a fault between intervals 10 and 11.
11	3	D	6	2	4	38.0	60.40	6	2	10	118.0	56.22	62.90	Poikilitic Gabbronorite	2.50	S	SI	GS	I	N	Medium grained poikilitic gabbronorite described in hand specimen as olivine-bearing gabbronorite with variable amounts of olivine, generally less than 5%, even in olivine-rich zones. No olivine seen in the single thin section, however, which did contain 5-10% orthopyroxene oikocrysts and 1.5% oxide.

APPENDIX (continued)

Leg 147 Igneous Contacts Log — Hole:894G

Inter.	Ign. Unit	Plut. Unit	Top C	Top S	Top Pc	Top cm	expan. Depth	Bottom C	Bottom S	Bottom Pc	Bottom Cm	Curat. Depth	Exp. Depth	Lithology	Expan. Thick.	Description Type	Nat.	Asp.	Mor.	Def.	Notes
12	3	D	6	2	10	118.0	62.90	6	2	10	124.0	56.22	63.08	Gabbronorite	0.18	M		GS			Coarse grained interval, mineralogically similar to above, with subhedral granular to oikocrystic orthopyroxene in hand specimen
13	3	E	6	2	11	124.0	63.08	7	1	12	73.0	64.80	66.04	Olivine Gabbronorite	2.96	M		GS			Medium-grained ophitic olivine gabbronorite with about 10% olivine in thin section. Contains about 10% orthopyroxene and 0.25% oxide.
14	3	F	7	1	13	73.0	66.04	7	2	2	22.0	66.20	67.56	Poikilitic Gabbornorite	1.52	M		GS			Coarsens from fine to medium-grained (0.5-4 mm) poikilitic gabbronorite for first 50 cm downwards to 2-10 mm medium to coarse-grained, and is then fairly uniform in grain size to the end of the interval, though varitextured on a thin section scale. Possible olivine pseudomorphs present in thin section from coarse interval with15% granular orthopyroxene and 2% oxide.
15	3	F	7	2	3	22.0	67.56	9	3	1c	33.0	76.88	76.85	Poikilitic Gabbronorite	0.05	S	SI	GS	I	N	Medium-grained poikilitic gabbronorite with local coarse-grained patches. Contains 10 to 15% orthopyroxene oikocrysts, from 0.2 to 2% oxide and has an equigranular texture but highly variable grain size in thin section. The interval has a steeply dipping contact with coarse grained gabbronorite below. Thin sections 32, 33, 34, 35 are heavily altered making it dificult to estimate the proportions of mafic silicates.
16	3	F	9	3	1c	33.0	76.85	9	3	5f	92.0	76.88	77.37	Gabbronorite	0.57	S	SI	GS	I	N	Coarse-grained gabbronorite with about 10% granular orthopyroxene pseudomorphs, and locally10% oxide. It has a very steep contact with finer-grained gabbro which curves downward and then dies out into varitextured gabbronorite. apatite present. Zircon locally abundant (up to 1/2% in patches), and appears to be associated with blue-green amphibole (possible deuteric origin).
17	3	G	9	3	5f	92.0	77.37	9	5	3	31.5	79.47	79.10	Olivine Gabbronorite	1.73	G		M		N	Medium-grained ophitic olivine gabbronorite with 5-10% granular to ophitic orthopyroxene, 10% olivine, and 0.1-0.5% oxide.
18	3	H	10	1	1	0.0	79.10	10	2	5	43.0	80.48	84.10	Gabbro	5.00	S	SI	GS			Fine to medium-grained (0.2-3 mm) averaging 0.5 mm with medium-grained patches (occasional grains up to 6 mm). Three thin sections are olivine-free gabbro with 1-2% subophitic orthopyroxene and 1% oxides. Lower contact is inclined about 30° and is very sharp.
19	3	I	11	1	1	0.0	84.10	11	3	3	31.0	87.00	92.58	Gabbronorite	8.48	M		GS			Medium-grained (2-5 mm). Thin section shows no evidence of olivine, and contains subhedral to euhedral medium-grained granular orthopyroxene.
20	3	J	11	3	4	31.0	92.58	11	3	10	76.0	87.00	93.77	Olivine Gabbronorite	1.19	M					Fine to medium-grained poikilitic gabbronorite. Thin section shows a medium grained varitextured-granular gabbronorite, with a small amount of fresh olivine, perhaps up to 7% originally present, 15% orthopyroxene oikocrysts and 0.2% oxides.
21	3	K	12	1	1	0.0	93.77	12	2	4f	68.0	95.29	96.41	Gabbronorite	2.64	M					Coarse-grained with 15% euhedral to granular orthopyroxene, and 0.5 to 1% oxide. A few grains of coroded olivine were seen in one thin section from this interval. Vein on last piece has no evidence of faulting.

Leg 147 Igneous Contacts Log — Hole:894G

Inter.	Ign. Unit	Plut. Unit	Top C	Top S	Top Pc	Top cm	expan. Depth	Bottom C	Bottom S	Bottom Pc	Bottom Cm	Curat. Depth	Exp. Depth	Lithology	Expan. Thick.	Description Type	Nat.	Asp.	Mor.	Def.	Notes
22	3	K	12	2	5	68.0	96.41	12	3	4b	78.0	96.73	98.27	Poikilitic Gabbronorite	1.86	G	Sl	GS		N	Fine-grained poikilitic gabbronorite with 5 to 10% oikocrysts and subophitic orthopyroxene and less than 0.5% oxide. A vertical 2 cm thick, 40 cm long, band of coarse gabbronorite has abundant euhedral to granular orthopyroxene and up to 4% oxide.
23	3	K	12	3	4b	78.0	98.27	12	3	8a	140.0	96.73	99.02	Gabbronorite	0.75	G	Sl	GS		N	Medium to coarse-grained (1-5 mm) with abundant euhedral coarse orthopyroxene.
24	3	L	12	3	8b	140.0	99.02	12	3	8b	151.0	96.73	99.15	Gabbro	0.13	M					Fine to medium-grained olivine-bearing gabbro with rare 4-7 mm orthopyroxene oikocrysts. Thin section has an excellent plagioclase lamination, disrupted locally by a small coarse-grained gabbronorite patch with subhedral orthopyroxene.
25	3	M	12	4	1	0.0	99.15	13	1	14	130.0	103.40	106.42	Gabbronorite	7.27	S	Sl	M	P	N	Fine to coarse-grained gabbronorite and gabbro. There is abundant fine-grained gabbro down to the end of Section 4 of Core 12 with patches of medium-grained gabbronorite. Lower, it is consistently medium to coarse grained (up to 6-7 mm) equigranular gabbronorite with 15-20% coarse euhedral to granular orthopyroxene. Oxide increases sharply in these areas and is irregullarly distributed in patches containing up to 4%. The igneous lamination seen in interval 24 persists, and is well developed in some medium to coarse grained intervals (Pc. 894G 12-5:7B) where stubby 4x2 mm orthopyroxene euhedra are aligned with the plagioclase laths dipping about 65°. The lower contact is sharp and planar on a hand specimen scale, about 60°, but is irregular on a thin section scale, and marked by an fairly sharp increase in intergranular oxide. Thin section from near the base of the interval contains about 5% talc-magnetite pseudomorphs after olivine,.
26	3	M	13	1	14	130.0	106.42	13	1	14	137.0	103.40	106.58	Oxide Gabbronorite	0.16	M					Ten percent iron oxide (ilmenite) in relatively coarse medium-grained interval with 12% coarse blocky subhedral orthopyroxene.
27	3	M	13	2	1	0.0	106.58	13	2	4	28.5	104.77	107.24	Gabbronorite	0.66	M					Coarse grained gabbronorite with abundant euhedral orthopyroxene. Vein on last piece is probably not a fault with no evidence of shearing.
28	3	M	13	2	5a	28.5	107.24	13	2	9d	114.0	104.77	109.22	Poikilitic Gabbronorite	1.98	M		GS			Fine to medium-grained poikilitic gabbronorite with 21% orthopyroxene oikocrysts and 0.3% oxides.
29	3	M	13	2	10a	114.0	109.22	13	3	11	106.0	106.23	112.43	Gabbronorite	3.21	M					This interval starts medium-grained and gradually increases to coarse grained and then fines downward again to medium to fine-grained at the bottom of the section. Thin section of medium to coarse zone contains 12% subhedral to granular orthopyroxene and 0.9% oxide.
30	3	M	13	3	11	106.0	112.43	13	3	13b	130.0	106.23	112.98	Poikilitic Gabbronorite	0.55	S	Sl	GS	P	N	Identified in hand specimen. Medium-grained with poikilitic orthopyroxene
31	3	M	13	3	13b	130.0	112.98	14	1	11	73.0	113.10	118.80	Gabbronorite	5.82	M					Coarse to medium grained gabbronorite. Coarse patches have about 20% stubby subhedral to granular orthopyroxene and 1% oxide. Identified in hand specimen at the bottom of Core 13 and in Core 14 (mostly rubble recovered with core cuttings) in the last piece of core (believed to have been drilled) .

APPENDIX (continued)

Leg 147 Igneous Contacts Log — Hole:894G

Inter.	Ign. Unit	Plut. Unit	Top C	Top S	Top Pc	Top cm	expan. Depth	Bottom C	Bottom S	Bottom Pc	Bottom Cm	Curat. Depth	Exp. Depth	Lithology	Expan. Thick.	Description Type	Nat.	Asp.	Mor.	Def.	Notes
32	3	M	15	1	1	0.0	118.80	15	1	6	40.0	118.00	119.55	Rubble	0.75						Core 15 was taken after drilling through rubble fill in hole. Pieces 1-6 look like they could be redrilled rubble fill.
33	3	M	15	1	7	40.0	119.55	15	1	12	71.0	118.00	120.76	Gabboronorite	1.21	S	SI	GS	P		Coarse-grained with euhedral OPX. Contact dips at 47°
34	3	M	15	1	12	71.0	121.56	15	1	16	103.0	118.00	122.80	Poikilitic Gabbronorite	0.44						Medium-grained poikilitic gabbronorite with approximately 5% orthopyroxene oikocrysts and 1% oxides.
35	3	M	16	1	1	0.0	122.80	16	1	7	46.0	122.80	122.80	WASH	0.00						Assorted rubble from bottom of hole. Last piece in core may have been drilled, but rig floor does not believe any penetration made during this core.
Drilled							122.80						125.80		3.00						No Recovery
36	3	M	17	1	1	0.0	125.80	19	1	8	48.0	140.50	141.48	Poikilitic Gabbronorite	15.68	M					Fine to medium-grained with occasional coarse patches. Contains sparse olivine, with a slight concentration at the top of the interval, and poikilitic pyroxene.
37	4		19	1	9	141.8	141.48	19	1	20	139.0	140.50	143.32	Olivine-Plagioclase Phyric Diabase	1.84	S	I	Cs	I	N	Fine-grained diabase with abundant olivine, plagioclase and spinel phenocrysts. Contact is highly irregular, and runs subvertical apearring in a number of pieces downcore adhering to coarse-grained gabbronorite.
38	5	M	19	1	11	61.0	141.74	20	1	1	6.0	145.60	145.77	Gabbronorite	4.03						Coarse-grained with 10-20% euhedral to granular orthopyroxene. Intergranular oxide is irregularly distributed, occuring in patches where it locally amounts to 10%. The gabbronorite first appears in subvertical contact with the diabase part of the section. Contact with overlying gabbronorite
39	5	M	20	1	2	6.0	145.77	20	1	22	139.0	145.60	149.60	Poikilitic Gabbronorite	3.83	M					Medium grained poikilitic gabbronorite with about 5% orthopyroxene oikocrysts.
40	5	M	20	1	23	139.0	149.60	20	2	2	12.0	147.02	150.04	Gabbronorite	0.44	S	SI	GS	P	N	Coarse-grained gabbronorite with granular orthopyroxene. Contact subhorizontal
41	5	M	20	2	2	12.0	150.04	20	3	5	26.5	147.41	151.58	Poikilitic Gabbronorite	1.54	M					Medium-grained poikilitic gabbronorite with 5% or less orthopyroxene oikocrysts with coarser patches with more abundant (15-20%) granular to subhedral orthopyroxene. Contains about 1-2% irregullarly distributed oxides.
42	5	M	20	3	6	26.5	151.58	20	3	6	33.0	147.41	151.76	Gabbronorite	0.18	M					Coarse-grained granular gabbronorite.
43	5	M	20	3	6	33.0	151.76	20	3	17	128.0	147.41	154.50	Poikilitic Gabbronorite	2.74	M					Medium-grained olivine-bearing (~1%) gabbronorite with granular orthopyroxene in coarser patches, subophitic in medium grained portions, and about 2% oxides.

Notes: Location is that of lower contact of interval: (C) core, (S) section, (Pc) piece, (cm) curated depth in section. Type: (S) sharp, (G) gradational, (F) fault, (M) missing. Nature: (SI) sutured igneous, (I) intrusive, Aspect: (Cd) chilled down, (Cu) chilled up, (Cs) chilled sideways, (GS) grain size, (M) modal. Morphology: (I) irregular, (P) planar. Deformation: (N) none, (W) weakly foliated, (S) moderately foliated, (M) mylonite. Ap. - Apparent dip 1 & 2. Orientation is in core reference frame.